

Aus dem Institut für Schlaganfall- und Demenzforschung

Klinikum der Universität München, Großhadern

Direktor: Prof Dr. Martin Dichgans



**First and Second Generation CXCR4 Peptide Mimics to Block  
MIF Pathways in Atherosclerosis**

Dissertation

zum Erwerb des Doctor of Philosophy (Ph.D.)

an der Medizinischen Fakultät der

Ludwig-Maximilians-Universität zu München

vorgelegt von

Ying Gao

aus:

Pingdingshan, China

Jahr

2023

---

Mit Genehmigung der Medizinischen Fakultät der  
Ludwig-Maximilians-Universität zu München

Erstes Gutachten: Prof. Dr. Jürgen Bernhagen

Zweites Gutachten: Prof. Dr. Aphrodite Kapurniotu

Drittes Gutachten: Prof. Dr. Michael Weis

Viertes Gutachten: Prof. Dr. Sabine Marten-Steffens

Dekan: Prof. Dr. med. Thomas Gudermann

Tag der mündlichen Prüfung: 19.10.2023

# Table of Contents

<b>Table of Contents</b> .....	<b>II</b>
<b>List of Figures</b> .....	<b>VI</b>
<b>List of Table</b> .....	<b>IX</b>
<b>Abbreviations</b> .....	<b>X</b>
<b>List of Publications</b> .....	<b>XIV</b>
<b>Abstract</b> .....	<b>1</b>
<b>1 Introduction</b> .....	<b>3</b>
1.1 Atherosclerosis .....	3
1.1.1 Pathogenesis and Pathological features.....	3
1.1.2 Inflammation in atherosclerosis .....	6
1.1.3 Chemokines and their receptors in atherosclerosis.....	8
1.1.4 Anti-inflammatory therapy.....	13
1.2 MIF and its receptors .....	13
1.2.1 MIF .....	13
1.2.2 CD74.....	16
1.2.3 CXCR2 and CXCR4 .....	17
1.2.4 ACKR3/CXCR7 .....	20
1.2.5 MIF in atherosclerosis .....	21
1.3 Anti-MIF therapeutic strategies .....	22
1.3.1 Small molecule inhibitors.....	23
1.3.2 Antibody-based inhibitors .....	24
1.3.3 Peptide-based inhibitors .....	25

---

Aims .....	28
<b>2. Materials and Methods.....</b>	<b>30</b>
2.1 Materials .....	30
2.1.1 Reagents and chemicals .....	30
2.1.2 Cell culture reagents and media .....	33
2.1.3 Primary and secondary antibodies.....	34
2.1.3 Solutions and buffers .....	34
2.1.4 Laboratory equipment and software .....	35
2.2 Methods.....	35
2.2.1 <i>In vitro</i> drug testing and screening methods .....	35
2.2.2 Plasma degradation and protein interaction methods .....	43
2.2.3 <i>In vivo</i> murine experiments and bulk RNA-seq .....	45
<b>3. Results .....</b>	<b>49</b>
3.1 Characterization of the first generation CXCR4 ectodomain-derived peptide msR4M-L1 <i>in vitro</i> .....	49
3.1.1 MIF induces Dil-LDL phagocytosis in macrophages .....	49
3.1.2 msR4M-L1 inhibits MIF-induced Dil-LDL uptake in human PBMC-derived macrophages .....	50
3.1.3 Mutated msR4M-L1 loses capacity to block MIF/CXCR4-mediated LDL uptake ..	52
3.1.4 msR4M-L1 inhibits MIF-triggered Dil-oxLDL uptake in PBMC-derived macrophages .....	53
3.1.5 msR4M-L1 partially reverses MIF-induced integrated cellular responses as read out by DMR methodology .....	54
3.1.6 msR4M-L1 does not disrupt the MIF/CD74 interaction .....	55
3.2 Characterization of the inhibitory potential and pharmacological properties (IC <sub>50</sub> curves) for the next generation CXCR4 mimics (NGMs).....	56
3.2.1 Potency of the NGMs (IC <sub>50</sub> curves) as assessed by a Dil-oxLDL uptake assay ...	58

---

3.2.2 Inhibitory potency of NGMs (IC <sub>50</sub> curves) as assessed by a 3D monocyte chemotaxis assay.....	59
3.2.3 Inhibitory potency of NGMs (IC <sub>50</sub> curves) as assessed by Transwell B cell migration assay .....	61
3.2.4 Determining the selectivity of NGMs between MIF and CXCL12 .....	63
3.2.5 Summary of the inhibitory potential (IC <sub>50</sub> values) and selectivity of the NGMs .....	65
3.3 Degradation and albumin binding characteristics of NGM-D3 .....	67
3.3.1 Proteolytic stability of TAMRA-NGM-D3 in human plasma.....	67
3.3.2 Investigation of the interaction between albumin and NGM-D3.....	69
3.3.3 Investigation of the interaction between NGM-D3 and albumin using native PAGE .....	71
3.4 Therapeutic effects of NGM-D3 in early plaque development.....	73
3.3.1 Treatment with NGM-D3 does not attenuate plaque development and lesional macrophage content in an <i>ApoE</i> <sup>-/-</sup> mouse model or early atherogenesis.....	74
3.3.2 Circulating T-cell numbers are reduced in mice subjected to NGM-D3 treatment	76
3.4.4 Bulk RNA-seq unveils numerous differentially expressed genes in NGM-D3 treated atherogenic mice .....	78
3.4.5 NGM-D3 attenuates multiple atherogenesis-related pathways.....	81
3.4.6 NGM-D3 reprograms molecular landscape of plaques by downregulating non-immune cell-associated atherogenic genes and enhancing mitochondria metabolism..	83
<b>4 Discussion .....</b>	<b>86</b>
4.1 msR4M-L1 .....	86
4.2 Next generation mimics.....	90
4.2.1 <i>In vitro</i> screening .....	90
4.2.2 Degradation and albumin binding feature of NGM-D3 .....	93
4.2.3 <i>In vivo</i> study .....	96
<b>References.....</b>	<b>101</b>

<b>Acknowledgements.....</b>	<b>119</b>
<b>Affidavit.....</b>	<b>121</b>
<b>Confirmation of congruency.....</b>	<b>122</b>

# List of Figures

Figure 1: Initiation of atherosclerosis .....	5
Figure 2: Complexity and specificity of chemokine-receptor network .....	9
Figure 3: Chemokine activities in cardiovascular disease .....	11
Figure 4: MIF signaling pathways .....	17
Figure 5: Structural comparison between CXCL12/CXCR4 and MIF/CXCR4 binding models .....	20
Figure 6: Summary of inhibition strategies to target MIF-receptor axes in atherosclerosis	23
Figure 7: The design scheme for the generation of CXCR4 peptide inhibitor msR4M-L1.	27
Figure 8: MIF induces Dil-LDL uptake in primary human monocyte-derived macrophages	50
Figure 9: The inhibitory effect of AMD3100 and msR4M-L1 on MIF-associated Dil-LDL uptake in primary human monocyte-derived macrophages .....	51
Figure 10: Mutated msR4M-L1(7xAla and 2xAla) loses the capacity to block MIF/CXCR4- mediated LDL uptake .....	52
Figure 11: msR4M-L1 dose-dependently reverses MIF-mediated oxLDL uptake.....	53
Figure 12: Dynamic mass redistribution analysis of the inhibition effect of msR4M-L1 on MIF- stimulated HEK293-CXCR4 transfectants. ....	54
Figure 13: Transfection efficiency of CD74minRTS-FLAG in HEK293T cells.....	55
Figure 14: msR4M-L1 does not disrupt MIF/CD74 interaction .....	56
Figure 15: Sequences of msR4M-L1 and six NGMs. ....	58
Figure 16: Determination of IC50 curves for the inhibitory effects of NGMs on MIF-elicited Dil- oxLDL uptake .....	59
Figure 17: Determination of IC50 curves for the inhibitory effect of NGMs on MIF-induced 3D monocyte chemotaxis.....	60

---

Figure 18: Determination of IC50 curves for the inhibitory effect of NGMs on MIF-induced murine B-cell chemotaxis .....	62
Figure 19: NGMs do not inhibit CXCL12-mediated murine B-cell migration in a Transwell setting .....	64
Figure 20: Differential effects of NGMs on CXCL12-mediated 3D human monocyte chemotaxis .....	65
Figure 21: TAMRA-NGM-D3 reveals appreciable proteolytic stability in human plasma	68
Figure 22: Cy7.5-NGM-D3 partially co-electrophoreses with human serum albumin .....	70
Figure 23: The interaction of Cy7.5-NGM-D3 with human albumin is dependent on disulfide bonds .....	71
Figure 24: Cy7.5-NGM-D3 interacts with human serum albumin in a dose-dependent manner – evidence from native PAGE analysis.....	72
Figure 25: Experimental scheme.....	74
Figure 26: Lesions and macrophage content were not significantly altered by NGM-D3 in 5-week HFD <i>ApoE</i> <sup>-/-</sup> mice .....	75
Figure 27: Gating strategy for different leukocyte populations in circulation.....	76
Figure 28: Effect of NGM-D3 treatment on circulating leukocyte counts .....	77
Figure 29: Weight change over the course of the 5-week HFD diet.....	78
Figure 30: Principal component analysis (PCA) of RNA-seq data of atherosclerotic plaque samples from saline- and NGM-D3-treated mice .....	79
Figure 31: Volcano plot of highly differentially expressed genes identified in each group	80
Figure 32: Transcriptome analysis reveals distinct gene expression between saline and NGM-D3 treated mice.....	81
Figure 33: Downstream enrichment analysis of genes down-regulated in the NGM-D3 group .....	82
Figure 34: Heatmap of genes mediating TNF signaling pathway in bulk RNA-seq.....	83
Figure 35: Downstream enrichment analysis of upregulated genes in the NGM-D3 group.	84



Figure 36: Violin plots of non-immune cell signatures comparing control and NGM-D3 mice identified in bulk RNA-seq data ..... 85

# List of Table

Table 1: Summary of IC <sub>50</sub> values of NGMs obtained from screening using <i>in vitro</i> cell assays mimicking atherogenic processes.....	66
--	----

# Abbreviations

ACKs	Atypical chemokines
ACKR3	Atypical chemokine receptor 3
AMPK	AMP-activated protein kinase
APCs	Antigen-presenting cells
ASCVD	Atherosclerotic cardiovascular disease
APOA-1	Apolipoprotein A-I
APOE	Apolipoprotein E
BC	Brachiocephalic artery
CD74	Cluster of differentiation 74
CD184	Cluster of differentiation 184
CRP	C-reactive protein
CVD	Cardiovascular disease
CXCL12	CXC motif chemokine ligand 12
CCR5	C-C motif chemokine receptor 5
CXCR2	CXC chemokine receptor 2
CXCR4	CXC chemokine receptor 4
CK	Creatine kinase
CRL	Cullin-ring ligase
DAMPs	Damage-associated molecular patterns
DMR	Dynamic mass redistribution
DTT	Dithiothreitol

---

ECs	Endothelial cells
ECLs	Extracellular loops
ECM	Extracellular matrix
FMI	Forward migration index
FSC	Forward scatter cytometer
GBD	Global Burden of Disease, Injuries, and Risk Factors Study
GO	Gene ontology
GM-CSF	Granulocyte-macrophage colony stimulating factor
GPCRs	G-protein-coupled receptors
HFD	High-fat diet
HIV	Human immunodeficiency virus
HSA	Human serum albumin
ICLs	Intracellular loops
IFN- $\gamma$	Interferon-gamma
IRI	Ischemia-reperfusion injury
IL-1 $\beta$	Interleukin-1 $\beta$
KEGG	Kyoto encyclopedia of genes and genomes
LDL	Low-density lipoprotein
LESTR	Leukocyte-derived seven-transmembrane domain receptor
LFA1	Lymphocyte function-associated antigen 1
MAPK	Mitogen-activated protein kinase
MCP-1	Monocyte chemoattractant protein-1
MHCII	Major histocompatibility complex II
MIF	Macrophage migration inhibitory factor

---

M-CSF	Monocyte-colony stimulating factor
MS	Multiple sclerosis
MyD88	Myeloid differentiation factor 88
NK	Natural killer
NF- $\kappa$ B	Nuclear factor $\kappa$ B
NETs	Neutrophil extracellular traps
NGMs	Next generation mimics
OCT	Optimal cutting temperature
PAMPs	Pathogen-associated molecular patterns
PBMCs	Peripheral blood mononuclear cells
PCA	Principal component analysis
PPIs	Protein-protein interactions
PLC	Phospholipase C
RA	Rheumatoid arthritis
RLR	Arg-Leu-Arg
SARs	Structure-activity relationships
SLE	Systemic lupus erythematosus
SMDs	Small molecule drugs
SSC	Side scattered light
TCA	Citric acid
Th1	T helper cell 1
TIA	Transient ischemic attack
Tr1	Type 1 regulatory T
TLRs	Toll-like receptors

TNF	Tumor necrosis factor
VCAM-1	Vascular cell adhesion molecule-1
VLA4	Very late antigen 4
VSMCs	Vascular smooth muscle cells
4-IPP	4-iodo-6-phenylpyrimidine

# List of Publications

## Published paper:

Kontos C, El Bounkari O, Krammer C, Sinitski D, Hille K, Zan C, Yan G, Wang S, **Gao Y**, Brandhofer M, Megens RT. Designed CXCR4 mimic acts as a soluble chemokine receptor that blocks atherogenic inflammation by agonist-specific targeting. *Nat Commun* 2020; Nov 25;11:5981.

Wang S, El Bounkari O, Zan C, Tian Y, Gao Y, Bernhagen J. Classical chemokines, atypical chemokines, and MIF proteins in ischemic stroke: effects, mechanisms and roles in conditioning. *Cond Med* 2021; 4: 39-57

## Manuscript in preparation:

Kontos C\*, Gao Y\*, Ebert S, Wunderlich H, Yang B, Ji H, Gokce O, Bernhagen J#, Kapurniotu A#. Minimized CXCR4 receptor peptide mimics with tailored ligand recognition and anti-atherogenic properties. in preparation 2023

# Abstract

## Background:

Chemokines have a pathogenic role in atherosclerosis, but chemokine targeting strategies have been hampered by the redundancy of the chemokine/receptor network. Complexity is further complicated by atypical chemokines (ACKs) such as macrophage migration inhibitory factor (MIF), an inflammatory mediator that signals through CXCR2 and CXCR4 to promote atherogenic leukocyte recruitment. CXCR4 is also the *bona fide* receptor of the homeostatic chemokine CXCL12. Our laboratory recently developed a 31-residue anti-atherogenic ectodomain-derived peptide mimic of CXCR4, msR4M-L1, which selectively binds MIF but spares CXCL12 and this contributed to the characterization of the inhibitory profile of msR4M-L1. Moreover, guided by structure-activity studies on relevant CXCR4 ectodomain sequences, work in this PhD thesis also focused on the design of next generation mimics (NGMs) with a minimized size of only 20 residues, non-natural or native amino acid-based linkers, and improved solubility.

## Methods:

Using freshly isolated primary human monocytes, LDL or oxLDL uptake assays were established to determine the inhibitory capacity of msR4M-L1 against MIF. DMR and receptor binding experiment were used to examine the selectivity of MIF between its receptors CXCR4 and CD74. For NGMs, *in vitro* 2D and 3D cell migration and oxLDL uptake assays were performed to examine their potency and efficacy by constructing IC<sub>50</sub> curves. The lead minimized peptide NGM-D3 was chosen for degradation and stability studies. Additionally, *ApoE*<sup>-/-</sup> mice were treated with NGM-D3 to evaluate its therapeutics in atherosclerosis and bulk RNA sequencing of plaque tissue was performed.



**Results:**

As the proof-of-concept CXCR4 ectodomain-derived peptide inhibitor, msR4M-L1 showed robust and specific inhibition on MIF-driven inflammatory responses *in vitro* and *in vivo*. LDL/oxLDL uptake in macrophages induced through MIF/CXCR4 were dose-dependently blocked by msR4M-L1. msR4M-L1 selectively targeted the MIF/CXCR4 pathway without interfering MIF/CD74. NGMs were generated with improved conformational flexibility and solubility, while maintaining the preferential selectivity of binding to MIF over CXCL12. NGMs such as NGM-D3 inhibited MIF-elicited macrophage foam cell formation and attenuated MIF-induced chemotaxis as determined by constructing IC<sub>50</sub> curves. Dose titrations of NGMs revealed IC<sub>50</sub> values in the range of 10-100 nM for all bioassays. NGM-D3 exhibited favorable stability and half-life in human plasma *ex vivo*, partially due to its binding capacity to albumin as indicated by albumin binding assays using TAMRA-NGM-D3. Although NGM-D3 did not reduce plaque size and macrophage burden in a 5-week high-fat diet (HFD) *ApoE*<sup>-/-</sup> mice model of early atherogenesis, it led to reprogramming of the transcriptional profiles of the atherosclerotic plaque tissue. Extracellular matrix regulatory and pro-inflammatory signatures were found to be significantly downregulated in plaque tissue of NGM-D3-treated mice compared to vehicle control, exemplified by enrichment in extracellular matrix organization, cell adhesion and migration, and TNF signaling pathway. In addition, NGM-R3 not only block MIF-driven pathways, but also CXCL12-mediated signaling.

**Conclusions:**

The first generation ectodomain mimic msR4M-L1 and minimized ectodomain mimics of CXCR4 (“NGMs”) such as NGM-D3 were designed and verified to selectively bind to MIF. They are promising inhibitors of atherogenic MIF activities *in vitro*. NGM-D3 modulates atherogenic transcriptional signatures *in vivo* in an early mouse model of atherosclerosis. Interestingly, dual-specific NGMs such as NGM-R3 binding to MIF and CXCL12 could have a utility in conditions driven by MIF and CXCL12.

# 1 Introduction

## 1.1 Atherosclerosis

### 1.1.1 Pathogenesis and Pathological features

The latest Global Burden of Diseases, Injuries, and Risk Factors Study (GBD) 2019 reported that cardiovascular diseases (CVD) led to approximate one-third of mortality globally (1). The increasing prevalence of major risk factors, including dietary risks, high low-density lipoprotein cholesterol, air pollution, high body mass index, and smoking, largely attribute to the high death rate for atherosclerotic cardiovascular diseases (ASCVD).

Atherosclerosis is a disease, in which plaque grows on the inside of the wall of arteries. Plaque lesions are composed of fat, cholesterol, calcium, infiltrated immune cells, and other substances. Plaque build-up exerts detrimental effects, hardening and narrowing of the arteries and reducing the blood flow delivered to tissues. Tissue infarction and death could happen when obtaining non-sufficient oxygen and nutrients from the blood, resulting in severe clinical outcomes. Sometimes a piece of plaque can break-off and travel somewhere else throughout the circulation to block blood flow, causing ischemic damage or thrombotic occlusion. Atherosclerosis often doesn't cause symptoms until an artery becomes more than 50-70% obstructed. Some early signs warning of the presence of the disease include chest pain, intermittent claudication, and transient ischemic attack (TIA). The location of the vascular artery impacted presents with different clinical manifestations.

Atherosclerosis has been a human disease for >3,500 years, dating back to when the pathology was found in Egyptian mummies (2). It was initially identified as a lipid-driven disease. The initial step occurs, when low-density lipoprotein (LDL) levels increase, particularly in body parts where the vessel wall undergoes disturbed or low laminar shear stress flow (3,

4). Once the endothelial barrier disrupts, LDL particles can cross the endothelial layer, break through into the intima and start to accumulate. Those LDL droplets often undergo oxidative or other forms of modifications (5, 6), converting into pro-atherogenesis particles, setting off the innate inflammatory reactions within the intima. Activated endothelial cells (ECs) express elevated adhesion molecules like vascular cell adhesion molecule-1 (VCAM-1) and release cytokines and chemokines to attract monocytes, lymphocytes, and neutrophils and draw them into the intimal space. Upon entry, transmigrated circulating monocytes transform into macrophages in response to the local monocyte-colony stimulating factor (M-CSF) release, take up lipids, and transform into foam cells. Foam cells are the hallmark of atherosclerosis. Not only do they promote the enlargement of lipid-rich compartments, but they also secrete a variety of inflammatory mediators. Another major resource of cellular components, vascular smooth muscle cells (VSMCs), may also give rise to lipid-laden cells and contribute to the disease progression by secreting various pro-inflammatory cytokines, such as interleukin (IL)- $1\beta$ , tumor necrosis factor (TNF)  $\alpha$  and  $\beta$ , MCP-1, and IL-18. All those cellular components' activation form an infinite loop, elaborating recruitment and proliferation of VSMCs, further LDL oxidation, and constant endothelial impairment and leukocyte recruitment (**Figure 1**). Additionally, many atherogenic molecules promote VSMCs to produce proteoglycans to augment the retention of LDL core proteins, increase lipid content and accelerate plaque formation (7, 8).

The first visible evidence of atherosclerosis is a fatty streak, which is a yellow-colored streak on gross inspection. They mainly consist of macrophage foam cells stratified in adjacent layers (9). Up to this point, the pathologic alterations are considered reversible. As the disease progresses, lipid accumulation begins to form an extracellular lipid pool with decreased cellularity.

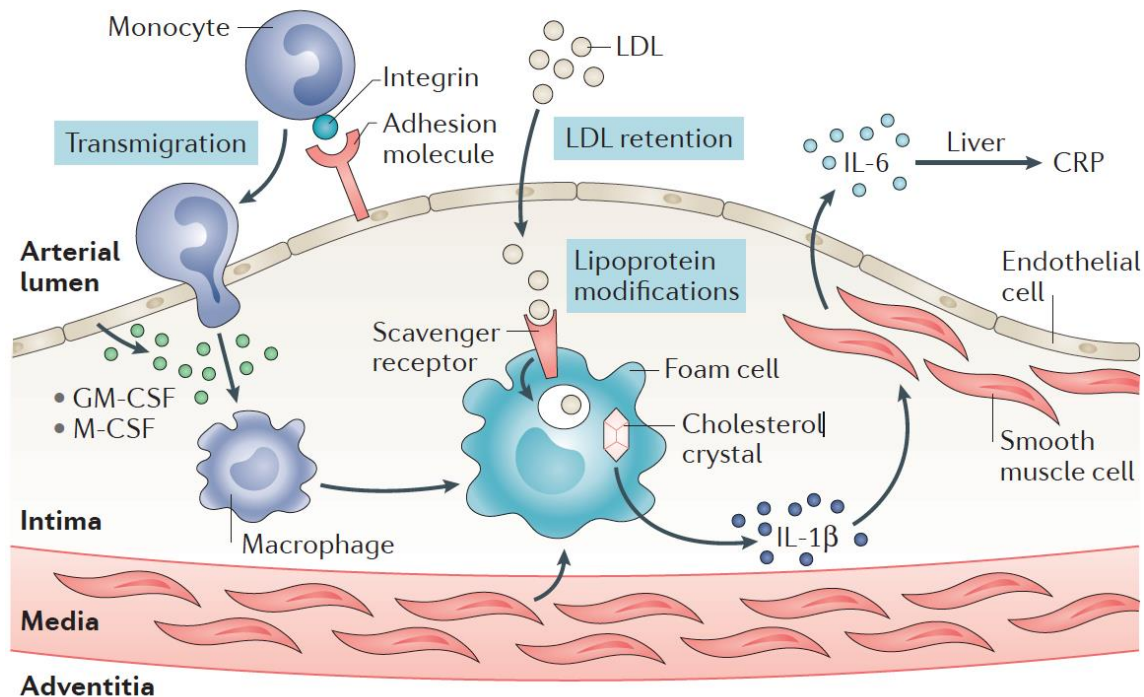


**Figure 1: Initiation of atherosclerosis.** Lipoprotein retention initiates innate immunity, which leads to the up-regulation of leukocyte adhesion molecules (such as VCAM-1 and ICAM-1) on the endothelium, facilitating the rolling, adherence, and eventually transmigration of blood neutrophils, monocytes, and lymphocytes to the subendothelial layer. Within the intima, macrophage-colony stimulating factor (M-CSF) and granulocyte-macrophage colony stimulating factor (GM-CSF) promote monocytes to differentiate into macrophages which take up lipoproteins and transform into foam cells. Smooth muscle cells can migrate into the intima space and proliferate. In addition, SMCs have been recognized to undergo metaplasia and give rise to macrophage-like cells. Cholesterol crystals are a critical mediator in activating the inflammasome synthesis and causally releasing of IL-1 $\beta$  and its downstream signaling IL-6. IL-6 participates in the production of C-reactive protein (CRP). Increased levels of CRP indicate an increased risk for atherosclerotic cardiovascular disease. Taken from Gisterà A et al, *Nat Rev Nephrol* 2017 (10).

The evolution of atherosclerotic lesions is characterized by gradual enlargement over time. Accumulating lipid droplets within foam cells, the proliferation of VSMCs, and the production of intracellular matrix slowly constitute fibroatheroma. At this stage, macrophages and VSMCs could die in plaques through apoptosis (11). The defective clearance of apoptotic bodies is associated with secondary necrosis. Cellular debris arising from apoptotic cells, the release of cellular contents, and accumulating extracellular lipids aggressively distort the normal

architecture of the intima, ultimately forming enlarging pools termed lipid-rich necrotic cores (12-14). Fibrous tissue adds and forms in and around regions of the intima, in which lipid cores are stacked irregularly. (15). Sometimes the fibrous tissue represents the greater thickness of the lesion than the underlying lipid cores. As a result, arteries are narrowed with a higher occurrence of clinically relevant complications.

In more advanced stages of plaque development, plaques can develop a thin cap and become unstable, which may lead to rupture (16, 17). Clinical morbidity and mortality are highly associated with this type of lesion, in which plaque rupture, hematoma or hemorrhage, and thrombosis are most likely to occur. They are often found among people at age  $\geq 55$  years, and the thickness for 95% of ruptured caps is below 65  $\mu\text{m}$  (18). Ruptured lesions revealed heavy macrophage-derived foam cell infiltration and less VSMC content (17, 19). The imbalance between collagen production and proteolytic degradation facilitates plaques to rupture, inducing thrombotic formation eventually. The clinical consequences of thrombosis vary, largely depending on the regions and sites. It only becomes life-threatening when a major blood vessel is affected. Nevertheless, silent plaque ruptures are of utmost importance for plaque growth and acute coronary syndrome (20, 21). Scarring of fibrous tissue has been viewed as a cause for the constrictive remodeling seen in patients with severe stenosis (22).

### **1.1.2 Inflammation in atherosclerosis**

Despite dyslipidemia, substantial experimental and clinical investigations indicate that the immune system fundamentally shapes atherosclerosis and contributes to the etiology of ischemic injuries. The initial insight that atherosclerosis is a lipid-driven inflammatory disease arises from studies of classical acute phase reactant proteins. For instance, concentrations of C-reactive protein (CRP) show associations with levels of creatine kinase (CK) MB, implicating that inflammation correlates to myocardial infarction (23). CRP levels are an independent risk

factor in predicting cardiovascular events. They could also be utilized as an indicator of vascular inflammation in patients with elevated lipid levels (24).

As part of innate immunity, macrophages express multiple Toll-like receptors (TLRs), including TLR2 and TLR4, which are crucial sensors for pathogen-associated molecular patterns (PAMPs) and damage-associated molecular patterns (DAMPs). In plaques, TLR2 and TLR4 recognize and bind to their endogenous ligands LDL and its modified products. Apart from lipoproteins, Other endogenous and exogenous ligands, such as heat shock proteins (25), fibronectin (26), and bacterial toxins, might also activate TLRs. The common downstream pro-inflammatory pathways of TLRs were succeeded by the myeloid differentiation factor 88 (MyD88) (27). Lack of MyD88 in mice causes reductions in lesion size, lipid content, and circulating levels of pro-inflammatory genes (28).

Cellular immunity has been extensively investigated in atherosclerosis. CD4<sup>+</sup> T cells recognize exogenous epitopes loaded on major histocompatibility complex (MHC) I, and CD8<sup>+</sup> T cells recognize endogenous peptides presented by MHC class II on antigen-presenting cells (APCs). CD4<sup>+</sup> T cells have the potential to differentiate into T<sub>H</sub> subset (T<sub>H</sub>1, T<sub>H</sub>2, T<sub>H</sub>9, T<sub>H</sub>17, T<sub>H</sub>22, follicular helper T (T<sub>FH</sub>) and CD28<sup>-</sup> T cells) or T<sub>reg</sub> subset (FOXP3<sup>+</sup> T<sub>reg</sub> cells and type 1 regulatory T (Tr1) cells) (29, 30). TH cells exert pro-inflammatory effects, whereas T<sub>reg</sub> cells hinder immune cell responses. Lack of CD4<sup>+</sup> T cells has a protective impact on atherosclerotic lesion formation (31, 32). Among T<sub>H</sub> cells, T<sub>H</sub>1 cells are the dominant T cell population in lesions (33), which express the C-C motif chemokine receptor 5 (CCR5), which is needed explicitly for CD4<sup>+</sup> T cell homing to the atherosclerotic plaques (34). The depletion of CD4<sup>+</sup> T<sub>reg</sub> cells exacerbates atherosclerosis (35). CD8<sup>+</sup> T cells compose a prominent population in atherosclerosis, especially in the advanced stage. The functions of CD8<sup>+</sup> T cells have been debated. Both pro-atherogenic and atheroprotective observations have been made in experimental studies. CD8<sup>+</sup> T cells promote vulnerable plaque development, and depletion of

CD8<sup>+</sup> T cells led to a decrease in plaques with increased levels of IFN- $\gamma$  and granzyme B in atheroprone mice, suggesting the pro-atherogenic effect of CD8<sup>+</sup> T cells (36, 37). Conversely, one study suggests that mice developed less stable lesions with increased macrophage burden and necrotic core area in *Ldlr*<sup>-/-</sup> mice lacking CD8<sup>+</sup> T cells (38).

Genome-wide association and transcriptomic studies highlight the fundamental role of B cells in atherosclerosis. As the reservoir of B cells in the body, splenectomy markedly sabotages atherosclerotic lesions in hypercholesterolemic apolipoprotein E knock-out mice (*ApoE*<sup>-/-</sup> mice). Those splenectomized mice receiving a transfer of spleen cells separated from *ApoE*<sup>-/-</sup> mice show decreased plaque size in contrast to the control (39). Similarly, *Ldlr*<sup>-/-</sup> mice with lethal irradiation grow increased lesions after injection of bone marrow from a B cell-deficient (uMT) donor (40). Those studies appear to favor an atheroprotective role of B cells. Nevertheless, B cells consist of multiple different functional subsets. Animal studies have demonstrated that distinct B cell subset targeting leads to contradictory outcomes, either pro-atherogenic or anti-atherogenic effects.

### **1.1.3 Chemokines and their receptors in atherosclerosis**

Chemokines are small molecule proteins (8-12 kDa) and belong to the large family of secreted proteins-cytokines. The fundamental function of chemokines is to regulate inflammatory responses with the ability to promote cell migration to target tissues, a biological process known as chemotaxis. Besides, chemokines are believed to participate in other processes beyond immune cell migration, such as embryogenesis, homeostasis, proliferation, and differentiation (41).

Classical chemokines can be divided into four subtypes based on the presence of N-terminal conserved cysteine residues, including CC-, CXC-, C-, and CX<sub>3</sub>C-. Chemokine receptors

belong to the family of G-protein-coupled receptors (GPCRs) and specifically bind to their cognate chemokine ligands via a two-site model (42). Chemokines and their interactions with their receptors constitute a complex network. Multiple chemokine ligands can bind different receptors with close affinity. Some receptors also present a wide range of binding specificities, unraveling the abundance and redundancy of the interaction network between ligands and receptors (**Figure 2**). When interacting with different ligands, receptors may exert different bio-activities by triggering specific downstream signaling. Regarding chemokine-receptor interactions, selectivity, specificity, and binding affinity are of prime importance. I will introduce several common relevant chemokine-receptor pathways in the context of ASCVDs (**Figure 3**).

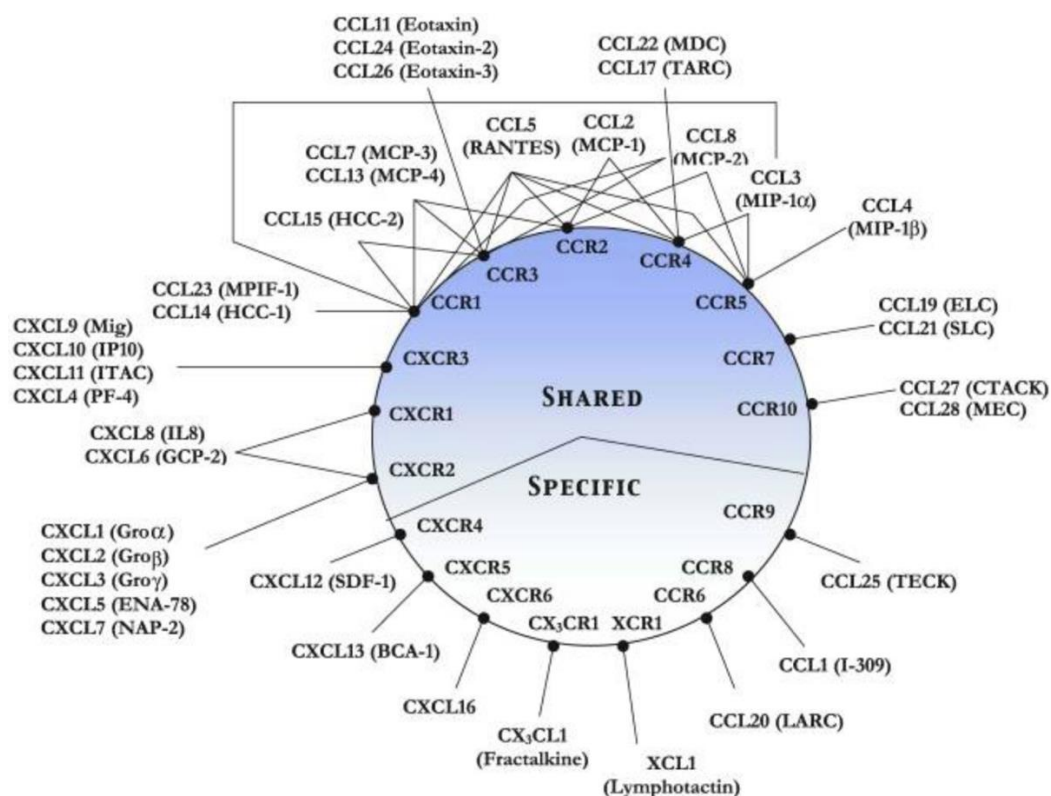


**Figure 2: Complexity and specificity of chemokine-receptor network.** The ligands are displayed outside the circle, while the receptors are depicted inside. The names of frequently used ligands are listed in brackets. The well-recognized nomenclature for chemokine ligands and receptors is employed. Some chemokines have more than one name. For the sake of simplicity, one of the names was chosen. Taken from Rajagopalan L et al, *Biosci Rep* 2006 (42).



**CCL2/CCR2 axis**

The CC chemokine CCL2, also known as the monocyte chemoattractant protein-1 (MCP-1), is the first identified chemokine and elicits, but is not limited to, potent classical monocyte chemoattractant impacts through its cognate receptor CCR2 (43, 44). Its pro-atherosclerotic role has been extensively investigated since the evidence came out as early as 1998. CCL2 plasma levels are linked to increased mortality in human acute coronary syndrome (45). *Ldlr*<sup>-/-</sup> mice lacking the expression of CCL2 developed less lipid burden with less macrophage content (43). *Ccr2*-knockout in the *Apoe*<sup>-/-</sup> background also revealed reduced plaque development (46). The athero-driving feature is accomplished by directing leukocytes to the inflamed arterial sites.

**CXCL8-CXCR2 axis**

CXCL8 is one of the important inflammatory mediators that chemo-attract neutrophils and T cells in atherosclerosis. CXCL8 binds to receptor CXCR2 with greater affinity than that of receptor CXCR1 (47). Other than its chemoattractant effect, CXCL8 is an ELR<sup>+</sup> chemokine, which promote angiogenesis (48, 49).

CXCL8 has an emerging role in the metabolism of VSMCs, suppressing the proliferation and migration of VSMCs through AKT/GSK3 $\beta$ /Cyclin D1 signaling (50). On the other hand, CXCL8 was found to down-regulate ABCA1 expression, thereby decreasing cholesterol efflux via miR-183 (51). However, further research must be done based on the latest contradictory outcomes to validate the findings.

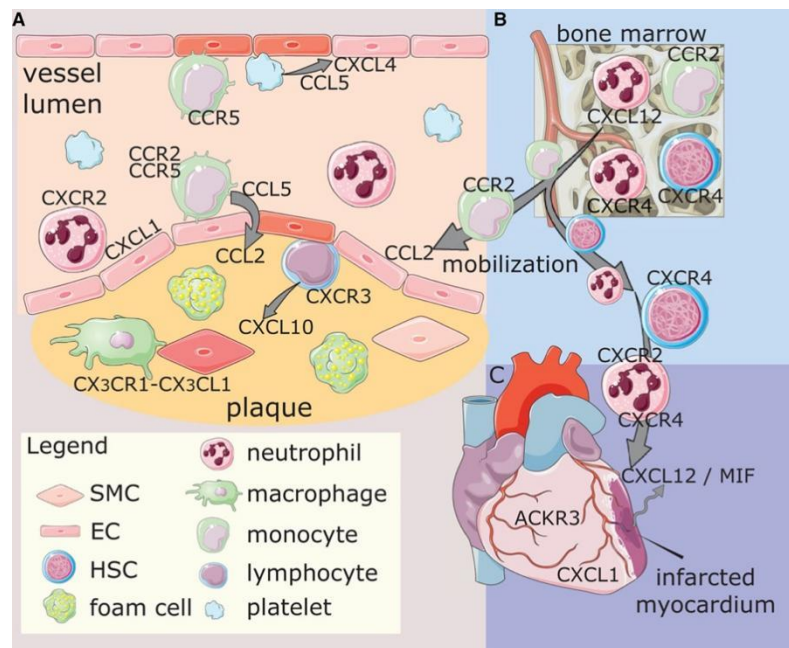


**Figure 3: Chemokine activities in cardiovascular disease.** Chemokines impact the development of atherosclerosis and other cardiovascular diseases by mediating leukocyte recruitment, or involving in hematopoiesis in the bone marrow, or initiating survival signaling in myocardial infarction. Chemokine deposition in platelets also contributes to monocyte adhesion. ACKR3, atypical chemokine receptor 3; EC, endothelial cell; MIF, macrophage migration inhibitory factor; SMC, smooth muscle cell. Taken from Noels et al, *Arterioscler Thromb Vasc Biol* 2019 (52).

### CXCL12-CXCR4/ACKR3 axis

CXCL12 (SDF-1 $\alpha$ ) is an essential player in numerous physiological and pathological processes. It functions at various levels, regulating the homing of hematopoietic progenitor cells, endothelial cell functions, and migration of leukocytes (53-56). Interaction with receptor CXC chemokine receptor 4 (CXCR4) and atypical chemokine receptor 3 (ACKR3) enables CXCL12 to perform its functions under healthy and disease conditions. CXCL12 activity is exerted by the NH<sub>2</sub>-terminal amino acids with the remarkable dedication of the first two amino acids, lysine, and proline (57, 58). Additionally, the sequence RFFESH strengthens the binding of the NH<sub>2</sub>-terminal motif to CXCR4 by altering CXCL12 conformation (59). Even though this two-site binding model between the chemokine and the receptor has been established and recognized over decades, recent findings have shown the advances in chemokine-receptor

interaction where the interaction engages other domains (60). RFFESH-motif was shown to be important for the binding. But N-terminal binding to receptor helices V/VI induces a conformational change which leads to intracellular G-protein signaling activation (61, 62). CXCR4 action is predominantly conferred by a G protein-coupled signal and amplified by a continuous sequence of signaling cascades, such as mitogen-activated protein kinase (MAPK), phospholipase C and phosphatidylinositol-3-kinase pathways, leading to migration or neovascularization (63).

From a clinical aspect, serum CXCL12 levels were associated with CVD severity (64, 65). In addition, a genome study disclosed the contributions of the CXCL12 gene to CVD and myocardial infarction (66).

Due to its role in the regulation of progenitor cells, CXCL12 was shown to promote the healing process of injured vasculature by boosting endothelial progenitor cell recruitment (67). In the context of atherosclerosis, CXCL12 demonstrates a cell-specific effect. Global CXCL12 knockout did not alter lesion phenotype, whereas non-hematopoietic and EC-knockout models developed less lesions and increased collagen content (68). The data suggest the pro-atherosclerotic role of CXCL12. Atherosclerotic studies were also done on the CXCL12-CXCR4 axis with a focus on CXCR4. Bone marrow CXCR4 deficiency promoted lesion growth in *ApoE*<sup>-/-</sup> mice, and antagonizing CXCR4 with AMD3465 resulted in a more significant number of leukocytes and fewer SMCs presented in the lesions (69). In 2018, Döring et al. elucidated the comprehensive cell-specific actions of the CXCL12/CXCR4 pathway in EC- and VSMC-deficiency models. Both mice models showed a more severe atherosclerotic phenotype, pinpointing to a protective function of CXCL12/CXCR4 pathway (70). Overall evidence suggests debated functions of CXCL12-CXCR4 pathway in atherosclerosis. Because CXCR4 has two ligands, CXCL12 and MIF, future research needs to separate each axis to understand this chemokine-receptor relationship.

### **1.1.4 Anti-inflammatory therapy**

Considerable evidence from preclinical experimental models has inculcated inflammation in the prevalence of atherosclerosis and its complications (71, 72). Unfortunately, several trials have failed to alter cardiovascular outcomes. One adhesion molecule, P-selectin, augments acute inflammation complicated by thrombosis. SELECT-ACS trial (Effects of the P-Selectin Antagonist Inclacumab on Myocardial Damage After Percutaneous Coronary Intervention for Non-ST-Segment Elevation Myocardial Infarction) did not reduce adverse events in patients with acute coronary syndrome (73). Methotrexate inhibits the synthesis of DNA and might also have an impact on JAK/STAT protein kinase pathway to confer the anti-inflammatory effect. Patients receiving low-dose methotrexate did not show reduced clinical outcomes in CIRT (Cardiovascular Inflammation Reduction Trial) (74). However, the CANTOS (Canakinumab Anti-inflammatory Thrombosis Outcomes Study) raised the attention to targeting inflammation in atherosclerosis (75). Neutralizing IL-1 $\beta$  antibody reduced recurrent cardiovascular events in patients with acute myocardial infarction 30 days before enrollment. Another anti-inflammatory agent, colchicine, pioneered the utilization of colchicine to prevent coronary artery events (LoDoCo trial, Low-Dose Colchicine for Secondary Prevention of Cardiovascular Disease) (76). Other potential immunotherapies target IL-2, IL-6, NLRP3, and vaccine strategies.

Beyond CANTOS trial, there are trials targeting chemokines and their receptors ongoing. Maraviroc, a small molecule CCR5 inhibitor decreased various markers of cardiovascular risk in HIV patients accompanied by atherosclerosis (77). The inhibition of CXCR2 with AZD5069 in coronary heart disease is under evaluation (78).

## **1.2 MIF and its receptors**

### **1.2.1 MIF**

Macrophage migration inhibitory factor (MIF) was first discovered as a lymphokine in guinea pig, in which its expression levels were associated with delayed hypersensitivity and cellular

immunity (79, 80). The human MIF is located in chromosome 22q, and its cDNA was successfully isolated in 1989 (81). Mouse MIF was discovered in 1993 (82). Having access to recombinant MIF allows for a deeper understanding of MIF functions in different disease models. In 1994, Paralkar and Wistow reported the small genetic structure of human MIF that has three exons separated by two introns (83). Next year, one study found that the structure of mouse *Mif* gene resembles its human counterpart (84). Unlike the human *MIF* gene, mouse *Mif* maps to chromosome 10 and has nine processed pseudogenes on chromosomes 1, 2, 3, 7, 8, 9, 12, 17, and 19 (84).

*MIF* gene is highly conserved across many species, including mammals, nematodes, bacteria, and plants (85, 86). Human MIF sequence is 90% similar to mouse and rat *Mif* (87). Two polymorphisms in the gene that have been associated with human disease. One is a single nucleotide polymorphism (SNP) -173 G/C (rs755622) that reveals an association with autoimmune, infections, and age-related diseases, and the other one is CATT- repeat -794, which correlates with kidney and heart disease (88, 89).

MIF protein is comprised of 114 amino acids. It can present as monomer, dimer, and trimer. The monomer features two anti-parallel  $\alpha$ -helices and a four-stranded  $\beta$ -sheet. Even if there is no extended sequence similarity between MIF and classical chemokines, the conformation of the MIF monomer resembles the dimer of CXCL8 and other CXC chemokines (90). Only the homotrimer harbors the unique tautomerase enzymatic activity of MIF, which mediates the tautomerization of the non-physiological substrates D-dopachrome and hydroxylphenyl pyruvate (4-HPP). The essential amino acid for the MIF enzymatic activity is proline residue at the N-terminal (proline-2). Blockade of the site would slow down the enzymatic reaction.

MIF was identified as a protein secreted by anterior pituitary cells upon stimulation with lipopolysaccharide (LPS) in 1993 (82). It appeared to be a critical molecule in the toxic

circumstances in dealing with endotoxemia or septic shock. This unraveled a key role for MIF as inflammatory cytokine. Later, one paper recapitulated the notions of MIF being a pituitary mediator that functions as a counter-regulatory hormone for glucocorticoid actions in immunity (91). MIF could balance the potent inhibition of steroids in the immune response. MIF can be detected in various tissues and is localized in intracellular vesicles, the nucleus, and the exosomes (92-94). Due to the lack of an N-terminal signal required for the classical translocation into the endoplasmic reticulum (ER), MIF secretion follows a non-classical secretory pathway mediated by ATP binding cassette transporter subfamily 1 (ABCA1) (95, 96). The intracellular reservoir of MIF has been implicated to be driven through clathrin-mediated endocytosis (97, 98). However, the underlying mechanisms of how MIF passes endosomal or other vesicular membranes have yet to be known. Release of MIF can be triggered by several stimuli, including LPS, corticosteroids, and adrenocorticotrophic hormone (ACTH). A recent study suggested that the release of MIF is regulated by necroptosis and pyroptosis (99).

MIF exerts biological actions through extracellular and intracellular pathways, while by far most of the evidence is available for MIF's extracellular cytokine/chemokine activity (**Figure 4**). The ultimate effects are determined by which receptor or intracellular protein MIF interacts with. MIF acts at sites in a paracrine or autocrine manner and binds to intracellular proteins or surface receptors to initiate signal transductions. The intracellular actions of MIF encompass its binding to a couple of different intracellular effectors to alter their signaling pathways. Subunit 5 of COP9 signalosome (CSN5) is one of the best understood proteins. MIF is expected to be an anti-inflammatory mediator concerning its intracellular interaction with CSN5/c-Jun signaling (100, 101). The extracellular chemokine-like functions of MIF are regulated through the interaction with classical chemokine receptors CXCR2 and CXCR4 as a non-canonical ligand. It is an atypical chemokine. In 2007, Bernhagen et al established its

pro-inflammatory effect by facilitating leukocyte influx, particularly in the pathogenesis of atherosclerosis (102).

### **1.2.2 CD74**

The first identified cognate receptor for MIF is cluster of differentiation 74 (CD74). CD74 is a type II transmembrane glycoprotein containing an N-terminal cytosolic tail and an extended C-terminal luminal/extracellular region. CD74 is widely expressed in classical antigen-presenting cells (APCs) as a cofactor for MHCII (103, 104). A small portion of CD74 is expressed on the cell surface and binds to MIF (105).

MIF interacts with CD74 with high affinity ( $K_d=1.4$  nM) and triggers the protein kinase A-dependent phosphorylation of the intracellular portion of CD74, which subsequently leads to kinase-1/2 MAP kinase cascade activation (105, 106). This effect relies on the coordination of CD74 and CD44 (107). One of the major biological functions of MIF regulated through the MIF/CD74 signaling is to sustain monocyte and macrophage activation (108). On the other hand, CD74 participates in the mediation of cell proliferation (105, 109, 110). The interaction between MIF and CD74 triggers the Syk tyrosine kinase and the PI3K/Akt pathway (111, 112). A novel form of CD74 termed soluble CD74 (sCD74) was found in liver cells that is produced from proteolytic shedding of the ectodomain area (113). One study suggested the release of sCD74 is driven by either a disintegrin and metalloproteinase-mediated cell-surface cleavage or cysteine-protease-mediated lysosomal cleavage (114). However, more data are needed to deeply understand the molecular mechanism of sCD74.

In cardiac ischemia-reperfusion injury (IRI), MIF/CD74 signaling exhibits beneficial effects. During IRI, MIF is released from the cardiomyocytes under hypoxia and oxidative stress. This locally secreted MIF triggers the AMP-activated protein kinase (AMPK) pathway via the interaction with the CD74/CD44 complex, boosting glucose metabolism to provide a protective

influence for injured tissue (115, 116). As a result, the ischemic heart tissue undergoes metabolic adaption to recover. Moreover, MIF appeared defensive of ischemic damages, given its capacity of inhibiting stress kinase JNK during the reperfusion phase, which reduced cardiomyocyte apoptosis (117). Those findings emphasize the protective impacts of MIF/CD74 signaling in ischemia.

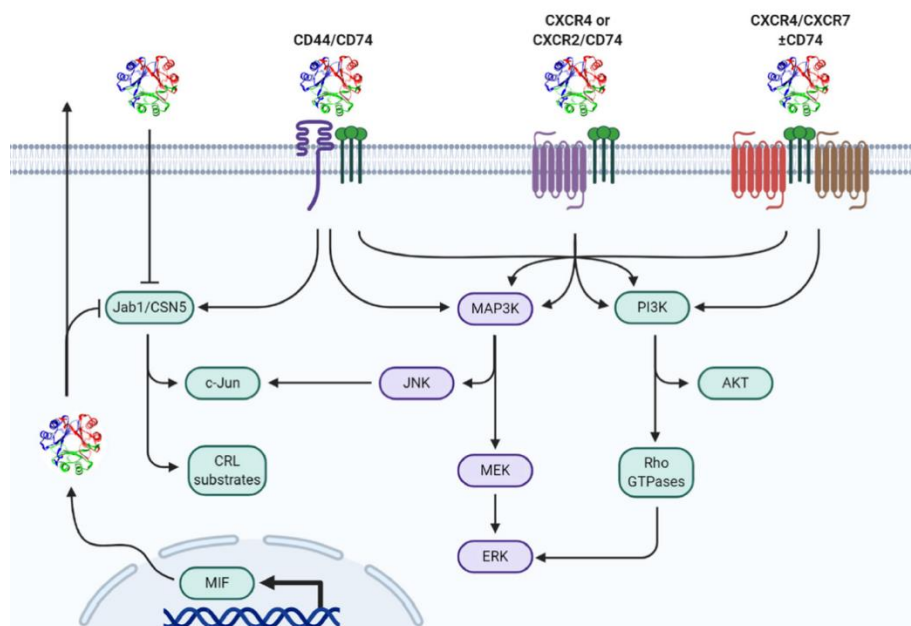


**Figure 4: MIF signaling pathways.** Secreted extracellular MIF or endogenously generated MIF interaction with Jab1/CSN5 mediates cullin-ring ligase (CRL) substrate proteasomal degradation and c-Jun phosphorylation/AP-1 activity. Moreover, MIF binds to CD74 in cooperation with CD44 or CXCR2 and CXCR4 to trigger MAPK and/or PI3K/Akt signaling. Taken from Noet al, *Front Immunol* 2020 (118).

### 1.2.3 CXCR2 and CXCR4

CXCR2 was cloned in 1991 (119). It is expressed in several immune cell types. CXCR2 is a crucial chemokine receptor on neutrophils with the highest binding affinity to CXCL8 (120). Other ligands include CXCL1, 2, 3, 5, 6, and 7 and the atypical chemokine MIF (102, 121). MIF possesses an indispensable motif for receptor interaction, named “pseudo-(E)LR”, mimicking the N-terminal ELR motif in the CXC- chemokines (90). The MIF motif consists of Asp45-X-Arg12 with the substitution of glutamate (Glu/E) with an aspartic acid (Asp/D) (90, 122). Mutagenesis studies in MIF showed a partial or complete loss of CXCR2 binding and



leukocyte arrest activity. Later, the N-like loop in MIF, particularly the region 50-65, was uncovered to be involved in the binding to CXCR2 (123-126). Site-specific mutations within the fragment caused MIF activity disruption. On the CXCR2 side, the extracellular loops, ECL2 and ECL3, are the interaction regions for MIF (123). The binding model of MIF/CXCR2 follows a similar pattern to that of between CXCL8 and CXCR2.

Leukocyte recruitment process consists of three steps: rolling, adhesion, and transmigration. Chemokines trigger leukocyte integrin activation to facilitate leukocyte arrest on the endothelium through their corresponding GPCRs, inducing inside-out signaling activating integrins. MIF was confirmed to induce monocyte/neutrophil adhesion through CXCR2 (102). Like other chemokines, this process is mediated by the activation of leukocyte integrins, lymphocyte function-associated antigen 1 (LFA1), and very late antigen 4 (VLA4, integrin  $\alpha 4\beta 1$ ) (102). Gai proteins and PI3K cascade is suggested to be the downstream mediators for CXCR2 to regulate leukocyte adhesion. Also, MIF could trigger CXCR2-dependent calcium influx. Nonetheless, little is known about the precise molecular mechanism of MIF-triggered integrin activation.

CXCR4 is also named cluster of differentiation 184 (CD184). The CXCR4 gene maps to chromosome 2, encoding two alternative isoforms: isoform 1 and isoform 2. Both isoforms are functionally active. Isoform 1 is predominant in all tissue tested (127). The protein is comprised of 352 amino acids, featuring an extracellular N-terminal domain, seven transmembrane helices, three extracellular loops (ECLs), three intracellular loops (ICLs), and an intracellular C-terminal end (128). There are multiple multimerization states of CXCR4 on the membrane, including monomer, dimer, oligomer, or nanoclusters (129). CXCR4 could also form heterodimers with ACKR3 (another receptor bound to MIF, known as CXCR7) and CD74, exerting distinctive signaling functions (130).

CXCR4 was initially recognized as a co-receptor on CD4<sup>+</sup> T cells in human immunodeficiency virus (HIV) cell entry. After that, CXCL12 was discovered to be its cognate ligand (131). From the structural perspective, CXCR4 has two unique, longer helical turns than other receptors at the end of helix VII, which enables a disulfide bond formation between Cys274 and Cys2, contributing to the interaction with CXCL12 (132, 133). Many tissues and cells express CXCR4 in physiological and pathological conditions, not only in myeloid-derived cells and lymphocytes but also in lung, spleen, small intestine, and non-hematopoietic cells (127). The intracellular signaling of CXCR4 is mediated by heterotrimeric G proteins, among which G $\alpha_{i1}$ , G $\alpha_{i2}$ , G $\alpha_{i3}$ , G $\alpha_q$ , and G $\alpha_o$  are reported to be responsible for CXCR4 activation (134). Activated downstream pathways include MEK/ERK pathway, phospholipase C (PLC) beta and gamma 2, PI3K/Akt/mTOR pathway, and nuclear factor  $\kappa$ B (NF- $\kappa$ B) pathway (135, 136), which are involved in regulating vasculopathy, inflammation, and proliferation (132, 137).

The vast majority of classical chemokines bind to their receptors following the two-site binding pattern (42, 138). Site one refers to the interaction between the chemokine N-loop and the receptor N-terminal area. Site two involves the N-terminal residues of the chemokine and the extracellular loops of the receptor. Previous studies have addressed the structure elements critically required for the interaction of MIF with CXCR4 (139). The N-like loop of MIF required for CXCR4 interaction encompasses the residues 43-98, which have an extended length than what is observed in CXCL12. There is an overlap between the CXCL12/CXCR4 and MIF/CXCR4 interaction regarding the interaction region on the CXCR4 side. The N-terminus of CXCR4 for CXCL12 and MIF are located in close proximity. ECL1 and ECL2 of CXCR4 take part in the second binding site of MIF/CXCR4. But no evidence showed the interaction of MIF with the transmembrane cavity. Moreover, using a MIF catalytic inhibitor and mutation of the catalytic site suppressed CXCR4 signaling induced by MIF stimulation, indicating the catalytic site Pro-2 contributes to the MIF/CXCR4 binding. MIF acts as a partial allosteric agonist, distinguishing its interaction with CXCR4 from that of the cognate CXCL12 (**Figure 5**). Another

study came out identifying the Arg-Leu-Arg (RLR) sequence at the C-terminal end of MIF participates in the site one interaction between MIF and CXCR4 (140). Those findings provide valuable insights into understanding the structural basis for MIF/CXCR4 interaction. It also helps to illuminate the path for designing structure-based MIF inhibitors.

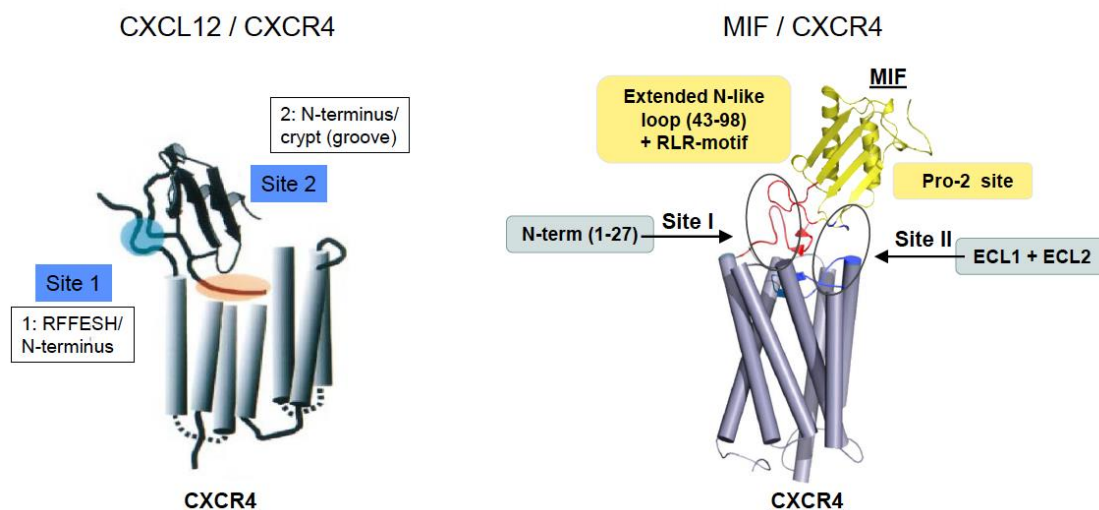


**Figure 5: Structural comparison between CXCL12/CXCR4 and MIF/CXCR4 binding models.** Two-site binding models are established for CXCL12/CXCR4 and MIF/CXCR4 axes. They partially overlap in the N-terminal end of CXCR4 bound to CXCL12 and MIF. The CXCR4 transmembrane cavity attached to CXCL12 does not interact with MIF. A higher concentration of CXCR4 antagonist AMD3100 could inhibit MIF-initiated signaling. MIF is considered an allosteric agonist in contrast to CXCL12. Kindly provided by J. Bernhagen.

#### 1.2.4 ACKR3/CXCR7

As another important category in the chemokine receptor family, atypical chemokine receptors (ACKRs) share structural similarities with classical chemokine GPCRs. But given the lack of a specific amino acid motif, they fail to couple with G-proteins. Thus, ACKRs do not play a role in leukocyte recruitment that relies on the GPCR-dependent intracellular pathways. Nevertheless, ACKRs are confirmed to regulate receptor internalization and scavenging (141, 142). Among them, ACKR3 can interact with CXCL12 and MIF. ACKR3 is primarily documented to negatively regulate CXCL12 actions by internalizing it for lysosomal degradation (143). The activation of ACKR3 occurs through  $\beta$ -arrestin binding (144, 145).

MIF/ACKR3 binding triggers multiple pathways, including phosphoinositide-3-kinase-Akt signaling, JAK2/STAT3 pathway, and ERK1/2 pathway (146, 147). *In vivo* study also showed that *Ackr3*-knockout mice would die in utero because of defective cardiovascular system development (148). In atherosclerosis, the functions of ACKR3 remain debated (147, 149-151). Due to its emerging role as an alternative receptor for CXCL12 and MIF in cardiovascular disease, ACKR3 further complicates the CXCL12/MIF/CXCR4 signaling.

### **1.2.5 MIF in atherosclerosis**

In hyperlipidemia, MIF expression was shown to be higher in cells, like ECs, VSMCs, monocytes, and T cells (152, 153). As hyperlipidemia is proven to be a high-risk factor for atherogenesis, enhanced MIF levels could imply detrimental function of MIF in lesion growth. In 2007, Bernhagen et al. discovered a chemokine-like activity of MIF and identified CXCR2 and CXCR4 as non-cognate MIF receptors (102). Furthermore, MIF was implicated in promoting atherogenic leukocyte arrest, inflammation, and epithelial-mesenchymal interaction in tumors through its engagement of these two chemokine receptors (102, 154). MIF triggers T cell, neutrophil, and monocyte chemotaxis in an integrin-dependent way. *In vitro* flow assay indicated that aortic endothelium stimulated with MIF induced increased leukocyte arrest, implying a significant role of MIF in driving immune cell recruitment. High plasma MIF levels correlate with coronary events in patients with CVD and type 2 diabetes mellitus (155). MIF markedly contributes to atherosclerosis exacerbation through the regulation of leukocyte recruitment. MIF was found to be up-regulated in human atherosclerotic plaques, particularly in unstable plaques (156), but a recent study found no difference in MIF mRNA expression levels between stable and unstable atherosclerotic plaques obtained from carotid endarterectomy. Animal studies showed that MIF depletion in *Ldlr*<sup>-/-</sup> caused a marked reduction in lesion sizes in the abdominal aorta and decreased intimal thickening in the arch (157). When treated with monoclonal MIF antibody, *ApoE*<sup>-/-</sup> mice developed decreased macrophage content together with lower expression of inflammatory molecules, but no

prominent change in plaque size was shown (158). In addition, the blockade of MIF reduced foam cell content and increased VSMCs and collagen in mice, meaning MIF positively impacts advanced plaque stability (159). In *ApoE*<sup>-/-</sup> mice, lack of MIF reduced lesions in brachiocephalic artery (BC) and abdominal aorta, and correlated with enhanced B cell hypersensitivity (160). MIF can also induce B cell migration by coordinating CXCR4 and CD74 (161). The effect was linked to a rapid calcium flux and F-actin polymerization. Recent study implied a complex function of MIF in aged mice with atherosclerosis (162). Transcriptomic analysis indicated MIF- and aging-dependent pathways enriched in lipid synthesis, metabolism and storage. The observed MIF atheroprotection is lost upon aging. All those data highlight the profound role of MIF in atherosclerosis. Targeting MIF represents a promising novel therapeutic approach for atherosclerosis.

### 1.3 Anti-MIF therapeutic strategies

Leukocyte recruitment is a hallmark of inflammation. Based on the essential role of MIF in the leukocyte recruiting process, MIF inhibition could be effective for patients with pronounced inflammatory responses, for example atherogenic inflammation. Accordingly, MIF-directed therapeutics could potentially benefit atherosclerotic patients with high background MIF levels. The established anti-MIF approaches can be divided into three categories, small molecule drugs (SMDs), antibodies, and peptides. **Figure 6** gives a detailed overview of three MIF-targeted inhibition approaches with a focus on atherosclerosis (163).

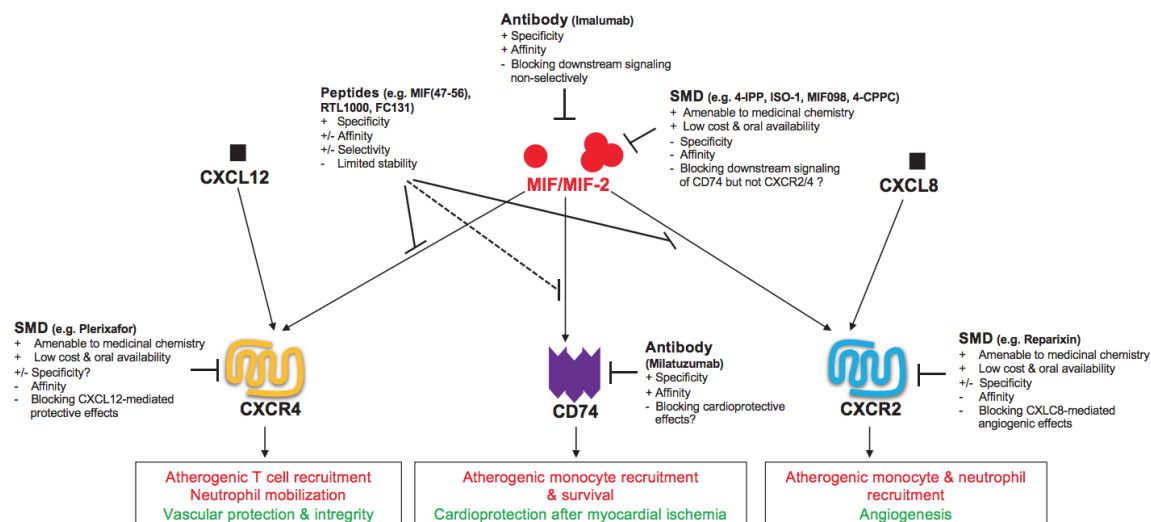


**Figure 6: Summary of inhibition strategies to target MIF-receptor axes in atherosclerosis.** The current availability of three categories of MIF inhibitory agents that mitigate atherosclerosis evolution include small molecule drugs (SMDs), antibodies, and peptides. Inhibitors targeting MIF or one of the receptors are depicted by scoring their features with +, +/-, or -. The text boxes are color-coded (red, pro-atherogenic; green, athero-/cardioprotective). Taken from Sinitski et al, *Thromb Haemost* 2019 (163).

### 1.3.1 Small molecule inhibitors

SMDs are the most common type of drugs in conventional drug development. MIF inhibitors have been identified through either virtual or high-throughput screening with a particular interest in the tautomerase activity site. Even though physiological substrates have not been documented yet, the MIF inhibitors targeting the tautomerase could possibly alter MIF activities by inducing structural changes, in particular to block MIF/CD74-mediated pathological pathways such as in cancer (139, 164-166).

The commonly used inhibitors, iso-oxazoline compound ISO-1 (167), 4-iodo-6-phenylpyrimidine (4-IPP) (168), and SCD-19 (169), act at the MIF tautomerase site. In autoimmune encephalomyelitis and multiple sclerosis, mice receiving ISO-1 revealed less severe phenotype (170). 4-IPP suppresses tumor growth and angiogenesis in experimental melanoma (171). Ebselen induces MIF trimer dissociation to disrupt MIF/CD74 signaling (172).

p425 interferes with CD74 binding by binding to the MIF trimer surface (173). In the clinic application, it is worth noting that ibudilast is a non-competitive inhibitor, harnessing the MIF enzymatic activity. It can decrease mononuclear cell migration and synthesis of MIF-stimulated cytokines (174). Unfortunately, none of those compounds have been studied in atherosclerosis or CVD models. Future research needs to be done in the field of CVD.

### **1.3.2 Antibody-based inhibitors**

Monoclonal antibody therapy is viewed as being specific and efficacious. As mentioned in the prior chapter, neutralization of MIF with antibody, NIH/IIID.9, has been examined in atherosclerotic models. It is generated against the full-length mouse MIF, although the epitope has not been recognized. IIID.9 has been shown to slow down disease progression in various inflammatory, autoimmune and cardiovascular conditions (158, 175, 176). The MIF antibody imalumab has undertaken clinical trials against colorectal cancer and lupus nephritis (177). It demonstrates potent anti-inflammation capacity, reducing circulating TNF- $\alpha$ , IL-6, and CCL2 and alleviating disease severity in glomerulonephritis and cancer.

Antibodies against CD74 harness many signaling pathways that can be blocked by MIF antibodies. However, it should be pointed out that the utility of CD74-directed strategies might be confined in CVD due to the protective effect of the CD74/AMPK metabolic pathway. In addition, CXCL12/CXCR4 axis has homeostatic functions and presumable cardio-protective actions. Thus, caution should be taken while developing CXCR4 antibody without sparing CXCL12. The first GPCR-directed antibody, erenumab, was approved in 2018 (178). As an emerging class of drugs, discovering and developing other GPCR antibodies have a long way to go. In MIF/CXCR2/CXCR4 axes, both receptors could be promising targets in vascular inflammation.

### 1.3.3 Peptide-based inhibitors

Peptides represent a unique form of pharmaceutical agent. They are well-ordered natural amino acids with molecular weights ranging from 500-5000 Da (179). The first peptide drug was insulin, which came out in 1921. More peptide hormones and their receptors with therapeutic capacity were discovered and characterized in the late 20<sup>th</sup> century (180). With the advancement of technologies required for protein purification, sequencing, and structure elucidation, 40 therapeutic peptides so far have been approved globally, and more than 170 peptides are actively undergoing clinical development with more of them in pre-clinical studies (179, 180).

Peptide drugs usually take effect in the outer space of cells. They bind to cell surface receptors or to receptor ligands, and may exhibit relatively high binding affinities. The physiochemical natures of peptides allow them to block proteins over a larger surface than small molecules. They can bind to the grooves or clefts on an interacting face (181). Besides, amino acids can interact with other residues at protein-protein interfaces (182). Of note, peptides show less immunogenicity and can be manufactured at lower production costs than antibodies (183, 184). SMDs have a long therapeutic history and have a good reputation for low production costs, oral administration, and intrinsically good membrane penetration rate (185). On the flip side, the therapeutic effects of SMDs often come with various side effects, given their low specificity and selectivity. More importantly, their small size makes it difficult to interfere with large surface interactions, such as protein-protein interactions (PPIs) (186). On the contrary, the biophysical characteristics of peptides allow them to become a better candidate for PPI suppression (187). Regardless of all the advantages, peptide drugs have some drawbacks, like poor stability, rapid renal clearance, and membrane impermeability. The weak membrane permeability of peptide drugs limits their use against intracellular targets (180). Due to small sizes and lack of (secondary or) tertiary structure, peptides could be easily digested by abundant enzymes and eliminated through the urinary tract in a living organism (188).



PPIs exist in most cellular pathways and biological functions in human diseases, presumably making them excellent therapeutic targets. Investigation of the structure-activity relationships (SARs) enables identifying the crucial amino acids or fragments for PPIs. Chemokine-chemokine or chemokine-receptor interactions account for a large group of intrinsic PPIs. Selective inhibition of their interactions could favor disease resolution without compromising defensive host immunity. For example, designed peptide inhibitors that specifically interrupt CCL5-CXCL4 pro-inflammatory effects avoid the side effects of simply targeting CCL5 (189, 190). Because of the extraordinary complexity of the chemokine-receptor network and their cell- or tissue-specific effects, rational peptide drug design should take into account the specificity and selectivity of signaling pathways to reduce the off-target effects.

Peptide drugs have been explored in atherosclerosis, including targeting lipid metabolism and inflammatory regulators (189, 191). Apolipoprotein A-I (apoA-I) serves as the major component of high-density lipoprotein (HDL), facilitating off-loading and elimination of cholesterol through the liver. Peptides mimicking the structure of apoA-I revealed protective functions against CVD (191). CCL5-derived peptides MKEY and CKEY interfere with pro-inflammatory CCL5-CXCL4 interaction, subsequently slow down plaque progression (189). Also, some peptides have been designed and synthesized to block MIF pathways. For example, C36L1, a 17-mer peptide bound to CD74, inhibits immunosuppressive activities in melanoma models (192, 193). Other peptides disrupting MIF/CD74 axis have been developed and tested in experimental autoimmune encephalomyelitis and multiple sclerosis (194, 195). However, the utility of CD74 inhibitors in cardiovascular conditions should be well considered because of the protective function of the MIF/CD74 axis in ischemic heart disease.

Some CXCR2 and CXCR4 peptide inhibitors have been synthesized through different development approach and assessed in disease models. A cyclic peptide CVX15, developed

by co-crystallization, was proven to interfere with HIV entry and inhibit tumor metastasis (128, 196, 197). By mimicking part of the chemokine-receptor interface, CXCL12 N-terminus-originated peptide inhibitors were generated with characteristic CXCL12/CXCR4 inhibition and tumor-resistant activity (198, 199). These examples highlight the new way of peptide drug discovery through the deep understanding of SARs.

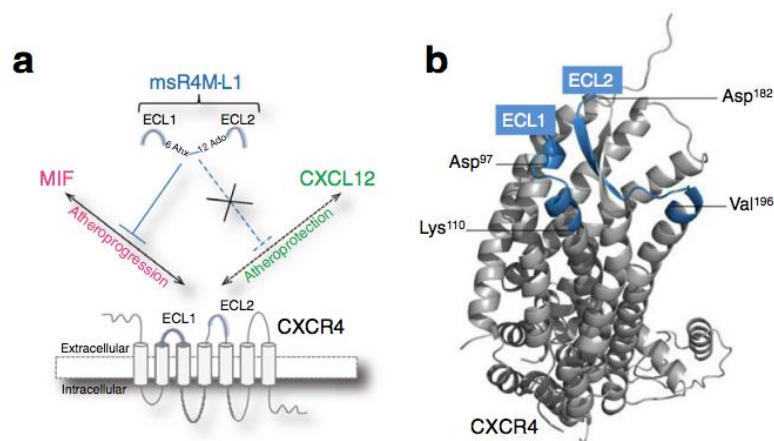


**Figure 7: The design scheme for the generation of CXCR4 peptide inhibitor msR4M-L1.** Figure taken from Kontos et al, *Nat Commun* 2020 (200).

Former studies have identified the distinct binding interfaces for MIF/CXCR2 in relation to CXCL8/CXCR2 (201). Thus, peptide MIF (47-56), derived from the N-like loop sequence of MIF, was synthesized to competitively block MIF interaction with CXCR2, reducing leukocyte recruitment (201, 202). Similar principle applies to the MIF/CXCR4 interaction surface that is distinct from CXCL12/CXCR4 binding. Based on this theory, my host laboratory, in collaboration with Prof. Kapurniotu's laboratory at Technical University of Munich (TUM), designed peptide drugs mimicking the extracellular domains of CXCR4 (**Figure 7**) in an attempt to inhibit detrimental MIF activities in disease models. The study about the proof of concept prototype, msR4M-L1, was published in 2020 in the field of atherosclerosis (200). I was involved in the study and took part in some of the cellular assays to assess the inhibitory capacity of the peptide. msR4M-L1 showed inhibitory effects on MIF/CXCR4 axis *in vitro*, and injection of msR4M-L1 mitigated early plaque formation in *ApoE*<sup>-/-</sup> mice. There are a few

limitations of msR4M-L1, such as relatively low solubility, length of still 31 residues, and the incorporation of two non-natural -chemical- moieties. To improve of some of these properties, next generation mimics (NGMs) were designed and synthesized by the collaborative laboratory for the optimization of CXCR4 ectodomain inhibitors. In my thesis, in addition to studying the *in vitro* inhibitory capacity of msR4M-L1, I focused on the characterization of the pharmacological features of NGMs and examined lead peptide called NGM-D3 in an atherosclerotic mouse model *in vivo*.

## Aims

Atherosclerosis is a lipid-driven disease, involves inflammation from the inception to the emergence of complications. Atypical chemokine MIF is known to induce leukocyte recruitment through CXCR4 to further worsen the disease. Prior knowledge on MIF-CXCR4 binding model allows to identify their binding interface. Based on that, we developed novel CXCR4 ectodomain mimics to block MIF pathways, including msR4M-L1 and NGMs. Therefore, the first aim of my thesis was to study the effect of msR4M-L1 on macrophage foam cell formation and MIF/CD74 cardio-protective signaling. My work was dedicated to characterize the functional roles of msR4M-L1 against MIF/CXCR4 signaling using LDL and oxLDL uptake in primary human macrophages and DMR, and determine impacts of msR4M-L1 on MIF/CD74 surface interaction using competitive receptor binding assay.

Secondary generation CXCR4 ectodomain mimics-NGMs consisting of minimal active binding sites were generated by our collaborator with improved conformational flexibility and solubility. Using primary human monocytes and murine splenic B cells to set up *in vitro* models including 3D chemotaxis live imaging, foam cell formation, and Transwell chemotaxis, I aimed to determine the inhibitory potency and efficacy of NGMs against MIF *in vitro* by constructing IC<sub>50</sub> curves, and assess the potential inhibitory capacity of NGMs to CXCL12. Based on the *in vitro* data, the lead peptide NGM-D3 was evaluated for the enzymatic stability and *in vivo*

pharmacological study of early atherosclerosis. The impacts of NGM-D3 on plaques and macrophage content were set to be assessed. To delineate the therapeutic effects of NGM-D3 at transcriptional levels, RNA was extracted from plaques and bulk RNA sequencing was performed.

## 2. Materials and Methods

### 2.1 Materials

#### 2.1.1 Reagents and chemicals

<b>Substances and catalog number</b>	<b>Manufacturer</b>	<b>City, Country</b>
Albumin fraction V, NZ-origin, 8076.4	Carl Roth	Karlsruhe, Germany
CountBright™ absolute counting beads, C36950	ThermoFisher Scientific	Karlsruhe, Germany
Rat tail collagen type I, 50201	Ibidi GmbH	Munich, Germany
Rat tail collagen type I, 08115	Merck Millipore	Darmstadt, Germany
Dulbecco's phosphate buffered saline (DPBS), D8537	Sigma-Aldrich	Deisenhofen, Germany
Dimethylsulfoxid (DMSO), D2650	Sigma-Aldrich	Darmstadt, Germany
Low density lipoprotein from human plasma, Dil complex (Dil LDL), L3482	ThermoFisher Scientific	Karlsruhe, Germany
Low density lipoprotein from human plasma, oxidized, Dil conjugate (Dil-oxLDL), L34358	ThermoFisher Scientific	Karlsruhe, Germany
CozyHi prestained protein ladder, PRL0202	highQu GmbH	Kraichtal, Germany
Tetramethylethylenediamine (TEMED), 1610801	Bio-Rad	Feldkirchen, Germany

---

Eosin Y solution, HT110232	Sigma-Aldrich	Darmstadt, Germany
Ethanol, 20821.310	VWR	Darmstadt, Germany
Ethylenediaminetetraacetic acid (EDTA), A3234	AppliChem	Darmstadt, Germany
Epic 96 well cell assay microplate, fibronectin coated, 5082	Corning	New York, USA
Ficoll-Paque™ PLUS, 17144002	GE Healthcare	Freiburg, Germany
Fluorescent mounting medium, F4680	Sigma-Aldrich	Darmstadt, Germany
Kaisers Glycerin-Gelatine Phenol-free, 6474.1	Carl Roth	Karlsruhe, Germany
Mayer's hematoxylin solution, MHS80	Sigma-Aldrich	Darmstadt, Germany
RBC lysis buffer (10x), 420301	BioLegend	California, United States
Oil Red O solution, O1516	Sigma-Aldrich	Darmstadt, Germany
Hanks' balanced salt solution (HBSS), 14025-050	ThermoFisher Scientific	Karlsruhe, Germany
HEPES, 7365-45-9	Carl Roth	Karlsruhe, Germany
Methanol, 0798.3	Carl Roth	Karlsruhe, Germany
Mounting medium with DAPI, H1200	Vector Laboratories	California, United States

Tricine 10 to 20% gels, EC6625BOX	ThermoFisher Scientific	Karlsruhe, Germany
Tricine SDS running buffer (10x), LC1675	ThermoFisher Scientific	Karlsruhe, Germany
Tricine SDS sample buffer (2x), LC1676	ThermoFisher Scientific	Karlsruhe, Germany
Tris-Glycine 10-20% gel, XP10200BOX	ThermoFisher Scientific	Karlsruhe, Germany
Tris-Glycine native sample buffer (2x), LC2673	ThermoFisher Scientific	Karlsruhe, Germany
Tris-Glycine native running buffer (10x), LC2672	ThermoFisher Scientific	Karlsruhe, Germany
Tween 20, P2287	Sigma-Aldrich	Darmstadt, Germany
DL-Dithiothreitol (DTT), D0632	Sigma-Aldrich	Darmstadt, Germany
Fluorescein (FITC) chrompure human albumin, 009-090-051	Jackson ImmunoResearch	Cambridgeshire, United Kingdom
FACSFlow™ sheath fluid, 342003	BD Biosciences	Heidelberg, Germany
FACSClean, 340345	BD Biosciences	Heidelberg, Germany
Recombinant Human M-CSF, 300-25	PeptoTech	Hamburg, Germany
Paraformaldehyde (PFA) 4% in PBS, 11762	Morphisto	Offenbach am Main, Germany
Tris-(hydroxymethyl)-aminomethan (Tris), 4855.2	Sigma-Aldrich	Darmstadt, Germany

Sodium dodecyl sulfate (SDS), 201139	SERVA Electrophoresis	Heidelberg, Germany
Xylene, 28973.294	VWR	Darmstadt, Germany
Trisodium citrate (3.2%)	Sigma-Aldrich	Darmstadt, Germany
Qiagen Plasmid mini kit	Qiagen	Hilden, Germany
Polyfect Transfection Reagent, 301105	Qiagen	Hilden, Germany
Mouse Pan B cell isolation kit II, 130104443	Miltenyi Biotec	Bergisch Gladbach, Germany
Human Pan monocyte isolation kit, 130096537	Miltenyi Biotec	Bergisch Gladbach, Germany

### 2.1.2 Cell culture reagents and media

Substances and catalog number	Manufacturer	City, Country
Dulbecco's modified eagle medium (DMEM), A1443001	ThermoFisher Scientific	Karlsruhe, Germany
Fetal bovine serum (FBS), 10270106	ThermoFisher Scientific	Karlsruhe, Germany
RPMI 1640 medium, GlutaMAX™ supplement, 61870036	ThermoFisher Scientific	Karlsruhe, Germany
Dulbecco's phosphate buffered saline (DPBS), D8537	Sigma-Aldrich	Deisenhofen, Germany
Penicillin/streptomycin, 15070063	ThermoFisher Scientific	Karlsruhe, Germany
Trypsin-EDTA (0.05%), 25300054	ThermoFisher Scientific	Karlsruhe, Germany



### 2.1.3 Primary and secondary antibodies

Antibodies and catalog numbers	Manufacturer	City, Country
V450 rat anti-mouse CD45 (1:100), 560501	BD Biosciences	Heidelberg, Germany
CD3-FITC, anti-mouse (1:100), 130119758	Miltenyi Biotec	Bergisch Gladbach, Germany
APC/Cyanine7 anti-mouse CD19 (1:100), 115530	Biolegend	Munich, Germany
PE anti-mouse CD11c (1:100), 117308	BioLegend	Munich, Germany
PE/Cyanine7 anti-mouse/human CD11b (1:100), 101216	BioLegend	Munich, Germany
PerCP anti-mouse Ly-6G (1:100), 127654	BioLegend	Munich, Germany
APC anti-mouse Ly-6C (1:100), 128016	BioLegend	Munich, Germany
Rat anti-mouse CD68 (1:100), MCA1957	Bio-Rad	Feldkirchen, Germany
Cy3 donkey anti-rat IgG (1:300), 712166153	Jackson ImmunoResearch	Cambridgeshire, United Kingdom

### 2.1.3 Solutions and buffers

1x Phosphate buffered saline (PBS)	137 mM NaCl
	2.7 mM KCl
	1.5 mM KH <sub>2</sub> PO <sub>4</sub>
	8.1 mM Na <sub>2</sub> HPO <sub>4</sub> x 2 H <sub>2</sub> O
DMR assay buffer	1x HBSS, pH 7.4

---

	20 mM HEPES
	1% DMSO
FACS buffer	1% BSA
	1x PBS, pH 7.4
MACS buffer	2 mM EDTA
	0.5% BSA
	1x PBS, pH 7.4

#### 2.1.4 Laboratory equipment and software

BD FACSVerser<sup>TM</sup> Cell Analyzer, BD Biosciences, Heidelberg, Germany

DMI8-Life Cell Imaging System with a DMC2900 Digital Microscope, Leica Microsystems, Wetzlar, Germany

Odyssey<sup>®</sup> Fc imager, LI-COR Biosciences, Bad Homburg, Germany

EnSpire<sup>®</sup> Multimode Plate Reader, PerkinElmer, Hamburg, Germany

BioWizard Silver Line Biosafety cabinet, Kojair Tech Oy, Ulm, Germany

TC20 automated cell counter, Bio-Rad Laboratories GmbH, Feldkirchen, Germany

ImageJ-Fiji

FlowJo\_V10 software, BD Biosciences

Manual Tracking tool (ibidi), Munich, Germany

Graphpad Prism 8.4.3, San Diego, CA, USA

R 4.2.2, RStudio

## 2.2 Methods

### 2.2.1 *In vitro* drug testing and screening methods

#### ***Cell culture***

Human embryonic kidney 293 (HEK293) cells were cultured in DMEM complete media in T75 flasks in a 37°C incubator with 5% CO<sub>2</sub> in the air. Cells were detached and passaged when they reached 80% confluency.

Primary human monocytes and murine B cells were cultured in RPMI1640 complete media in T25 or T75 flasks in a 37°C incubator with 5% CO<sub>2</sub>.

All procedures were performed in a sterile environment where cells were handled with sterile reagents under a biosafety cabinet (Kojair Tech Oy, Finland). Cell counts and viability were determined by trypan blue staining. Cell suspension was mixed with trypan blue at a ratio of 1:1 and counted by TC20 automated cell counter (Bio-Rad, Germany).

#### ***CD74 plasmid transformation and purification***

Transformation of pcDNA3.1-CD74minRTS-FLAG plasmid was performed using pET11b/*E.coli* BL21 Rosetta strain. 5 µl of DNA was added to 50 µl of bacteria in a microcentrifuge and gently mixed by flicking the bottom of the tube. The bacteria/DNA mixture was placed on the ice for 30 min and then heated by placing the tube into 42°C water for 45 s. The mixture was added to 250 µl LB media without antibiotics to enable it to grow in a 37°C shaking incubator for 45 min after it was put back on ice for 2 min. Transformed bacteria were allowed to grow on an LB agar plate containing Ampl at 37°C overnight. Purifying pcDNA3.1-CD74minRTS-FLAG plasmid was performed using Qiagen Plasmid Mini kit following the manufacturer's instruction (Qiagen, Germany). Obtained DNA was dissolved in a suitable volume of ionized water.

#### ***Transfection of CD74 into HEK293 cells***

The day before transfection,  $2 \times 10^6$  HEK293 cells were seeded in a 100 mm peri dish. Cell density should be 70-80% confluent on the day of transfection. 8 µg of pcDNA3.1-CD74minRTS-FLAG were diluted in 300 µl of growth media containing no serum or antibiotics.

Next, 80 µl of Polyfect Transfection Reagent (Qiagen, Germany) was added into the diluted DNA solution and mixed well. The mixture was incubated for 10 min at room temperature to allow DNA-Transfection reagent complex formation. While complexes took place, media were removed from the dish, and 7 ml of fresh media were added. On the other hand, 1 ml growth media was mixed well with the transfection complexes and immediately transferred into the dish. The dish was swirling gently to ensure uniform distribution of the complexes. The cells were incubated with the complexes in the incubator for 48 h and harvested for receptor binding assay. Additionally, the expression level of CD74 was validated by FACSVerse™ cell analyzer (BD biosciences, Germany).

### ***Receptor binding assay***

CD74 transfected HEK293 cells grew in a peri dish until they reached 70-80% confluency. Alexa-MIF was pre-incubated with inhibitors for 30 min. The cells were washed with PBS once, detached, and divided into 3 tubes,  $3 \times 10^5$  cells for each tube. Cells were stimulated with treatments at 4°C for 2 h. Then they were washed with 500 µl PBS, pH 7.4, containing 0.1% BSA and resuspended in 500 µl FACS buffer. Data was measured by FACSVerse™ cell analyzer (BD biosciences) and analyzed by FlowJo software.

### ***MIF protein purification***

Recombinant human and mouse MIF proteins were expressed in the pET11b/*E.coli* BL21 Rosetta system as previously described (203). Bacteria were cultured at 37 °C until an absorbance at 600 nm of 0.6 was reached. MIF expression was then induced by adding solid IPTG to a concentration of 1 mM and the bacteria were incubated for 4 h until harvested by centrifugation. Bacteria were subjected to French Press (EmulsiFlex-C5, AVESTIN) to release the protein. Protein was purified on a Mono Q column (Cytiva Europe GmbH, USA) and a C8 reverse-phase chromatography column (MZ-Analysentechnik GmbH, Germany), followed by lyophilization as well as dialysis-based renaturation. Protein with greater than 98% purity was

then utilized in all bio-assays. Protein concentration was re-measured regularly using standard Bradford assay.

### ***PBMC separation***

Human peripheral blood mononuclear cells (PBMCs) were separated using Ficoll-Paque density gradient centrifugation as previously described (200). Fresh buffy coats containing abundant white blood cells were obtained from the blood bank of Klinikum Großhadern (LMU, approval). The buffy coat was diluted with PBS without calcium and magnesium to a volume of 40 ml, followed by gently inverting the tube several times to mix it well. Next, 3 ml Ficoll-Paque media was added to the 15 ml centrifuge tube. 10 ml diluted blood sample was carefully layered onto each Ficoll-Paque media solution without mixing the Ficoll-Paque media solution and the sample, and then centrifuged at 2000 rpm for 30 min at room temperature with the brake turned off. The upper layer containing plasma and platelets was discarded using a sterile plastic pipette, and the mononuclear cell layer was left undisturbed at the interface. The mononuclear cell layers were collected in a sterile 50 ml tube, and cells were centrifuged at 300 x g for 5 min at room temperature. After centrifugation, the supernatant was removed, and 1x RBC lysis buffer lysed red blood cells for 3 min. The red blood cell lysis reaction was ended by adding RPMI 1640 full media to a volume of 40 ml. Then the cell suspension was filtered twice with 40 µm filters and centrifuged again at 300x g for 5 min at room temperature. The PBMCs were resuspended in RPMI1640 full media and stored in the incubator.

### ***Monocyte isolation***

Human monocytes were isolated from PBMCs using the Pan Monocyte Isolation Kit II (Miltenyi Biotec, Germany). This kit enables the simultaneous enrichment of classical (CD14<sup>++</sup>CD16<sup>-</sup>), nonclassical (CD14<sup>+</sup>CD16<sup>++</sup>), and intermediate (CD14<sup>++</sup>CD16<sup>+</sup>) monocytes. PBMCs were counted and centrifuged. The cell pellet was resuspended in 60 µl of MACS buffer per 25 x 10<sup>6</sup> cells. 20 µl of FcR Blocking Reagent per 25 x 10<sup>6</sup> total cells and 20 µl of biotin-antibody

cocktail per  $25 \times 10^6$  cells were sequentially added and incubated for 20 min in the refrigerator (4 °C). Afterward, 60  $\mu$ l of MACS buffer per  $25 \times 10^6$  cells was added, followed by adding 40  $\mu$ l of anti-biotin microbeads per  $25 \times 10^6$  cells in the suspension. The mixture was incubated for 30 min at 4°C. While waiting for the incubation, LS columns were placed in the magnetic field of a MACS separator and were rinsed with 3 ml MACS buffer.  $50 \times 10^6$  cell suspension was applied onto one column, and the columns were then washed with 3 ml MACS buffer 3 times. Unlabeled cells that flow through the column, representing the enriched monocytes, were collected and cultured in RPMI 1640 full media for further procedures. The purity of monocytes was validated using a FACSVerse™ cell analyzer (BD Biosciences).

### ***Mouse spleen dissection***

The whole mouse spleen was obtained freshly at the animal facility and placed into a 15 ml tube with 5 ml RPMI1640 complete media. The spleen was carefully minced into small pieces with a scalpel blade and put into a 40  $\mu$ m cell strainer over a 50 ml conical tube. The plunger end of a syringe was then used to mash the spleen through the strainer, followed by washing the strainer with 3 ml RPMI 1640 full media. After repeating the last two steps 2-3 times, the cells were centrifuged at 300 x g for 5 minutes at room temperature and resuspended in 3 ml of 1x RBC lysis buffer. The lysis was stopped by washing the cell suspension with 20 ml RPMI 1640 media. The cell pellet was resuspended in full media after centrifugation.

### ***Murine B cell isolation***

The murine B cells were isolated from the spleen using the Pan B Cell Isolation Kit (Miltenyi Biotec). In principle, non-B cells are labeled with a cocktail of biotinylated CD3, CD4, CD8a, CD49b, Gr-1, and Ter119 antibodies and subsequently magnetically labeled with anti-biotin microbeads. B cells are enriched by the depletion of magnetically labeled cells. The kit allows the untouched murine B-1 and B-2 B cell subsets from single-cell suspensions of the spleen. In detail, cell number was determined, and cells were centrifuged at 300 x g for 5 min.  $25 \times 10^6$

cells were resuspended in 70  $\mu$ l of MACS buffer, subsequently adding 10  $\mu$ l FcR Blocking Reagent and 20  $\mu$ l biotin-antibody cocktail. After 20 min incubation at 4°C, 60  $\mu$ l of MACS buffer and 40  $\mu$ l of anti-biotin microbeads. The mixture was incubated at 4°C for 30 min before proceeding to magnetic cell separation. LS column was placed in the magnetic field of the MACS Separator and rinsed with 3 ml of MACS buffer. Next,  $50 \times 10^6$  cell suspension was applied onto the column, followed by washing with 3 ml MACS buffer 3 times. Unlabeled B cells that pass through were collected in RPMI 1640 full media. The cells were verified with a high percentage of purity using FACSVerse™ cell analyzer (BD biosciences).

### ***Chemotaxis assay***

Chemotaxis is defined as the directed migration of cells toward a chemoattractant, distinguished from chemokinesis. It is an essential process involved in inflammation. Chemotaxis assays can be a useful tool to evaluate the effect of chemokines and chemokine inhibitors. Therefore, I investigated the impact of MIF inhibitors on MIF-exerted immune cell chemotaxis by employing Transwell migration assay and 3D chemotaxis assay.

### ***Transwell migration assay***

Transwell migration assay measures the chemotactic capability of cells towards the chemoattractant. In my setup, inserts with a pore size of 5  $\mu$ m were used in murine B cell migration. For the detailed procedure, murine B cells were spun down by centrifugation, and the supernatant was aspirated. Cells were then resuspended in serum-free RPMI1640 media at a density of  $7 \times 10^6$  /ml. 600  $\mu$ l of the serum-free RPMI1640 with the desired stimulus concentration was loaded into the lower chamber in a 24-well plate. 100  $\mu$ l of B cell suspension was pipetted on top of the filter membrane in a transwell insert. The insert was carefully placed over a chamber without creating any bubbles. Cells were allowed to migrate for 4 hours. For analysis of migrated cells, cells that migrated into the lower chamber were collected into an epi tube after the transwell inserts were removed from the plate. After centrifugation, 500  $\mu$ l

supernatant was aspirated, and 10  $\mu$ l counting beads were added. Analysis was accomplished by FACSVerse™ cell analyzer (BD biosciences).

### ***3D monocyte chemotaxis***

3D chemotaxis was accomplished using  $\mu$ -Slide Chemotaxis (ibidi, Germany), which measures real-time chemotaxis in 3D gel matrices. On one hand, cells were seeded in water-based gels, which does not hinder the movement. On the other hand, it provides a quick gradient with long-term stability mimicking the physiological condition. For the detailed procedures,  $\mu$ -Slides and serum-free RPMI 1640 media were placed in a cell culture incubator the day before. On day 2,  $5 \times 10^6$  monocytes were suspended in 40  $\mu$ l serum-free RPMI1640 media, and MasterMix was prepared based on the recipe mentioned in the Materials. To prepare  $\mu$ -slides, 16.6  $\mu$ l cell suspension was mixed with 20  $\mu$ l rat tail collagen type I gel (ibidi, Germany) and subsequently applied into the channel. Mixing it thoroughly helps the cells distribute homogeneously. Slides were then incubated at 37°C for 30 min to allow gelation of the mixture. After 30 min, reservoirs were filled with 65  $\mu$ l serum-free RPMI1640 media on both sides, followed by pipetting 15  $\mu$ l chemokine to the defined side of the reservoir. 15  $\mu$ l liquid was immediately aspirated out on the opposite filling port using the same pipetting strategy. The last two steps were repeated once again. Slides are ready to undergo live imaging by closing filling ports with plugs. For analysis of migration, a 90 min time-lapse experiment was started with 1 min intervals under a 10x objective. 30 cells were tracked for each video using ImageJ and the Manual Tracking tool.

### ***Macrophage differentiation***

After the isolation of primary human monocytes, cells were plated in a 96-well plate at a density of  $2 \times 10^5$  per well and cultured with RPMI1640 full media. 100 ng/ml M-CSF was used to stimulate monocytes to differentiate into macrophages every other day. After 7-8 days, cells attaching to the bottom reveal macrophage-like morphology.

### ***Dil-LDL and Dil-oxLDL phagocytosis assay***



Primary human monocyte-derived macrophages were starved for 3 h with serum-free RPMI1640 containing 0.2% BSA before treatments and then were stimulated with MIF in the absence or presence of different doses of inhibitors overnight. On the next day, cells were treated with 1% HPCD (Sigma, Germany) for 30 min to remove cholesterol by exchanging media. Cells were washed with media once before being treated with Dil-LDL or Dil-oxLDL (ThermoFisher, Germany). 25 µg/ml Dil-LDL or Dil-oxLDL were prepared in serum-free RPMI1640 media and incubated with cells for 4 h. After 4 h incubation, cells were washed with cold PBS once and fixed with 4% PFA for 15 min. For the analysis of Dil-oxLDL endocytosis, 8 images were obtained and analyzed for each well under 10x objective by DMI8 microscope. Corrected total cell fluorescence (CTCF) was calculated as the following formula:  $CTCF = \text{Integrated Density} - (\text{Area of selected cell} \times \text{Mean fluorescence of background readings})$ .

### ***DMR assay***

Dynamic mass redistribution (DMR) assay is a label-free technology that enables real-time detection of integrated cellular responses in living cells. On day one, HEK-CXCR4 stable transfectants were plated at a density of 40000 cells per well in 96-well Epic microplates (Corning, USA). In detail, 40 µl full media was first added, and the plate was centrifuged at 800 rpm for 1 min to remove bubbles. Next, 80 µl cell suspension was added, and cells grew overnight to reach 80% confluency. The next day, 85 µl media were removed, and 50 µl assay buffer was added. Once again, 50 µl media were removed, and 50 µl assay buffer was added. This step was repeated three times. After that, 45 µl assay buffer was added. The plate was equilibrated for 2 h at room temperature before an initial 10 min baseline readout was measured. After the baseline measurement, MIF with its preincubated different doses of inhibitors in 20 µl of assay buffer were added to the wells. DMR responses were monitored with EnSpire® multimode plate reader (PerkinElmer, USA) for 2 h to assess the inhibition of MIF-induced DMR responses.

**Flow cytometry****Cell number counting**

Relative cell count was achieved using CountBright™ Absolute Counting Beads (ThermoFisher, Germany). The beads must be mixed well to ensure a uniform suspension of microspheres by vortexing for 30 s before. The following equation was used to calculate the relative cell number:

$$A/B \times C/D = \text{concentration of sample as cells} / \mu\text{l}$$

A = number of cell events

B = number of bead events

C = assigned bead count of the lot (beads/50  $\mu\text{l}$ )

D = volume of sample ( $\mu\text{l}$ )

**Cell surface antibody staining**

Cell surface marker staining was measured using flow cytometry. It can be summarized as the following procedures. For each sample,  $1 \times 10^6$  single cells were suspended in 100  $\mu\text{l}$  cold FACS buffer. Then, antibodies of interest were added at a ratio of 1:100, and samples were incubated on the ice for 30 min. After 30 min, samples were washed twice with 500  $\mu\text{l}$  FACS buffer, and cells were resuspended in 500  $\mu\text{l}$  FACS buffer for flow cytometry analysis.

**2.2.2 Plasma degradation and protein interaction methods****Human plasma separation**

To separate human plasma, fresh blood was obtained from a healthy donor, and 105 mM trisodium citrate (pH=7) was used as the anti-coagulant (204). 2.2 ml anti-coagulant was employed for 20 ml blood. The blood was gently mixed with anti-coagulant and centrifuged at 2500 x g for 10 min at room temperature. The supernatant was transferred into a 15 ml conical tube and centrifuged once again at 2500 x g for 5 min at room temperature. The plasma was aliquoted into 10 x 500  $\mu\text{l}$  and frozen in liquid nitrogen. The aliquots were stored at - 80°C for long-term usage.

***Plasma degradation assay***

To examine the proteolytic stability of NGM-D3 in human plasma, TAMRA was conjugated to the N-terminus of NGM-D3 on solid phase following previously published protocol (205). Next, lyophilized TAMRA-NGM-D3 was reconstituted in PBS to a concentration of 50 µg/ml. TAMRA-NGM-D3 was added to plasma to a final concentration of 500 nM and incubated for 0 h, 1 h, 2 h, 4 h, 8 h, 24 h, 48 h, 120 h, and 168 h at 37 °C. Samples were then diluted in 2x Novex Tricine SDS sample buffer (Life Technologies) with or without DTT, boiled at 95°C for 10 min, and loaded onto a 10-20% Tricine gel (Life Technologies). DTT was used to reduce disulfide bonds. The fluorescent signal was imaged in the 600 nm channel with an Odyssey<sup>®</sup> Fc imager and quantified with Image Studio Lite Ver 5.2.

***Tricine SDS-PAGE gel electrophoresis***

The Tricine gel provides increased resolution of proteins with molecular weights as low as 2 kDa, which can be used to visualize the fluorescent signal of TAMRA-NGM-D3 and Cy7.5-NGM-D3. Tricine 10-20% gels and respective 2x Tricine SDS sample buffer and 10x Tricine SDS Running buffer were purchased from ThermoFisher. 100 ml of 10x Tricine SDS Running Buffer was diluted with 900 ml deionized water to prepare 1x Tricine SDS Running Buffer, and samples were heated at 95°C for 1 min. 500 ml 1x running buffer was filled in the tank. 25 µl of each sample was loaded in the gel wells and ran at 80 V for 20 min and 100 V for 100 min with protection from lights. The signal of TAMRA-NGM-D3 and Cy7.5-NGM-D3 was detected in 600 nm and 800 nm channels with the Odyssey<sup>®</sup> Fc imager.

***Cy7.5-NGM-D3-albumin interaction by native gel electrophoresis***

Native gels do not contain SDS and can be used to run proteins in their native forms, enabling the identification of protein-protein interactions. To investigate the potential interaction between human serum albumin (HSA) and NGM-D3, FITC-HSA and Cy7.5-NGM-D3 were used to determine the colocalization of fluorescent signals. Cyanine7.5 (Cy7.5, Lumiprobe

GmbH, Hannover, Germany) was linked to the N-terminus of NGM-D3 using the same molar excess of the label of the 2-(7-Aza-1H-benzotriazole-1-yl)-1,1,3,3-tetramethyluronium hexafluorophosphate (HATU) and 1.5-fold molar excess of N,N-diisopropylethylamine (DIEA) in N,N-dimethylformamide (DMF) for 2 h. The synthesis was performed by our collaborators at TUM. 500 nM Cy7.5-NGM-D3 was incubated with 1x, 2x, 5x, 10x, 20x, 50x fold of FITC-HSA for 0 h and 2 h. Samples were mixed with 2x Native Tris-Glycine Sample Buffer and ran onto 10-20% Tris-glycine native gel at 120 V for 90 min with being protected from lights. The fluorescent signals of Cy7.5-NGM-D3 and FITC-HSA were detected in the 800 nm and 600 nm channels, respectively, with the Odyssey<sup>®</sup> Fc imager.

### **2.2.3 *In vivo* murine experiments and bulk RNA-seq**

#### ***Animals***

All experiments were approved by the Animal Care and Use Committee of the local authorities and were performed under license (Vet\_03-21-40). *ApoE*<sup>-/-</sup> mice in the C57BL/6-J background were housed in a temperature-controlled environment at the Center for Stroke and Dementia Research (CSD), Munich, Germany and were originally obtained from Charles River Laboratories (Sulzfeld, Germany). I used female mice (8 weeks old) for the study, given that a previous study on the first-generation MIF inhibitor msR4M-L1 was performed with female mice. Mice were randomly assigned to either the control group or the NGM-D3 group and were fed a high fat diet (HFD) containing 0.21% cholesterol (ssniff Spezialdiäten GmbH, Soest, Germany) for 5 weeks. During these 5 weeks, mice were administrated either with saline or with 50 µg NGM-D3 three times a week. Mice were monitored regularly throughout the study. At the endpoint of the study, mice were anesthetized with midazolam-medetomidine-fentanyl (MMF) and exsanguinated by cardiac puncture, perfused with saline to remove any traces of blood. Aortic roots were embedded in optimal cutting temperature (OCT) medium and frozen immediately on dry-ice for further sectioning and staining.

#### ***Peripheral blood leukocyte separation***

Blood was centrifuged at 400 g, 4°C for 15 min to obtain the plasma. The remaining blood was mixed with PBS to a volume of 10 ml and was centrifuged at 300 g, 4°C for 10 min. The supernatant was discarded, and RBCs were lysed in 3 ml RBC lysis buffer for 5 min. After 5 min, 27 ml PBS was added, and cells were spun down and then resuspended in 5 ml PBS. Cell number was counted by the cell counter.

### ***Immunohistochemistry***

Aortic roots were placed in the specimen holder of a cryotome (ThermoFisher, Karlsruhe, Germany) and sectioned. 5 µm sections were collected on a glass slide when 1 or 2 valves of the aortic sinus started to appear. Serial sections were collected following a published method (206). For each mouse, 80-100 sections were collected. The first 10 sections were collected onto the top portion of labeled glass slides (slides labeled 1-10). Subsequent sections were collected following the same pattern. In this way, slide 1 holds sections 1, 11, 21, 31, 41, 51, 61, representing atherosclerotic lesions from the sinus to the ascending aorta. Analysis of lesions includes HE staining and Oil Red O staining. The remaining sections were stored at -80°C for immunofluorescence analysis. For HE staining, slides dry at room temperature for 30 min and rehydrated in PBS for 10 min. The slides were stained in Mayer's Hematoxylin solution for 10 min and rinsed with VE-water from the backside and then with warm tap water for 10 min. After washing with distilled water for 30 s, slides were immersed in Eosin Y solution for 1 min and dipped in distilled water until the eosin stopped streaking. Slides were dipped through 2 times of 95% EtOH, 2 times of 100% EtOH, and 2 times of xylene, each for 2 min. Slides were mounted with resinous mounting medium and covered with coverslips. For Oil Red O staining, slides were allowed to air dry at room temperature for 5 min and rinsed with PBS for 1-2 min. Slides were stained with Oil Red O solution (0.5% in propylene glycol, Sigma) at 37°C for 1 h. After 1 h, slides were washed with distilled water and stained with hematoxylin for 1 min. Then slides were rinsed with warm tap water for 5 min and mounted with Karsers Glycerine-Gelatin (Roth). Plaque size was quantified using ImageJ.

***CD68 staining***

Slides were thawed at 37°C for 1 min and dried at room temperature for 30 min. Pre-cooled 4°C acetone was used to fix the slides for 6 min at 4°C. After fixation, slides were allowed to air dry for 30 min and rehydrated in PBS for 10 min. Next, they were blocked with a solution containing 5% donkey and 1% BSA and stained with 1:100 rat-mouse CD68 antibody (Bio-rad) overnight. The next day, slides were washed with PBS 3 times, 5 min each, and then incubated with 1:300 donkey-rat Cy3 and DAPI for 1 h at room temperature. After washing with PBS 3 times, 5 min each time, they were mounted with Fluoromount G. Images were captured with a Leica DMI8 microscope and quantified using ImageJ.

***Isolation of RNA and library construction***

Aortic root sections were incubated with 50 µl RNA isolation buffer containing 20% proteinase K (Qiagen, Hilden, Germany) and 1:2400000 ERCC RNA spike-in mix in buffer PKD (ThermoFisher Scientific, Germany) at room temperature for 30 seconds, and were then dissected under the microscope. RNA samples were added to oligo dT25 magnetic beads (ThermoFisher Scientific) to allow mRNA hybridization, followed by washing two times with ice cold 1X HB and once with 1X PBS. Purified RNA was eluted at 80°C for 2 min, collected and stored at -80°C. For library preparation, 1 ng RNA from each sample was used and proceeded with reverse transcription and cDNA amplification following a prior published Smart-seq2 protocol (207)

***Bulk RNA sequencing and data analysis***

Sequencing was performed by BGI Tech Solutions (HongKong) Co., Limited (HongKong, China) on a DNB-seq platform for paired-end sequencing. Raw data was processed using Galaxy platform (208). Quality control was performed using FastQC Tool (Version 0.11.9). Sequencing reads was aligned to mouse GRCm38 (mm10) reference genome using RNA STAR (Version 2.7.8a). Aligned reads were generated using featureCounts (Version 2.0.1).

Differential gene expression was examined with DESeq2 (Version 1.34.0). *P* values were corrected by the Benjamini-Hochberg method. Genes with adjusted *P* value < 0.05 and log<sub>2</sub>FoldChange > 1 were considered significantly differentially expressed. Functional enrichment analysis was performed using g:Profiler (209).

### ***Statistical analysis***

GraphPad Prism 8.4.3 (GraphPad Software, San Diego, CA) was used for statistical analysis. Data are shown as means ± SEM from at least 3 independent experiments. Data with two groups were analyzed with unpaired, 2-tailed Student *t* test. For the data with ≥ three groups, one-way ANOVA test was performed, adjusted for multiple comparisons using Dunn post hoc test. For non-parametric data, analyses were performed using Mann-Whitney test. *P* ≤ 0.05 was considered significant.

---

## 3. Results

### 3.1 Characterization of the first generation CXCR4 ectodomain-derived peptide msR4M-L1 *in vitro*

#### 3.1.1 MIF induces Dil-LDL phagocytosis in macrophages

Increased levels of modified LDL, particularly oxLDL, are considered initiators of atherosclerosis. Beyond that, evidence has shown that native LDL contributes to foam cell formation (210). MIF has demonstrated its ability to drive macrophages to take up LDL through receptor CXCR4 (211). To verify whether MIF promotes LDL endocytosis in primary monocyte-derived macrophages, a Dil-LDL uptake assay was performed by stimulating cells with human MIF in the absence or presence of MIF inhibitors IIID.9 and ISO-1. IIID.9 is a known neutralizing MIF antibody. Addition of MIF enhanced LDL endocytic capability of macrophages. As expected, this effect was markedly reduced by 3-fold molar excess of IIID.9 but not by its isotype control IgG1 (**Figure 8**). To further validate the result, different concentrations of ISO-1 were added along with MIF. ISO-1 is a well-known small molecule MIF inhibitor that displays anti-MIF features through binding to its active catalytic active site (212). My data suggested ISO-1 inhibits MIF-related Dil-LDL uptake in human macrophages in a dose-dependent manner (**Figure 8B**). LDL uptake was diminished as much as adding 3-fold molar excess of IIID.9 when cells were treated with the highest concentration of ISO-1 (62.5-fold), which means ISO-1 has lower potency in suppressing MIF functions than neutralization antibody IIID.9 given its targeting site as well as small molecular size. Marked reduction of Dil-LDL uptake through co-stimulation with IIID.9 and ISO-1 emphasizes MIF regulates LDL endocytosis via CXCR4.



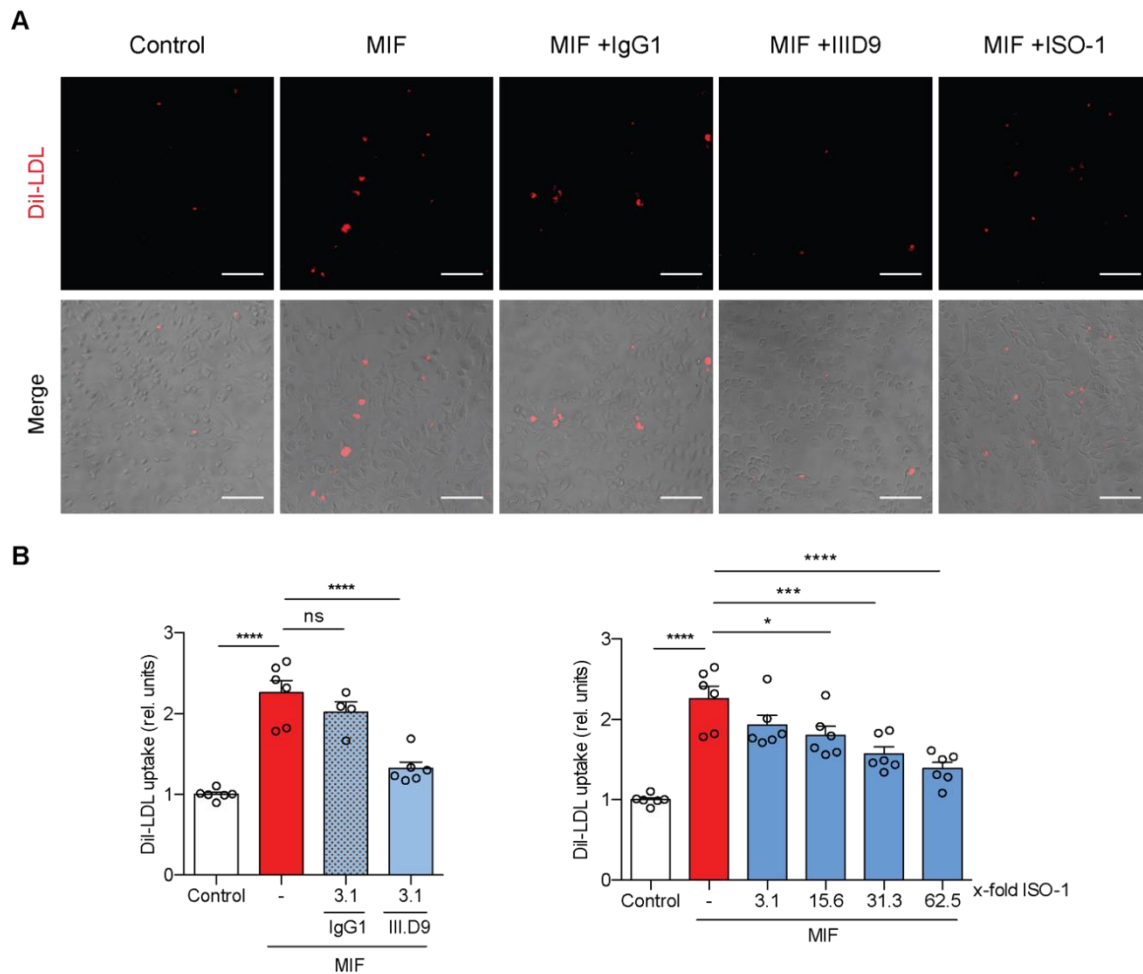


**Figure 8: MIF induces DiI-LDL uptake in primary human monocyte-derived macrophages. A** Representative images of DiI-LDL-positive macrophages. Images shown were merged with phase contrast. Cy3 red for DiI-LDL. **A-B** MIF increases LDL uptake in primary human monocyte-derived macrophages (cells were treated with 80 nM MIF). Addition of IIID.9, yet not isotype IgG1, and ISO-1 reduced the DiI-LDL positive fluorescent signals. X-fold concentrations of inhibitors correspond to the MIF concentration. Control indicates LDL uptake at baseline. Data are shown as means  $\pm$  SEM from three independent experiments. The scale bar in **A** is 75  $\mu$ m. MIF, macrophage migration-inhibitory factor; CXCR4, CXC motif chemokine receptor-4

### 3.1.2 msR4M-L1 inhibits MIF-induced DiI-LDL uptake in human PBMC-derived macrophages

AMD3100 is a small molecule that was discovered as a specific CXCR4 antagonist. To determine whether MIF-triggered LDL uptake is driven by receptor CXCR4, macrophages were stimulated with MIF with or without AMD3100. The MIF-driven LDL uptake was compromised by pretreating cells with 10  $\mu$ M AMD3100, indicating that MIF-mediated LDL uptake is

dependent, at least partially, on the receptor CXCR4 (**Figure 9B**). Based on that evidence, macrophages were treated with a range of msR4M-L1 concentrations to evaluate how the CXCR4-derived MIF inhibitor msR4M-L1 affects native LDL uptake by human macrophages. Similar to ISO-1, msR4M-L1 exhibited a dose-dependent inhibition on MIF-triggered native LDL uptake (**Figure 9B**). At 62.5-fold molar excess, which equals 5  $\mu\text{M}$  of peptide, msR4M-L1 was able to reduce the Dil-LDL signal approximately to the same level observed by 10  $\mu\text{M}$  AMD3100.

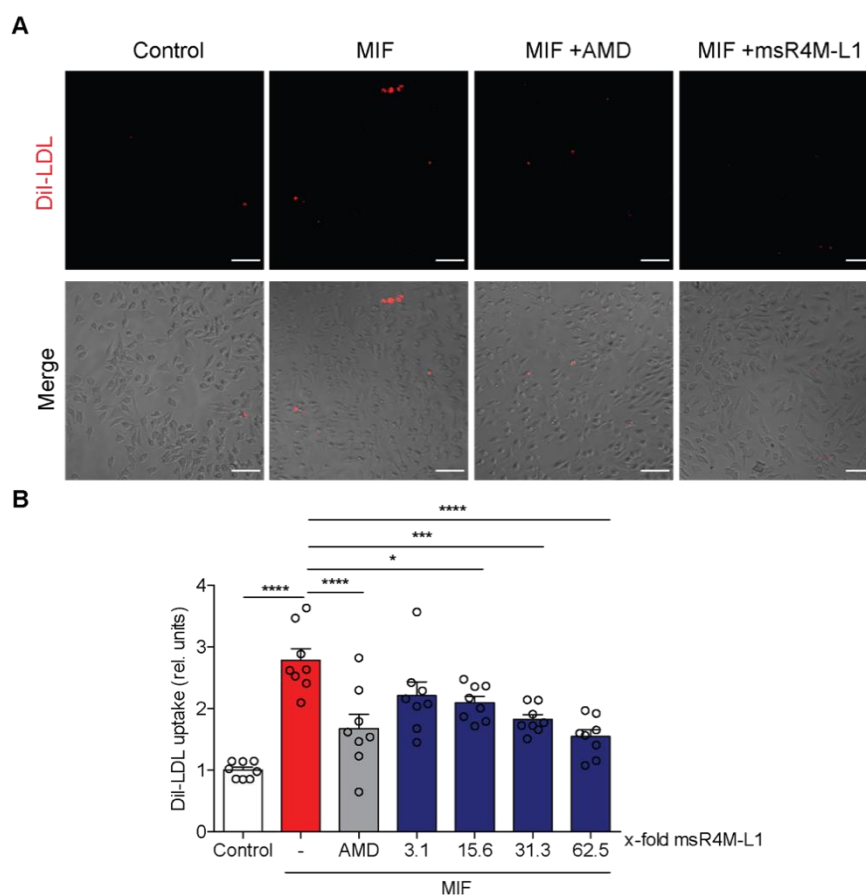


**Figure 9: The inhibitory effect of AMD3100 and msR4M-L1 on MIF-associated Dil-LDL uptake in primary human monocyte-derived macrophages.** **A** Representative images of Dil-LDL positive macrophages. Images shown were merged with phase contrast. Cy3 red for Dil-LDL. **A-B** MIF promoted the LDL endocytic ability of macrophages (cells were treated with 80 nM MIF +/- inhibitors, then incubated with 25  $\mu\text{g}/\text{ml}$  Dil-LDL for 4 h), which was then diminished by CXCR4 inhibitor AMD3100 and msR4M-L1. msR4M-L1 presents a dose-dependent response in the inhibition of Dil-LDL uptake. Control indicates LDL uptake at baseline. Data are shown as means  $\pm$  SEM from four independent experiments. The scale bar in A is 75  $\mu\text{m}$ . MIF, macrophage migration-inhibitory factor; CXCR4, CXC motif chemokine receptor-4.

### 3.1.3 Mutated msR4M-L1 loses capacity to block MIF/CXCR4-mediated LDL uptake

In a prior study, the amino acids in msR4M-L1 essential for MIF binding were identified by performing peptide array analysis and alanine-scanning (200). In ECL1, four aromatic residues in positions 102, 103, 104, and 107 were found to play a critical role. On the other hand, a remarkable interaction reduction of msR4M-L1 with MIF was seen upon substitution by Ala in positions 189, 190, and 195 in ECL2. To evaluate the importance of those amino acids to the specificity of msR4M-L1, they were substituted with alanine, which led to msR4M-L1(7xAla) synthesis. msR4M-L1(2xAla) was also synthesized, given that the alanine substitution of Phe-104 and Phe-107 caused a strong reduction in spot intensity. msR4M-L1(7xAla) and msR4M-L1(2xAla) showed no effects on MIF. Additionally, similar results were observed in Transwell B-cell migration assay. msR4M-L1(2xAla) demonstrated reduced ability in inhibiting MIF-initiated chemotaxis, whereas msR4M-L1(7xAla) activity was completely lost (**Figure 10**). These data are consistent with the biophysical properties of msR4M-L1 variants. The msR4M-L1 ability to block MIF activities correlates with the binding region on the molecule, which provided us insights into the optimization of the next generation peptide inhibitors.

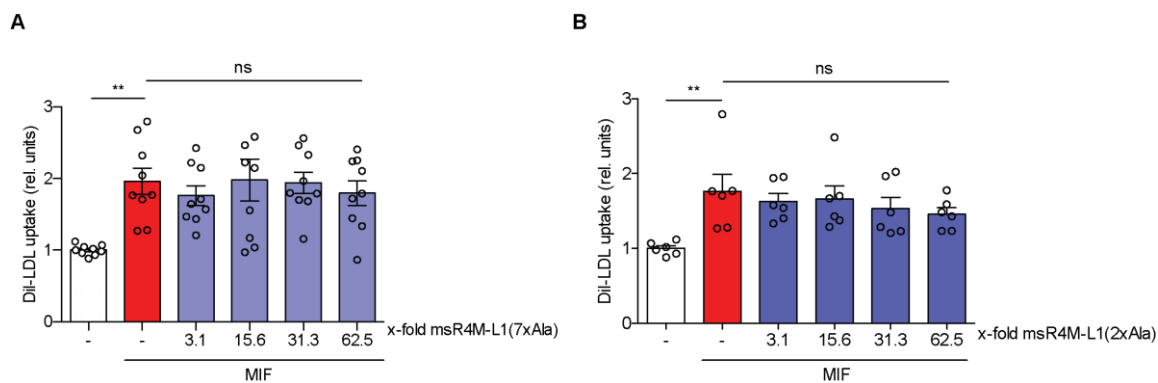


**Figure 10: Mutated msR4M-L1(7xAla and 2xAla) loses the capacity to block MIF/CXCR4-mediated LDL uptake.** Cells were treated with 80 nM human MIF +/- msR4M-L1 variants. **A** co-stimulated with msR4M-L1(7xAla); **B** co-stimulated with msR4M-L1(2xAla). The concentrations that were used for both variants were the same as msR4M-L1. Control (-) indicates LDL uptake at baseline. Data are shown as means  $\pm$  SEM from three or four independent experiments. MIF, macrophage migration-inhibitory factor; CXCR4, CXC motif chemokine receptor-4.

### 3.1.4 msR4M-L1 inhibits MIF-triggered Dil-oxLDL uptake in PBMC-derived macrophages

Among modified LDLs, oxLDL has been proposed as the main modification of LDL to promote foam cell formation, which in turn triggers immune responses. OxLDL initiates atherogenesis through various mechanisms. For example, oxLDL triggers the activation of endothelial cells and up-regulates adhesion molecules and MIF secretion, which facilitate blood leukocytes adhesion in the arterial wall. Macrophages take up oxLDL via CD36, among other scavenger receptors, resulting in the release of proinflammatory cytokines and chemokines. Thus, this brought us to the question, of whether MIF enhances oxLDL uptake in macrophages and how msR4M-L1 would influence the process. After stimulation of MIF in the absence or presence of msR4M-L1, cells were incubated with Dil-oxLDL. MIF increased oxLDL uptake by 1.8-fold, and the effect was dose-dependently reversed by adding msR4M-L1 (**Figure 11**). Although MIF enhanced oxLDL uptake in human monocyte-derived macrophages, the mechanism remains unclear and was not further studied in this thesis. Thus, the role of CXCR4 in oxLDL uptake and the involvement of CD36, needs to be further investigated.

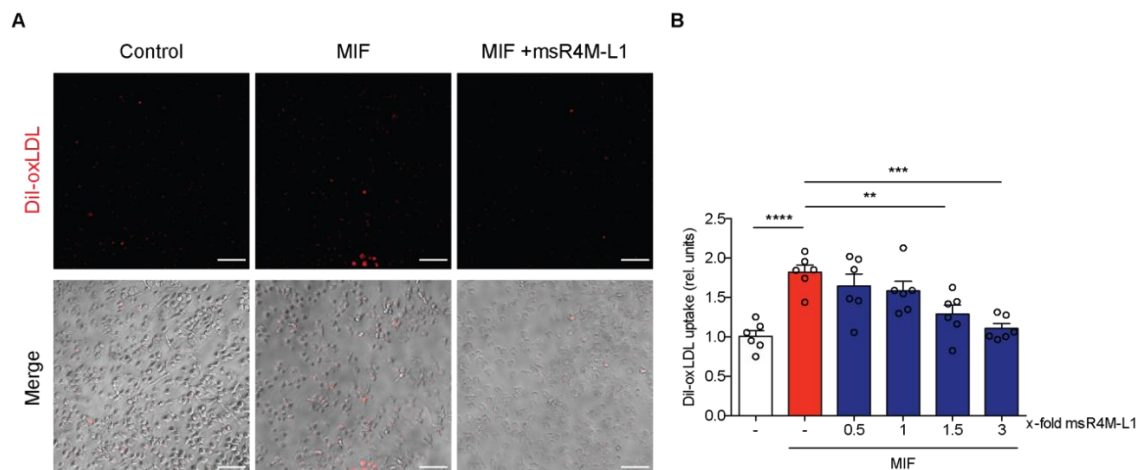


**Figure 11: msR4M-L1 dose-dependently reverses MIF-mediated oxLDL uptake.** **A** representative images of Dil-oxLDL positive macrophages. Images shown were merged with phase contrast. Cy3 greenish-yellow for Dil-oxLDL. **B** MIF promoted the oxLDL phagocytosis in human macrophages (cells were treated with 80 nM MIF overnight, then incubated with Dil-oxLDL at 37°C for 4 h), which was reversed by CXCR4 inhibitor msR4M-L1. msR4M-L1 produces a dose-dependent response in inhibiting Dil-oxLDL uptake. X-fold concentrations of inhibitors correspond to the MIF concentration. Control (-) indicates oxLDL uptake at baseline. Data are shown as means  $\pm$  SEM from three independent experiments. The scale bar in images is 75  $\mu$ m. MIF, macrophage migration-inhibitory factor; CXCR4, CXC motif chemokine receptor-4.

### 3.1.5 msR4M-L1 partially reverses MIF-induced integrated cellular responses as read out by DMR methodology

Chemokine receptors are one of the largest transmembrane proteins, G protein-coupled receptors (GPCRs). Activation of a single receptor may spike a complex of cellular responses. DMR detects biomolecules changes in their localization within a cell, when a cellular process occurs. An optical output is recorded by a change of wavelength of outgoing light when passing polarized broadband light through the bottom portion of cells on the plate surface. DMR provides a comprehensive picture of the action of agonists and antagonists. Stably transfected HEK-CXCR4 cells were used to investigate how msR4M-L1 affects the live-cell change sensing. 10  $\mu$ M MIF triggered the DMR response curve to rise, yet control treatment with solution buffer or msR4M-L1 alone did not cause any cellular changes (**Figure 12**). When cells were co-treated with MIF and msR4M-L1 at a molar ratio of 1:0.5, the DMR response curve was reduced and delayed. A dose-response curve needs to be evaluated to assess the concentration-dependent impact on the effect of MIF on HEK293-CXCR4 transfectants. However, due to the limited solubility properties of msR4M-L1 and the required optimization steps, these experiments could not be performed in the time line of my thesis.

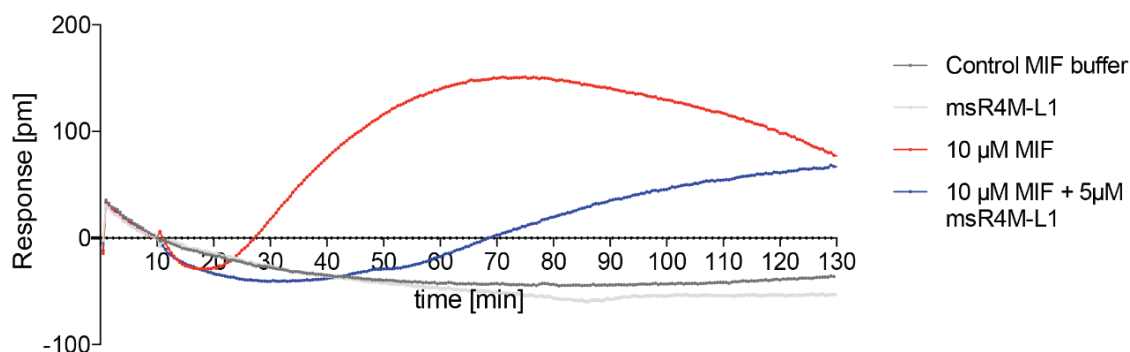


**Figure 12: Dynamic mass redistribution analysis of the inhibition effect of msR4M-L1 on MIF-stimulated HEK293-CXCR4 transfectants.** HEK293 cells stably transfected with CXCR4 were exposed to 10  $\mu$ M of MIF, and DMR was recorded for 120 min in combination with the application of 5  $\mu$ M of msR4M-L1 or solution buffer as control. Data are shown from a single experiment performed in technical triplicates. MIF, macrophage migration-inhibitory factor; CXCR4, CXC motif chemokine receptor-4.

### 3.1.6 msR4M-L1 does not disrupt the MIF/CD74 interaction

msR4M-L1 showed specificity in blocking MIF/CXCR4 signaling. As a cognate receptor, CD74 signaling was shown to have protective functions on cardiomyocytes in cardiac ischemic/reperfusion injury, an effect mediated by AMPK signaling (116). Activation of CD74 decreased infarct size and improved cell survival by triggering the AMPK signaling pathway to promote glucose uptake in cardiomyocytes (116). Therefore, to test whether msR4M-L1 would interfere the interaction between MIF and CD74 or would spare such interactions. To look at the ligand-receptor interaction, I transiently transfected CD74 into HEK293T cells and checked the expression level of CD74 on the cell surface by flow cytometry. **Figure 13** shows approximately 60% of cells express CD74 on the surface.

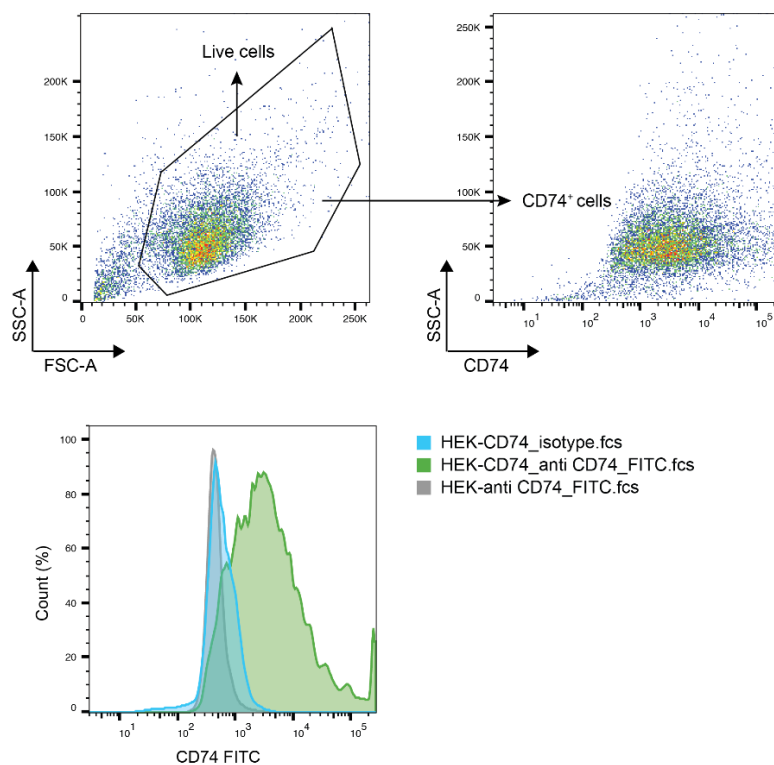


**Figure 13: Transfection efficiency of CD74minRTS-FLAG in HEK293T cells.** HEK293T cells were transfected with CD74minRTS-FLAG plasmid for 48 h. CD74 cell-surface expression on HEK293T cells was determined by flow cytometry analysis. MIF, macrophage migration-inhibitory factor; CD74, cluster of differentiation 74

Next, receptor binding assays were performed to study whether msR4M-L1 would interfere with MIF-CD74 binding. MIF was labeled with Alexa 488 to be detected by flow cytometry and

was incubated with CD74-expressing HEK cells for 2 h under equilibrium conditions. An untreated group was included to rule out unspecific fluorescence. **Figure 14** shows that Alexa 488-MIF bound to CD74, and co-incubation with msR4M-L1 did not perturb the interaction between MIF and CD74, suggesting the interface between MIF and CD74 is not affected by msR4M-L1/MIF binding. This result suggests msR4M-L1 could be selective in targeting MIF receptor pathways.

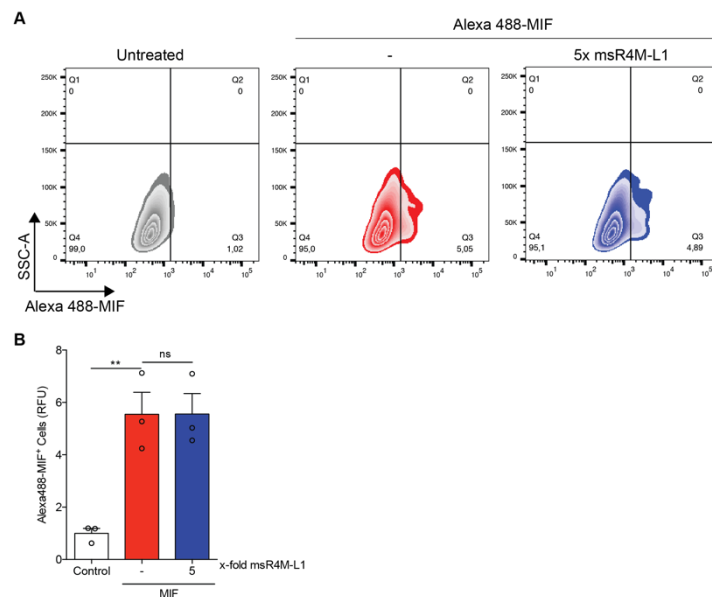


**Figure 14: msR4M-L1 does not disrupt MIF/CD74 interaction.** **A** Illustration of msR4M-L1 selectivity on CD74 surface binding. Percentage in **A** Q3 represents the number of cells bound to Alexa 488-MIF; **B** 5-fold molar excess of msR4M-L1 did not interfere with the binding of Alexa 488-MIF to CD74 on the cell surface (msR4M-L1 was pre-incubated with Alexa 488-MIF for 30 min, cells were treated with 400 nM MIF for 2 h). Data are shown as mean  $\pm$  SEM from three independent experiments. MIF, macrophage migration-inhibitory factor; CD74, cluster of differentiation 74.

### 3.2 Characterization of the inhibitory potential and pharmacological properties (IC<sub>50</sub> curves) for the next generation CXCR4 mimics (NGMs)

msR4M-L1 exhibited favorable selectivity and specificity to target MIF/CXCR4 interaction and attenuated atherosclerosis *in vivo*. To improve its solubility and generate minimum active sites, our collaborators at TUM conducted peptide array, alanine screening and other biophysical

experiments to identify the essential amino acids for MIF binding in msR4M-L1. As indicated in the scheme (**Figure 15**), ECL1[97-110] and ECL2[182-196] were shortened to ECL1[102-110] and ECL2[187-195] and connected by several linkers (8-Aoc, O1Pen2-O1Pen2, D-D-D, G-G-G, K-K-K, R-R-R) with enhanced solubility, which were termed 'NGMs'. Based on their biophysical characterization and their biochemical binding properties to MIF in comparison to CXCL12 as assessed by fluorescence titration spectroscopy (see also Discussion part) performed by our collaborators at the Division of Peptide Biochemistry at Technical University of Munich (TUM) (Head: Prof. Dr. Aphrodite Kapurniotu), four of the synthesized NGMs were selected for further screening using *in vitro* cell assays that mimic atherogenic MIF activities towards leukocytes. These were NGM-D3 ( $K_D(\text{MIF}) = 35.97 \text{ nM}$ ;  $K_D(\text{CXCL12}) > 2 \mu\text{M}$ ), NGM-R3 ( $K_D(\text{MIF}) = 16.82 \text{ nM}$ ;  $K_D(\text{CXCL12}) = 44 \text{ nM}$ ), NGM-K3 ( $K_D(\text{MIF}) = 36.4 \text{ nM}$ ;  $K_D(\text{CXCL12}) = 19.6 \text{ nM}$ ), and NGM-O1Pen2 ( $K_D(\text{MIF}) = 14.3 \text{ nM}$ ;  $K_D(\text{CXCL12}) > 2 \mu\text{M}$ ).

Measurement of drug potency is conventionally determined by the concentration of the drug that inhibits 50% ( $IC_{50}$ ) of targeted reaction in a dose-response assay *in vitro*. The  $IC_{50}$  value is the standard parameter used to establish experimental outcomes *in vitro* and to screen drugs with high potential for advancement into animal studies. It is a useful parameter that describes the inhibition capacity. I employed three functional assays, Dil-oxLDL uptake, 3D monocyte chemotaxis, and Transwell B-cell migration, to characterize dose-response inhibitory relationships for the NGMs and examine the specificity and selectivity of NGMs regarding their interactions with MIF and CXCL12.



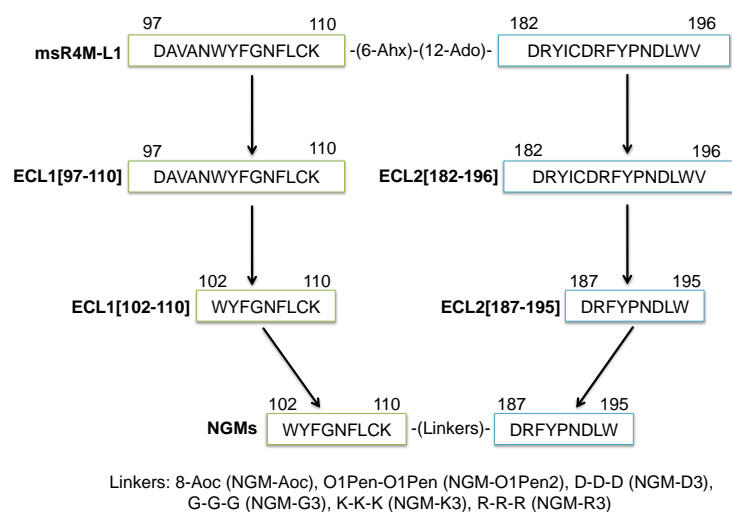


**Figure 15: Sequences of msR4M-L1 and six NGMs.** The backbone of NGMs consists of ECL1[102-110] and ECL2[187-195]. The original linker (6-Ahx)-(12-Ado) is replaced by six linkers (8-Aoc, O1Pen-O1Pen, D-D-D, G-G-G, K-K-K, R-R-R) to enhance solubility and optimize the structure. The design scheme was kindly provided by Dr. Christos Kontos and Prof. Aphrodite Kapurniotu (TUM).

### 3.2.1 Potency of the NGMs ( $IC_{50}$ curves) as assessed by a Dil-oxLDL uptake assay

To determine whether NGMs retain the anti-MIF functionality of msR4M-L1 and to assess potencies and efficacies, I performed a Dil-oxLDL uptake assay to acquire dose-response curves considering the essential role oxLDL plays in plaque formation. AMD3100 was also assayed to determine the dependence of MIF-induced oxLDL uptake on CXCR4. MIF enhanced oxLDL phagocytosis in human macrophages by a factor of 1.6-1.7-fold (**Figure 16B**). 100% at the starting point of curves refers to the effect elicited by MIF. The unstimulated cells also took up oxLDL, accounting for approximately 60% of MIF stimulation. AMD3100 exhibited a shallow dose-dependent reduction with the curve leveling at ca. 70% (**Figure 16C**), also indicating that the CXCR4-dependent part of MIF-elicited oxLDL uptake accounts for about 30% of the total MIF effect. The  $IC_{50}$  for AMD3100 was  $46.1 \pm 33.0$  nM. Inhibition curves for NGM-R3 ( $IC_{50}=10.7 \pm 3.4$  nM) and NGM-K3 ( $IC_{50}=8.2$  nM) reached plateaus below 60% with steeper slopes (**Figure 16D**). Curves for NGM-D3 ( $IC_{50}=4.6 \pm 5.7$  nM) and NGM-O1Pen2 ( $IC_{50}=63.5 \pm 171.4$  nM) slowly declined to the level slightly above 60% (**Figure 16D**). All NGMs achieved better effectiveness in suppressing oxLDL phagocytosis modulated by MIF as compared to AMD3100. Importantly, NGMs with an amino acid linker, namely NGM-D3, NGM-R3, and NGM-K3, showed greater potencies than NGM-O1Pen2, which suggests that independent of

structural similarities of NGMs related to CXCR4, solubility is strongly associated with the potency of CXCR4 mimics.

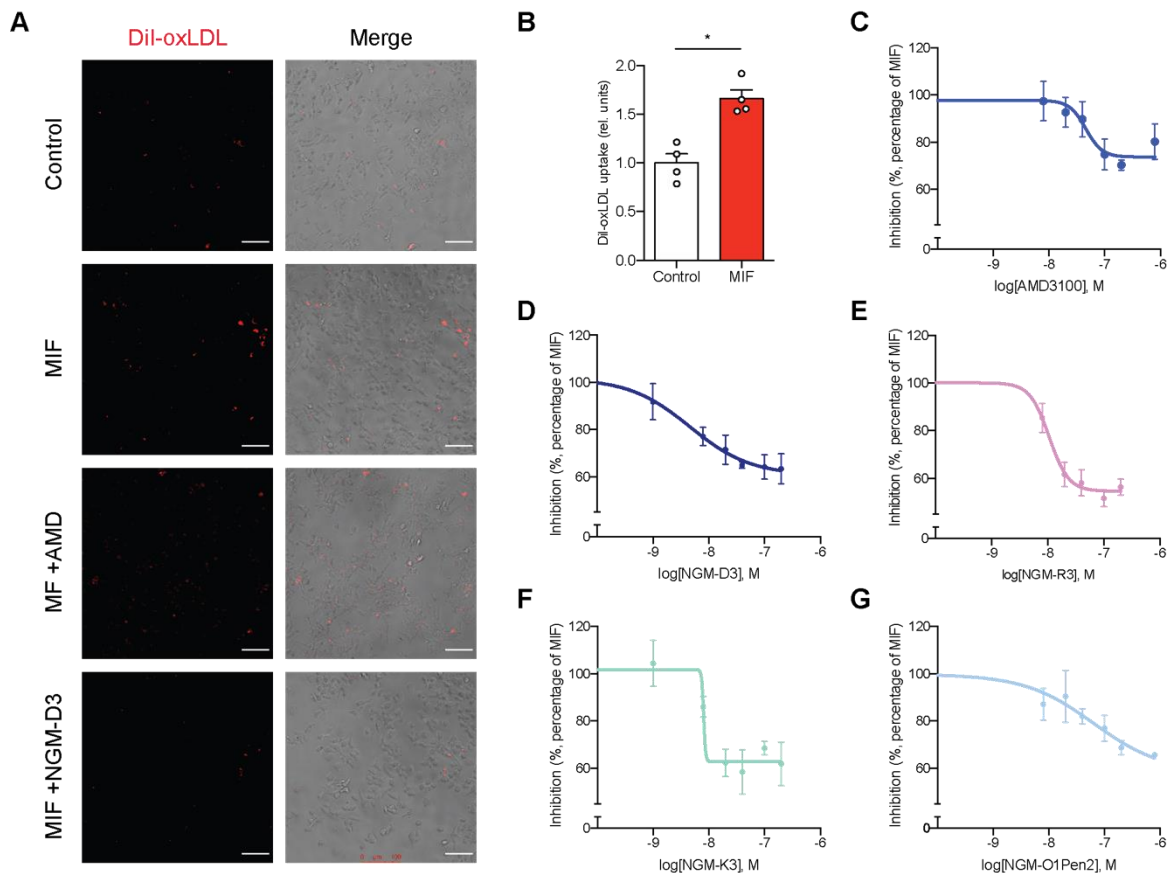


**Figure 16: Determination of IC<sub>50</sub> curves for the inhibitory effects of NGMs on MIF-elicited DiI-oxLDL uptake.** **A** Representative images of DiI-oxLDL-positive cells for the various treatment conditions. Data shown were merged with phase contrast, Cy3 red for DiI-oxLDL; **B** MIF increases oxLDL uptake in primary human monocyte-derived macrophages (cells were treated with 80 nM MIF); **C-G** Curves were plotted against MIF in the absence and presence of increasing doses of AMD3100 or NGMs indicated as log values (data from three independent experiments). MIF/CXCR4-mediated DiI-oxLDL uptake in primary human monocyte-derived macrophages is inhibited by adding inhibitor AMD3100 (**C**), NGM-D3 (**D**), NGM-R3 (**E**), NGM-K3 (**F**), NGM-O1Pen2 (**G**) in a dose-dependent manner. Data are shown as mean  $\pm$  SEM. The scale bar in **A** is 75  $\mu$ m. MIF, macrophage migration-inhibitory factor; CXCR4, CXC motif chemokine receptor-4; NGMs, next generation mimics.

### 3.2.2 Inhibitory potency of NGMs (IC<sub>50</sub> curves) as assessed by a 3D monocyte chemotaxis assay

The capacity of MIF to enhance monocyte recruitment has been well-established in earlier studies (102). It is viewed as one of the most crucial pro-inflammatory metrics for MIF in

atherogenic inflammation and is mediated by the cooperation of CXCR2 and CXCR4. Previous experiments showed msR4M-L1 dose-dependently inhibits MIF-elicited human monocyte 3D chemotaxis, an assay which mimics the migration process in physiological processes in the vessel.

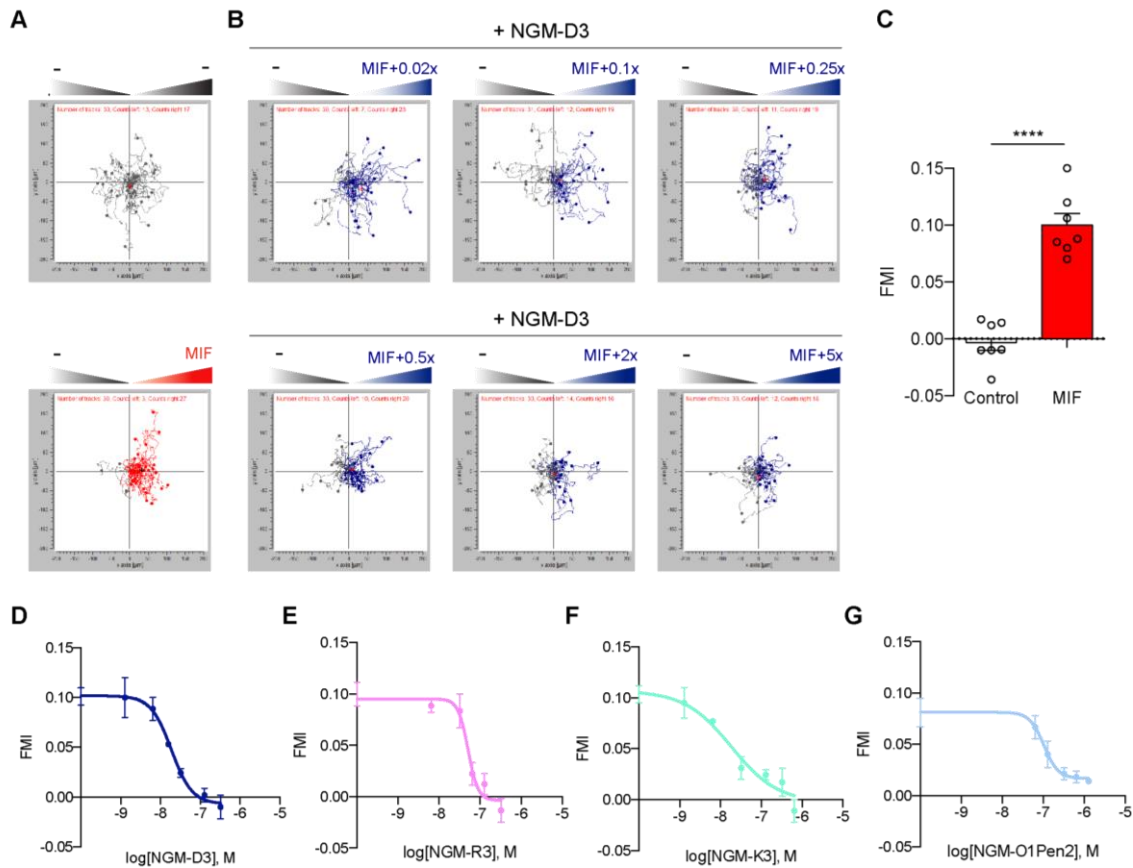


**Figure 17: Determination of IC<sub>50</sub> curves for the inhibitory effect of NGMs on MIF-induced 3D monocyte chemotaxis.** **A, B** Representative data reveal that NGM-D3 suppresses MIF-induced (red tracks) 3D chemotaxis of human monocytes in a dose-dependent manner, which was assessed by live-microscopy imaging of single-cell tracks in x/y direction in  $\mu\text{m}$ ; gradually increasing concentrations of NGM-D3 (blue tracks) is indicated as molar excess over MIF; unstimulated control (gray tracks) represents random motility. **C** Quantification of **A** (cells were treated with 64 nM MIF); the data points represent six independent experiments and the forward migration index (FMI) was plotted. In each experiment, the movement of 30 randomly selected cells was tracked. **D** Dose-response curves were plotted with MIF in the absence and presence of increasing concentrations of NGM-D3 (**D**), NGM-R3 (**E**), NGM-K3 (**F**), NGM-O1Pen2 (**G**) as indicated as log values (from three independent experiments, in each of which the movement of 30 randomly selected cells was tracked). Data are shown as means  $\pm$  SEM. \*\*\*\*,  $P < 0.0001$ . MIF, macrophage migration-inhibitory factor; NGMs, next generation mimics.

I tested the effect of the various NGMs and conducted dose-response curves to obtain their  $IC_{50}$  values. Forward migration index (FMI) was used to quantitate the degree of cell migration. FMI is a measure for directed, chemotactic cell migration. The normal FMI value for non-migrated cells is at about 0. The higher the FMI is, the stronger the chemotactic effect is. MIF (at a concentration of 64 nM) significantly increased the FMI of moving monocytes to 0.1 (**Figure 17C**). all four tested NGMs, NGM-D3, NGM-K3, NGM-R3, and NGM-O1Pen2, inhibited MIF-induced 3D monocyte chemotaxis in a dose-dependent manner (**Figure 17D, 17E, 17F, and 17G**). Except for NGM-O1Pen2, all other NGMs led to complete inhibition down to control level at their highest dose tested. The determined  $IC_{50}$  values for NGM-D3 and NGM-K3 are  $18.9 \pm 6.9$  nM and  $18.1 \pm 20.7$  nM, respectively. NGM-R3 and NGM-O1Pen2 showed lower inhibition potencies with an  $IC_{50}$  value of  $50.6 \pm 14.6$  nM and  $103.5 \pm 50.1$  nM, respectively.

### **3.2.3 Inhibitory potency of NGMs ( $IC_{50}$ curves) as assessed by Transwell B cell migration assay**

Previous work showed that MIF facilitates primary murine B lymphocyte migration through co-regulation of CXCR4 and CD74 (161). Addition of msR4M-L1 exerts a dose-dependent inhibitory effect on MIF-induced primary murine B lymphocyte migration, indicating that inhibitory effects of CXCR4 peptide mimics extend to B-cell migration responses and showing that the peptide inhibitor, which was designed based on the human CXCR4 ectodomain sequence, cross-inhibits murine MIF-mediated migration responses (200).  $IC_{50}$  curves were obtained for the inhibitory effect of NGMs on mouse B-cell migration. I treated freshly isolated mouse splenic B cells with 16 nM MIF, a concentration that was previously determined as a peak chemotactic MIF dose on B cells. 16 nM MIF enhanced the chemotactic index of mouse B cells by 1.6-fold (**Figure 18B**), in agreement with previous data (161). All tested NGMs led to a dose-dependent inhibition of MIF-elicited B-cell chemotaxis (**Figure 18**). The MIF effect was defined as 100%. Random migration as defined by control represented approximately 60%

of migration triggered by MIF.  $IC_{50}$  determinations showed that NGM-D3 had the most potent  $IC_{50}$  value ( $IC_{50} = 0.6 \pm 1.4$  nM), but maximal inhibition leveled off at 37%. The  $IC_{50}$  for NGM-R3 was  $14.4 \pm 9.3$  nM and the lowest reached inhibition value for this NGM was at around 50% of MIF. NGM-K3 had an  $IC_{50}$  of  $7.8 \pm 8.0$  nM and the  $IC_{50}$  of NGM-O1Pen2 was  $19.9 \pm 10.4$  nM with maximum inhibition plateauing at 35-40% of MIF effects. Together, NGM-D3, NGM-R3, NGM-K3, and NGM-O1Pen2 can block 100% of migratory effects of B cells induced by MIF. NGM-D3 and -K3 were the most efficient inhibitors in MIF-elicited murine B-cell chemotaxis.

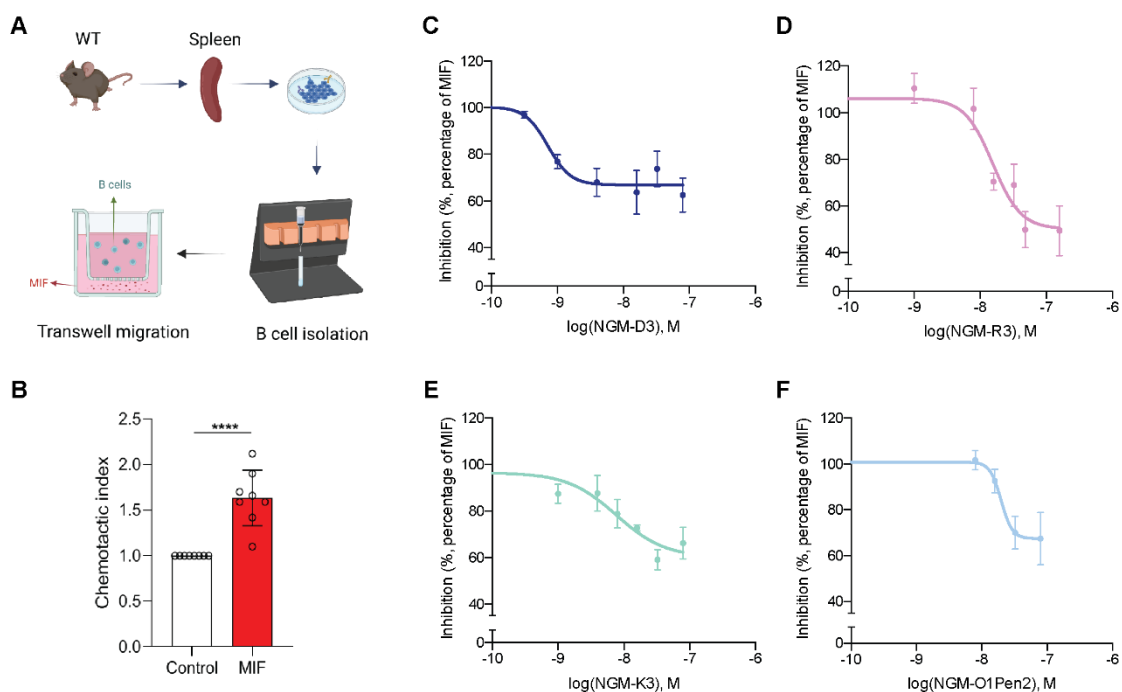


**Figure 18: Determination of  $IC_{50}$  curves for the inhibitory effect of NGMs on MIF-induced murine B-cell chemotaxis.** **A** Illustration of murine B-cell isolation from the mouse spleen using magnetic beads and principle of the Transwell-based 2D chemotaxis set-up. **B** MIF increases mouse B-cell chemotactic migration. Recombinant mouse MIF was added at its peak chemotactic concentration of 16 nM. Dose-response curves for NGM-D3 (**C**), NGM-R3 (**D**), NGM-K3 (**E**), and NGM-O1Pen2 (**F**) were plotted with MIF in the absence and presence of various concentrations of NGMs as being indicated as log values (three or four times independent experiments). Random migration represents 60% of B-cell migration elicited by MIF. NGMs inhibit MIF-mediated mouse B cell chemotaxis in a dose-dependent manner. Data are shown as means  $\pm$  SEM. \*\*\*\*,  $P < 0.0001$ . MIF, macrophage migration-inhibitory factor; NGMs, next generation mimics.

In aggregate, the inhibitory properties and determined IC<sub>50</sub> values of the CXCR4 ectodomain-derived NGMs as assessed in the above atherogenic assays indicated that peptide mimic NGM-D3 appeared to exhibit the most promising MIF-antagonizing inhibitor.

### **3.2.4 Determining the selectivity of NGMs between MIF and CXCL12**

The biochemical binding studies performed by our collaborators at TUM suggested that NGM-D3 and NGM-O1Pen2 were highly selective for MIF, while NGM-R3 and NGM-K3 also displayed high affinity binding to CXCL12. Here, I aimed to determine whether these selectivity properties would also extend to the inhibitory potential of the NGMs in atherogenic cell assays.

#### **3.2.4.1 NGM effects on CXCL12-mediated murine B-cell migration**

The first generation ectodomain-derived MIF inhibitor msR4M-L1 has a high selectivity for MIF without disrupting CXCL12/CXCR4 signaling. However, any sequence or linker change might alter the binding and/or activity features. As shown above, all four tested NGMs exhibited inhibitory activity against MIF with IC<sub>50</sub> values in the range of 10-100 nM. To test their selectivity for MIF over CXCL12, I first performed Transwell-based murine B-cell chemotaxis experiments, this time using CXCL12 as the chemoattractant. I applied two concentrations of NGMs (2x and 5x molar excess over CXCL12), as these excess ratios produced optimal inhibitory impacts on MIF. In line with the biochemical binding data performed by our collaborators, NGM-D3 did not inhibit CXCL12-mediated B-cell chemotaxis (**Figure 19**). Similarly, NGM-R3, NGM-K3, and NGM-O1Pen2 did not affect CXCL12-driven B-cell migration (**Figure 19**). This latter observation only partially concurred with the binding data, as NGM-R3 and NGM-K3 showed nanomolar binding to CXCL12, but did not lead to an inhibition of CXCL12-mediated B-cell chemotaxis. Overall, these data indicated that NGMs, despite their drastic reduction in size compared to msR4M-L1, can preserve the selectivity of msR4M-L1 for MIF/CXCR4 signaling over the CXCL12/CXCR4 axis.

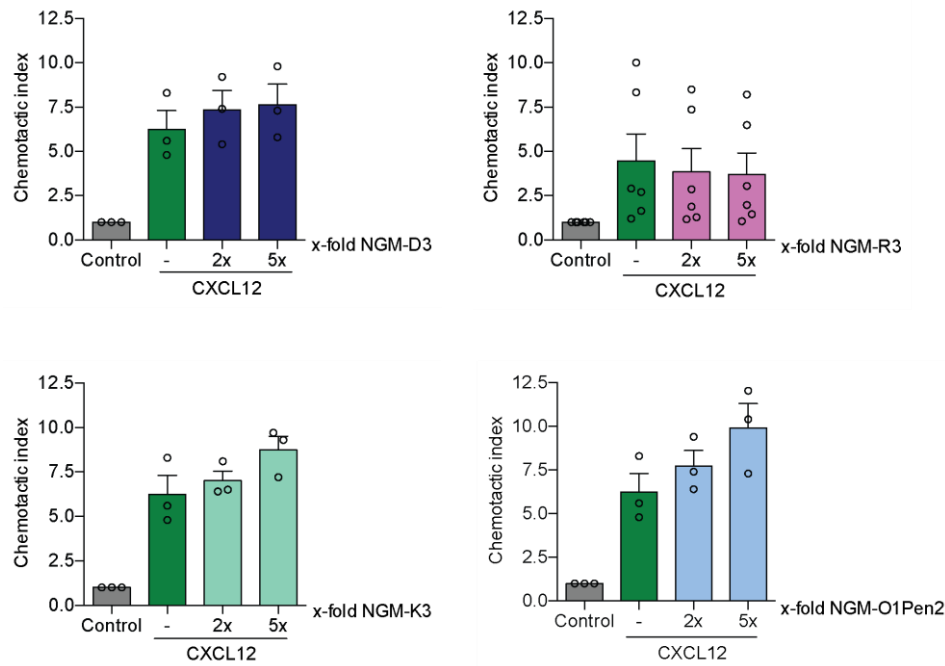


**Figure 19: NGMs do not inhibit CXCL12-mediated murine B-cell migration in a Transwell setting.** CXCL12 was used at a concentration of 16 nM, at which it increased mouse B-cell migration by 4-6-fold. NGMs were applied at 2- and 5-fold molar excess over CXCL12. Chemotaxis is plotted as chemotactic index. Data are shown as means  $\pm$  SEM (from three or six independent experiments as indicated). CXCL12, C-X-C motif chemokine 12; NGMs, next generation mimics.

### 3.2.4.2 NGM effects on CXCL12-mediated 3D monocyte chemotaxis

To further assess the selectivity of NGMs, I performed 3D human monocyte chemotaxis experiment using CXCL12 as chemoattractant (**Figure 20**). CXCL12 significantly increased monocyte migration (FMI  $\sim$  0.1). Similar to the results obtained in the murine B-cell migration studies, NGM-D3 and NGM-K3 did not affect CXCL12-induced monocyte chemotaxis. NGM-O1Pen2 showed a trend towards decreasing monocyte chemotaxis, but this effect did not reach statistical significance. In contrast, NGM-R3 profoundly blocked CXCL12-mediated monocyte migration.

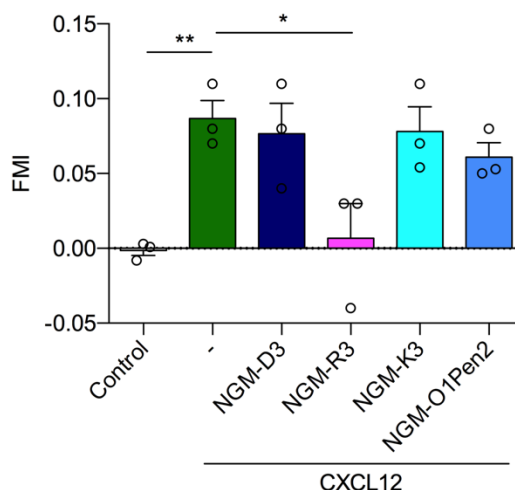


**Figure 20: Differential effects of NGMs on CXCL12-mediated 3D human monocyte chemotaxis.** CXCL12 was applied at a concentration of 64 nM, at which it significantly increased monocyte motility towards CXCL12. NGMs were applied at a 10-fold molar excess over CXCL12. Data are shown as means  $\pm$  SEM and are derived from three independent experiments; in each experiment 30 randomly selected monocyte trajectories were tracked. \*\*,  $P < 0.01$ . \*,  $P < 0.05$ . CXCL12, C-X-C motif chemokine 12; NGMs, next generation mimics.

### 3.2.5 Summary of the inhibitory potential ( $IC_{50}$ values) and selectivity of the NGMs

**Table 1** summarizes the  $IC_{50}$  values and maximum inhibitory effects obtained in the three atherogenic assays for NGM-D3, R3, K3, and O1Pen2 compared to msR4M-L1. For comparison, Table 1 also lists the binding affinities ( $K_D$  values) provided by our collaborators at TUM. Together, this indicates that the next generation CXCR4 mimics preserve the MIF-inhibitory effect of msR4M-L1, while retaining some of its selectivity. Most notably, the mimics with high solubility (data from the collaborators), including NGM-D3, R3, and K3, showed higher  $IC_{50}$  values than NGM-O1Pen2. The binding data from the collaborators indicate NGM-R3 and -K3 did bind to CXCL12 with appreciable affinity. Additionally, the inhibition of NGM-R3 on monocyte chemotaxis triggered by CXCL12 is quite prominent at 5x fold molar excess. The dual inhibition of MIF and CXCL12 seen in NGM-R3 could be potentially employed in cancer therapy. In the application of atherosclerotic disease, NGM-D3 stands out with multiple advantages, such as improved solubility, high binding affinity to MIF, and no interaction with CXCL12.



Table 1: Summary of IC<sub>50</sub> values of NGMs obtained from screening using *in vitro* cell assays mimicking atherogenic processes.

CXCR4 ectodomain mimics	OxLDL uptake		3D monocyte chemotaxis		2D mouse B cell migration		K <sub>D</sub> values*** (nM)	
	IC <sub>50</sub> values* (nM)	Maximum effect (%)	IC <sub>50</sub> values* (nM)	Maximum effect (%)	IC <sub>50</sub> values* (nM)	Maximum effect (%)	Fluos- peptide/MIF	Alexa- MIF/peptide
msR4M-L1	115.2 ± 97.5	51	55	100	10	70	40.7 ± 4.0	31.1 ± 16.6
NGM-D3	4.6 ± 5.7	65	18.9 ± 6.9	100	0.6 ± 1.4	67	36 ± 22.2	246.5 ± 21.7
NGM-R3	10.7 ± 3.4	54	50.6 ± 14.6	100	14.4 ± 9.3	50	16.8 ± 6.2	110.1 ± 28.1
NGM-K3	8.2 <sup>#</sup>	62	18.1 ± 20.7	100	7.8 ± 8.0	59	36.4 ± 7.5	44.7 ± 10.3
NGM- O1Pen2	63.5 ± 171.4	58	103.5 ± 50.1	85	19.9 ± 10.4	67	14.3 ± 5.7	41.8 ± 16.4

\* IC<sub>50</sub> values, concentrations of msR4M-L1 and NGMs that reduced the activity of MIF by 50%; data are shown in mean ± SD; <sup>#</sup> SD value was not available; \*\* maximum effect reached at highest dose (%), the normalized maximum inhibitory effect of msR4M-L1 and NGMs; \*\*\* K<sub>D</sub> values obtained for msR4M-L1 and NGM binding to MIF by fluorescence titration spectroscopy were kindly provided by Dr. C. Kontos and Prof. Dr. A. Kapurniotu (TUM). NGMs, next generation mimics; IC, inhibitory concentration; 2D/3D, 2-/3-dimensional.

### 3.3 Degradation and albumin binding characteristics of NGM-D3

Half-life is a measure to estimate how long it takes for a drug to be eliminated from the body. It is associated with bioavailability required for the optimal action. Short half-life is one of the major challenges in the development of peptide drugs. Thus, it is imperative to determine the half-life of NGM-D3.

#### 3.3.1 Proteolytic stability of TAMRA-NGM-D3 in human plasma

Proteolytic stability studies of the first generation CXCR4 mimic msR4M-L1 indicated that this peptide had good plasma stability with approximately 30% of TAMRA-msR4M-L1 preserved after 48 h exposure in mouse or human plasma. Before moving forward to *in vivo* studies, I tested the proteolytic stability of NGM-D3 in human plasma for an extended period of time (up to 7 days) using Tricine SDS-PAGE analysis as previously established for msR4M-L1(200). For detection purposes, a fluorescently labeled analog of NGM-D3 (N-terminal modified TAMRA-NGM-D3) was used and quantified after SDS-PAGE by infra-red Odyssey imaging. TAMRA-NGM-D3 showed appreciable plasma stability, with the TAMRA-NGM-D3 band detectable up to 120 h of plasma exposure (**Figure 21**). Overall, the observed plasma stability for TAMRA-NGM-D3 was similar to that of TAMRA-msR4M-L1.

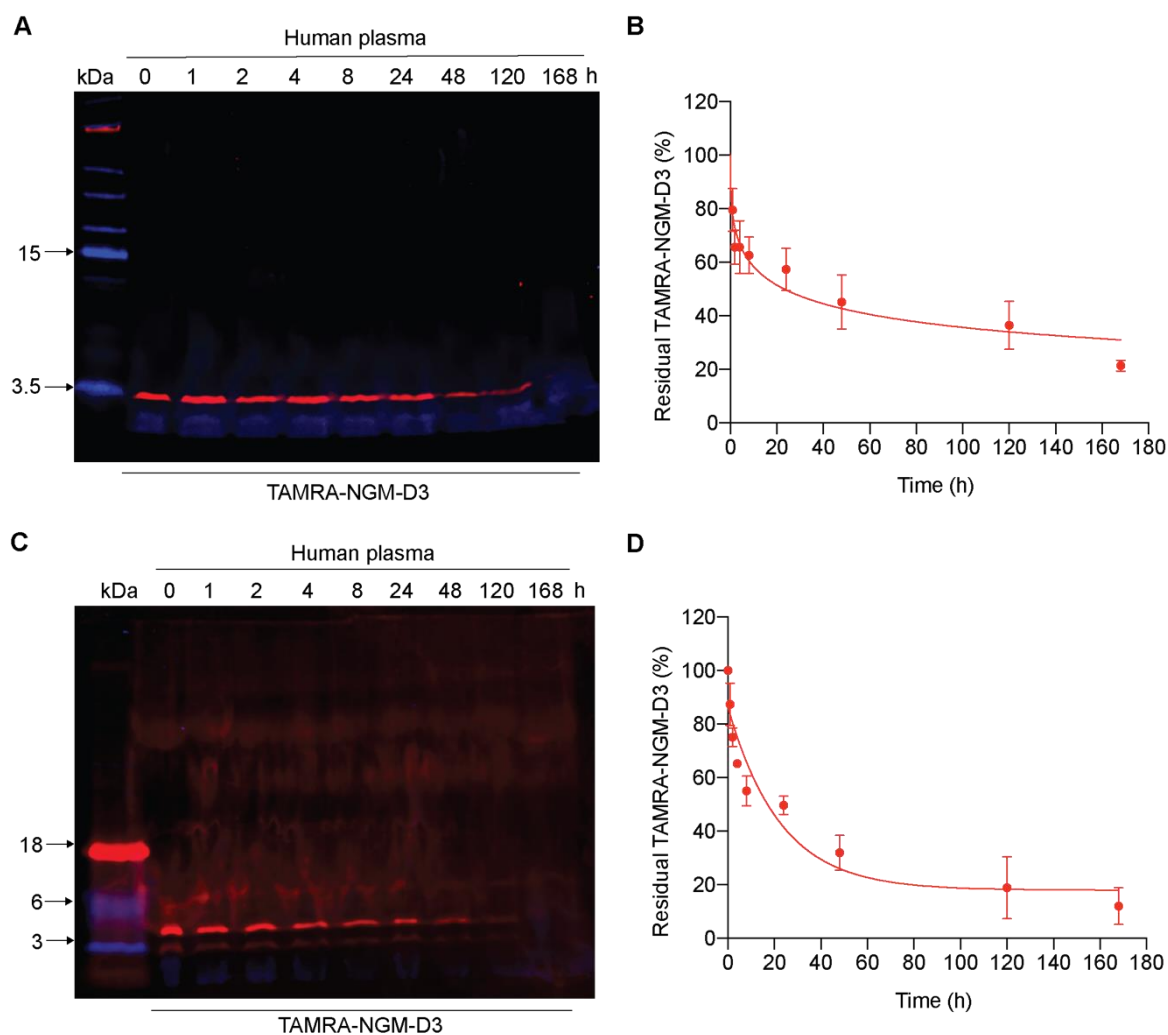


**Figure 21: TAMRA-NGM-D3 reveals appreciable proteolytic stability in human plasma.** **A** C 500 nM TAMRA-NGM-D3 was incubated in human plasma at 37°C over the time course of 0, 1, 2, 4, 8, 24, 48, 120, and 168 h. Samples were processed with DTT (**A**) and without DTT (**C**) then was loaded on a Tricine SDS-PAGE gel (red band, TAMRA-NGM-D3; blue band, running dye); **B** Nonlinear curve fitting (concentration vs time) for the degradation of TAMRA-NGM-D3 in human plasma. Data are shown as means  $\pm$  SEM and represent three independent experiments. **D** Nonlinear curve fitting (concentration vs time) for the degradation of TAMRA-NGM-D3 in human plasma. Data are shown as means  $\pm$  SEM (three times independent experiments).

According to the nonlinear curve fitting analysis of the TAMRA-NGM-D3 band in **Figure 21B**, the estimated half-life of TAMRA-NGM-D3 is 23.2 hours, showing reasonably good stability for a small peptide and being in line with the half-life previously determined for TAMRA-msR4M-L1 (200). I also performed SDS-PAGE electrophoresis under non-reducing conditions, meaning that the samples after plasma incubation of NGM-D3 were not processed by the

reducing agent, dithiothreitol (DTT). The curve (**Figure 21D**) manifested the same trend as **Figure 21B**. Overall, the SDS-PAGE gel was less “clean” and contained several bands and shadows that could represent disulfide-bonded oligomers or heteromers with plasma components. Three bands were noted that appeared to represent TAMRA-NGM-D3; these were an apparent monomer at 3 kDa, an apparent dimer at approximately 5 kD, and a band at around 6-8 kD, which could be a trimer or tetramer. Further blurred bands appeared in the high-molecular weight range of the gel between 40 and 80 kD, which might represent NGM-D3 bound to plasma proteins such as albumin by mixed disulfide formation. The estimated half-life acquired from the curve fit of TAMRA-NGM-D3 in **Figure 21D** was 15.6 hours. The disparity of half-lives acquired from the two approaches is considered in the range of experimental variations. Together, the plasma half-lives implicated that NGM-D3 has an overall good stability in human plasma.

### 3.3.2 Investigation of the interaction between albumin and NGM-D3

Based on the appreciable plasma stability of TAMRA-NGM-D3 as determined by *in vitro* incubations with human plasma, I wondered what mechanism could potentially protect TAMRA-NGM-D3 from more rapid degradation. One study found that human serum albumin (HSA) generates an endogenous peptide that antagonizes CXCR4 activity by binding to a region close to extracellular loop 2 of CXCR4 (213). In turn, this implicates that CXCR4 mimics encompassing ECL2 residues may have a binding affinity for albumin. Also, the above performed SDS-PAGE analysis of TAMRA-NGM-D3 following human plasma exposure showed diffuse weak bands in the 40-80 kD range, potentially indicating that NGM-D3 may partially form mixed disulfides with albumin.

To further investigate the possibility that NGM-D3 may covalently or non-covalently interact with albumin, I incubated red fluorescently-labeled Cy7.5-NGM-D3 with increasing concentrations of green fluorescently-labeled FITC-HSA or unlabeled HSA for 0 h and 2 h, and

imaged the resulting band patterns via Tricine SDS-PAGE under either reducing or non-reducing conditions. SDS-PAGE analysis under non-reducing conditions in **Figure 22** indicates that, in addition to the Cy7.5-NGM-D3 bands at 3 kD, 4-6 kD, and 6-8 kD, part of the Cy7.5-NGM-D3 fluorescence signal colocalizes with the FITC-HSA and unlabeled HSA bands at around 65 kD, following 2 h of coincubation of Cy7.5-NGM-D3 and FITC-HSA or unlabeled HSA, but not at time 0 h. The upper band fluorescence of Cy7.5-NGM-D3 enhanced as the concentration of HSA increased. The unbound fraction of Cy7.5-NGM-D3 at the bottom is most likely due to the saturation of binding. The unbound form of Cy7.5-NGM-D3 remained the same as the bound form increased. The maximum concentration (100x) of HSA applied is 3.3 g/L, which is 10 times lower than the normal range in circulation (35-50 g/L).

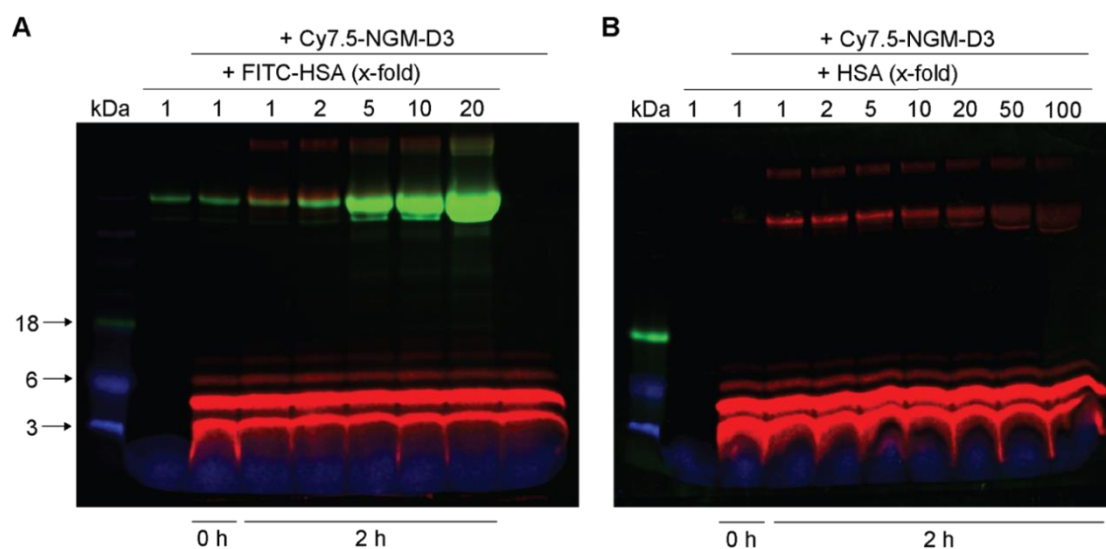


**Figure 22: Cy7.5-NGM-D3 partially co-electrophoreses with human serum albumin.** **A** 500 nM Cy7.5-NGM-D3 was incubated with increasing concentration of FITC-HSA (1-, 2-, 5-, 10-, and 20-fold molar excess of Cy7.5-NGM-D3) in PBS for 0 h and 2 h and imaged using red and green fluorescence channels following Tricine SDS-PAGE under non-reducing conditions (red band, Cy7.5-NGM-D3; green band, FITC-HSA; blue band, running dye). **B** 500nM Cy7.5-NGM-D3 was incubated with increasing concentrations of HSA (1-, 2-, 5-, 10-, 20-, 50-, and 100- fold molar excess of Cy7.5-NGM-D3) in PBS for 0 h and 2 h, then imaged using a red fluorescence channel following Tricine SDS-PAGE under non-reducing conditions (red band, Cy7.5-NGM-D3; blue band, running dye). Left hand lanes, molecular weight marker (kDa).

Next, I studied peptide-albumin binding under reducing Tricine SDS-PAGE conditions. Unlike the colocalization of Cy7.5-NGM-D3 and albumin under non-reducing conditions, the upper albumin-colocalizing band of Cy7.5-NGM-D3 was not detectable (**Figure 23**). As there is one cysteine residue present in the NGM-D3 sequence, peptide-albumin complex might, at least partially, be based on the formation of a mixed disulfide bond between NGM-D3 and albumin.

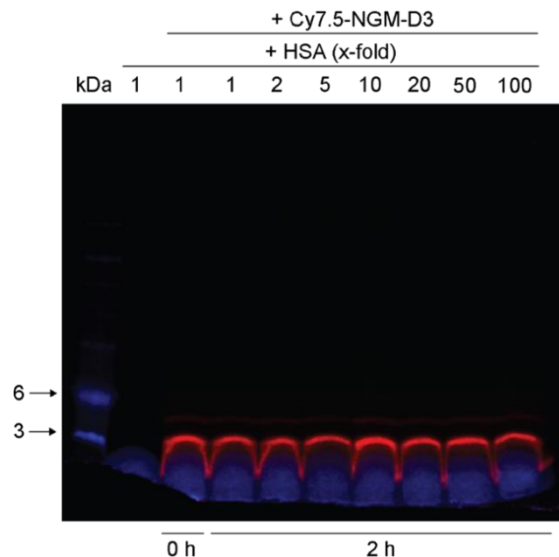


**Figure 23: The interaction of Cy7.5-NGM-D3 with human albumin is dependent on disulfide bonds.** 500 nM Cy7.5-NGM-D3 was incubated with increasing concentrations of HSA (1-, 2-, 5-, 10-, 20-, 50-, and 100-fold molar excess of Cy7.5-NGM-D3) in PBS for 0 h and 2 h, then imaged on Tricine SDS-PAGE gel (reducing condition; Red band, Cy7.5-NGM-D3; Blue band, marker). Left hand lanes, molecular weight marker (kDa).

### 3.3.3 Investigation of the interaction between NGM-D3 and albumin using native PAGE

The above described Tricine SDS-PAGE analyses were performed in the presence of SDS, i.e. a strong denaturing agent, which dissociates essentially all non-covalent protein complexes. Native electrophoresis does not contain denaturing agents and allows protein complexes to keep their natural interactions. It is a powerful tool for examining weak interaction forces between proteins and is used to study protein-protein-interactions (PPIs). However, the interpretation of the PAGE band pattern is more complicated because, owing to the lack of the “SDS charge effect”, proteins don’t run according to their size but electrophoretic running

behavior is governed by charge and size. I performed native electrophoresis after incubating Cy7.5-NGM-D3 with increasing concentrations of FITC-HSA or unlabeled HSA for 0 and 2 h. As shown in **Figure 24**, the Cy7.5-NGM-D3 band appeared alongside the labeled- or unlabeled HSA after 2 h but not 0 h incubation. The assembly of protein complexations is considered a dynamic process. Absence of Cy7.5-NGM-D3 at 0 h incubation supports the interaction between NGM-D3 and albumin.

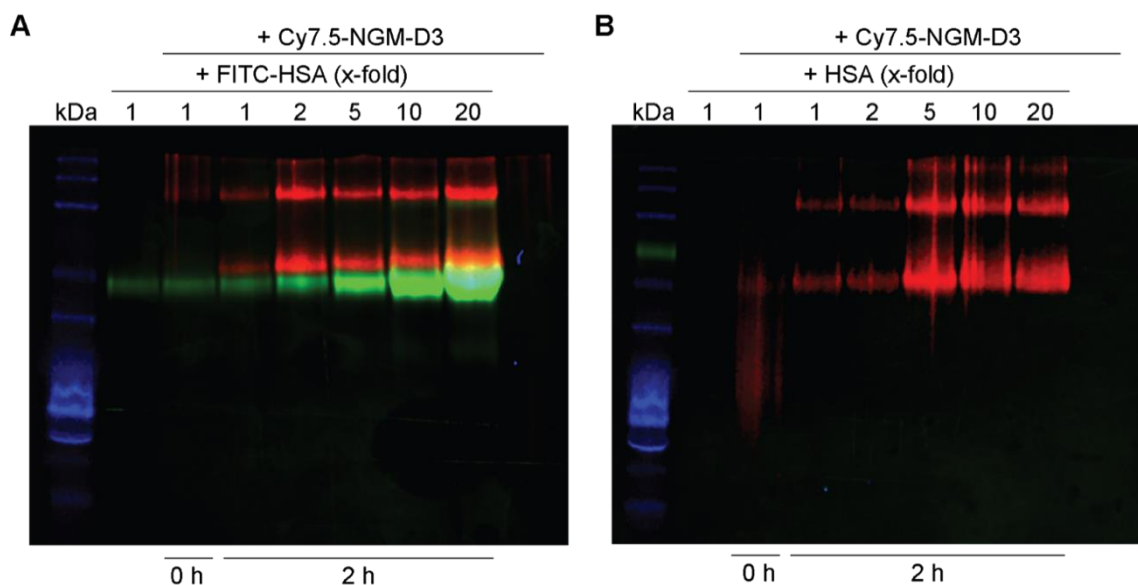


**Figure 24: Cy7.5-NGM-D3 interacts with human serum albumin in a dose-dependent manner – evidence from native PAGE analysis.** Native electrophoresis was used to identify the peptide-albumin protein complex formation. 500nM Cy7.5-NGM-D3 was incubated with increasing concentrations of **A** FITC-HSA or **B** HSA (1-, 2-, 5-, 10-, and 20- fold molar excess of Cy7.5-NGM-D3) in PBS for 0 h and 2 h, then imaged on the native tris-glycine gel (red band, Cy7.5-NGM-D3; green band, FITC-HSA; blue band, marker). The gels shown are representative of  $n = 3$  experiments.

Overall, the data from atherogenic cell assays suggest that the NGMs have well-preserved inhibitory effects against MIF. In contrast to msR4M-L1 and NGM-O1Pen2, NGM-D3, -R3, and -K3 are characterized by enhanced binding affinity and solubility. NGM-D3 and NGM-O1Pen2 showed robust inhibition on MIF over CXCL12, whereas NGM-R3 revealed prominent dual-inhibition on MIF and CXCL12. The selectivity of NGM-K3 needs to be further investigated because of inconsistency of *in vitro* data with biophysical evidence. The most promising

candidate peptide, NGM-D3, demonstrated good stability in plasma and I obtained evidence that it interacts with albumin. Further experiments will have to conclusively determine, whether this is covalent – disulfide-mediated – interaction or a non-covalent interaction.

### 3.4 Therapeutic effects of NGM-D3 in early plaque development

Mice are an attractive and effective animal model for the research of atherosclerosis. Two breeds of single gene deletion mice are commonly used in many studies, *ApoE*<sup>-/-</sup> and *Ldlr*<sup>-/-</sup> mice in the C57BL/6 background. Based on my above results, which showed a promising inhibitory activity profile of NGM-D3 in various atherogenic cell assays and good plasma stability, I next studied the inhibitory potency of NGM-D3 in a mouse atherosclerosis model.

The previous study on the parent-molecule msR4M-L1, tested in an *ApoE*<sup>-/-</sup> model of early atherogenesis, found that *ApoE*-deficient mice receiving msR4M-L1 intervention in parallel to a 4.5-week atherogenic high-fat diet (HFD) developed less pronounced lesions and had a lower number of plaque macrophages than mice receiving vehicle control. I therefore tested NGM-D3 in an *ApoE*<sup>-/-</sup> model of early atherogenesis as well. Mice were randomly assigned into two groups and fed an HFD for 5 weeks to induce early atherosclerosis. In parallel to HFD feeding, mice were either untreated or treated three times a week with 50 µg of NGM-D3 (corresponding to 2.5 mg/kg) each time (**Figure 25**).



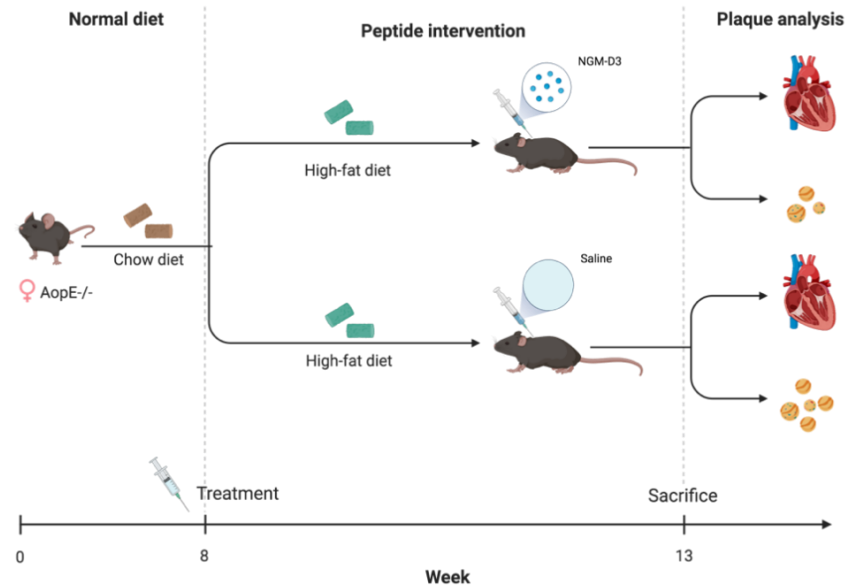


**Figure 25: Experimental scheme.** Female, 8-week-old *ApoE*<sup>-/-</sup> mice were randomized into two groups and fed a cholesterol-rich Western-type high-fat diet (HFD) for 5 weeks to develop early stage of plaques. 50  $\mu$ g NGM-D3 or saline were administered simultaneously to each mouse three times a week via intraperitoneal injection. During the time course of treatment, mice were monitored regularly, weighed weekly, and sacrificed after 5 weeks. Heart and peripheral blood were collected for lesion and inflammatory profiling analysis.

### 3.3.1 Treatment with NGM-D3 does not attenuate plaque development and lesional macrophage content in an *ApoE*<sup>-/-</sup> mouse model or early atherogenesis

To examine the potential anti-atherogenic therapeutic effect of NGM-D3, I analyzed the cross-sections from untreated and treated mice groups and quantified the plaque area in aortic roots using Oil Red O staining and HE staining (**Figure 26A and B**). NGM-D3 did not significantly decrease the plaque size (**Figure 26C and D**). Although there was a trend towards plaque reduction, NGM-D3 did not significantly attenuate plaque development in this early model of atherogenesis.

To further investigate the effect of NGM-D3 on plaque phenotype and assess its impact on inflammation, I performed CD68 immunofluorescence staining in aortic root sections from

untreated and treated mice and quantified the CD68-positive area, both expressed as total area and as percentage of lesion area. NGM-D3 did not show any impact on macrophage content in the aortic root in the 5-week HFD early atherogenesis (**Figure 26E**).

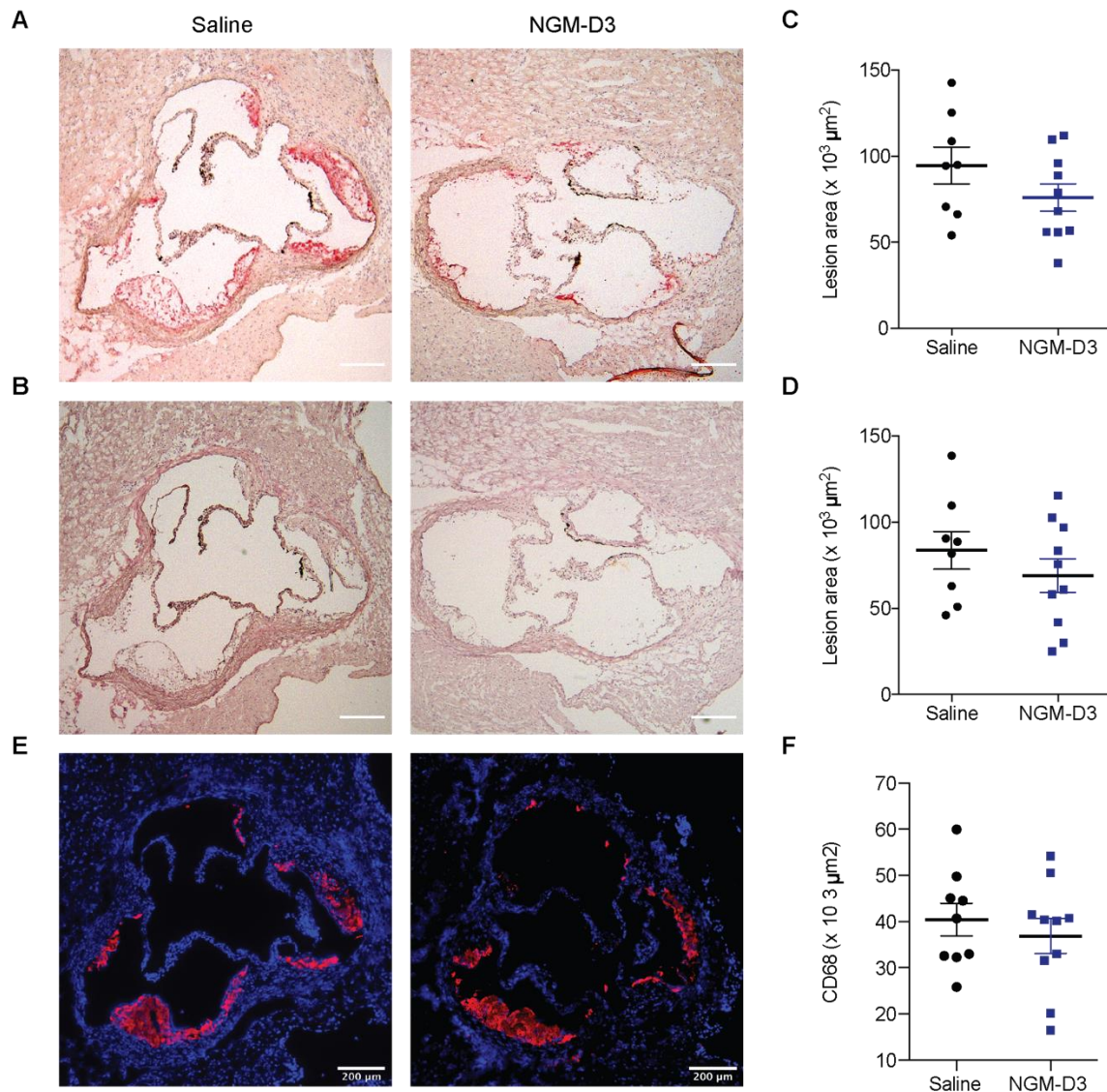


**Figure 26: Lesions and macrophage content were not significantly altered by NGM-D3 in 5-week HFD *Apoe*<sup>-/-</sup> mice.** Representative images of **A** Oil Red O-stained and **B** HE-stained lesions in aortic root from 5 weeks untreated and NGM-D3 treated mice are shown. Scale bars = 200 μm. **C, D** Cross-sectional analysis of atherosclerotic plaque area in the aortic root (saline n=8 mice; NGM-D3 n=10 mice). **C** Quantification of the oil red O-positive area in both groups. **D** Quantification of HE staining. **E** Representative immunofluorescence staining for CD68 in aortic root lesions after 5 weeks of HFD and NGM-D3 versus saline treatment (n=8-10 mice/group). Quantification is shown in **F**. Data are indicated as mean ± SEM. *P* values were calculated by Student *t* test; plaque size and macrophage content did not significantly differ between both groups

### 3.3.2 Circulating T-cell numbers are reduced in mice subjected to NGM-D3 treatment

Circulating immune cells represent an important part of systemic immune response, and they are the major source of recruited leukocytes contributing to lesion progression. To evaluate a potential impact of NGM-D3 on circulating leukocytes, I quantified T cell, B cell, neutrophil, and monocyte numbers in the circulation using flow cytometric marker analysis. The gating strategy is shown in **Figure 27**.

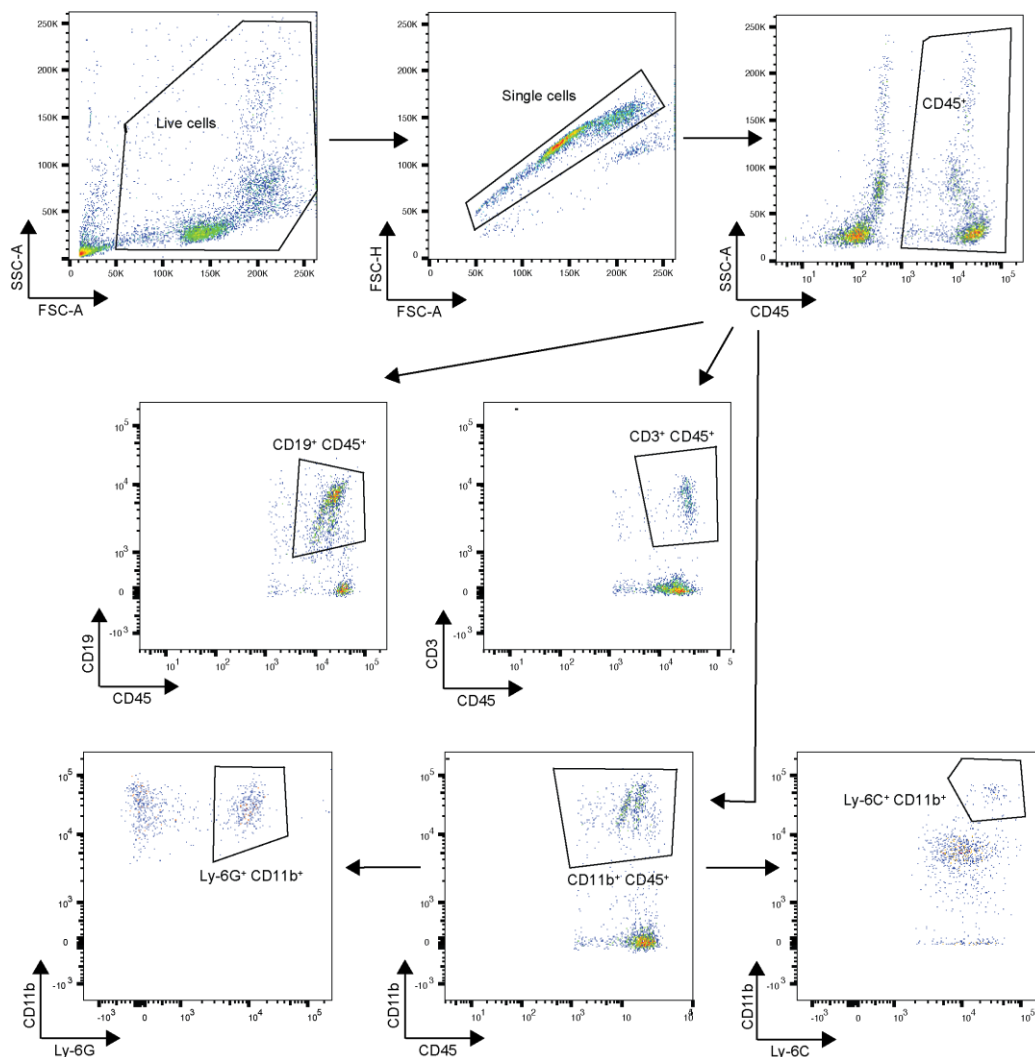


**Figure 27: Gating strategy for different leukocyte populations in circulation.** Circulating leukocytes were isolated from *ApoE*<sup>-/-</sup> untreated and treated mice and single cells were gated based on FSC-H and A. Total leukocytes were labeled with CD45. T cells and B cells are defined as CD3<sup>+</sup> and CD19<sup>+</sup>, respectively. Monocytes and neutrophils are defined as CD11b<sup>+</sup>Ly6C<sup>+</sup> and CD11b<sup>+</sup>Ly6G<sup>+</sup>. FSC, forward scatter cytometer; SSC, side scattered light.

Total CD3<sup>+</sup> T-cell percentage showed a 30% reduction in mice receiving NGM-D3 compared to the saline group (**Figure 28**). In contrast, B-cell, neutrophil and monocyte percentages remained unchanged (**Figure 28**).

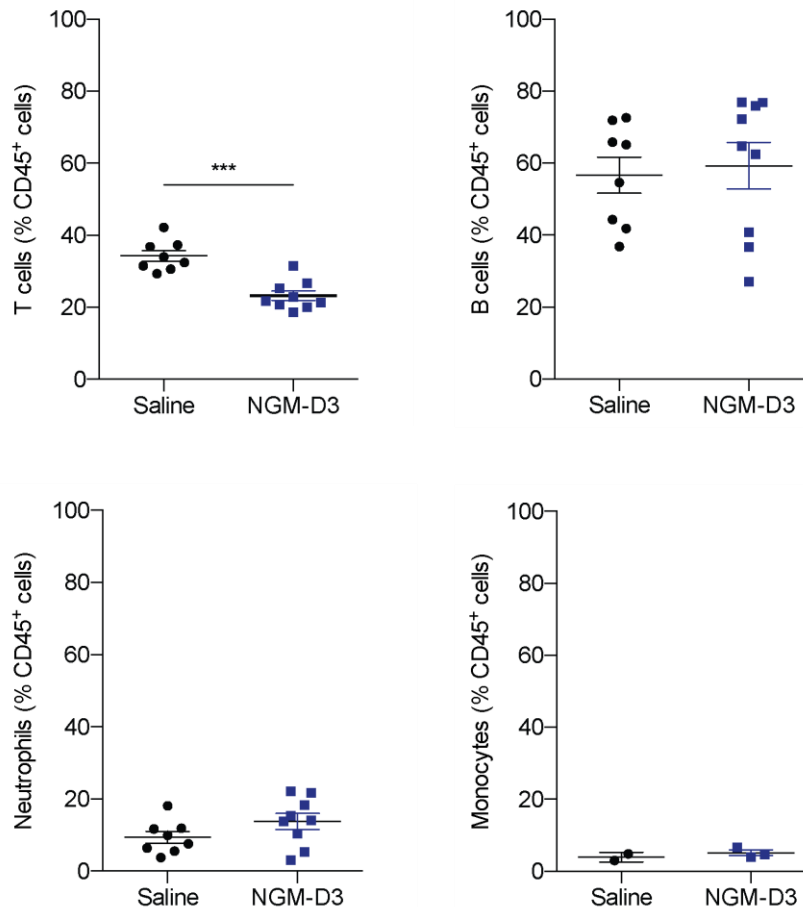


**Figure 28: Effect of NGM-D3 treatment on circulating leukocyte counts.** The total leukocyte number was determined via the CD45<sup>+</sup> marker. Quantification of CD3<sup>+</sup> T cells, CD19<sup>+</sup> B cells, CD11b<sup>+</sup> Ly6G<sup>+</sup> neutrophils (n=8-10 mice/group), and CD11b<sup>+</sup> Ly6C<sup>+</sup> monocytes (n=2-3 mice/group) is expressed as percentage of CD45<sup>+</sup> cells. Data are shown as mean ± SEM. *P* values were calculated by Student *t* test. \*\*\*, *P* = 0.001.

Mice weights were monitored every week. However, no difference was observed between the two groups, which also indicated that NGM-D3 has no effect on body weight (**Figure 29**).

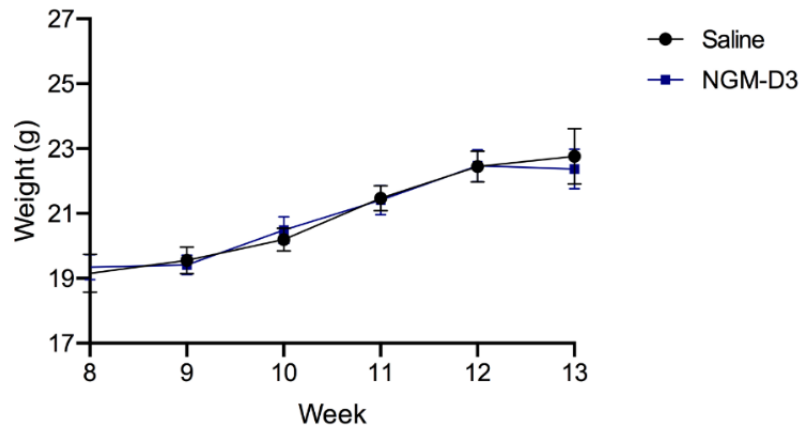


**Figure 29: Weight change over the course of the 5-week HFD diet.** During the 5-week HFD and treatment period, mice were weighed every week starting from 8 weeks. No difference was observed between two groups.

Although the next generation MIF/CXCR4 peptide inhibitor NGM-D3 did not have a significant attenuating effect early phase atherosclerotic lesion formation and plaque macrophage content after 5-week HFD, NGM-D3 treatment led to significantly reduced blood T-cell counts, indicating an impact of the peptide on the immune and inflammatory response in this early-stage atherosclerosis model.

#### **3.4.4 Bulk RNA-seq unveils numerous differentially expressed genes in NGM-D3 treated atherogenic mice**

To determine whether NGM-D3 may have had an impact on plaque inflammation and phenotype despite an lack of effect on lesion size, I next examined the plaque transcriptome by performing bulk RNA sequencing of freshly frozen aortic root plaque tissues. We made use of a recently developed procedure to isolate bulk RNA from frozen tissue sections and adapted the method to aortic root atherosclerotic plaque tissue. Following RNA extraction, libraries were prepared for bulk RNA-sequencing on DNB-seq platform for paired-end sequencing, comparing plaque tissue from NGM-D3-treated and vehicle-treated mice. Transcriptomic profiles of mice receiving NGM-D3 clustered together and segregated from those of mice

receiving saline, indicating that the transcriptional landscape of treatment group was remarkably altered compared to control (**Figure 30**).

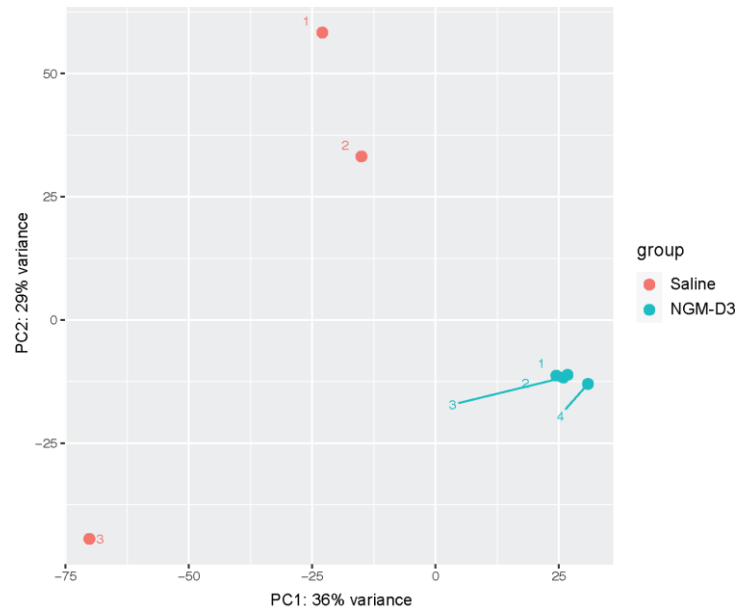


**Figure 30: Principal component analysis (PCA) of RNA-seq data of atherosclerotic plaque samples from saline- and NGM-D3-treated mice.** PC1 and PC2 indicate principal component 1 and 2. Mice number are indicated as dots (red, saline; blue, NGM-D3). Blue connecting lines indicate sample 3 and 4 in NGM-D3-treated group.

Differential gene analysis identified 2578 differentially regulated transcripts, in which 1639 transcripts were up-regulated and 939 transcripts were down-regulated in NGM-D3 treated mice compared to saline-treated mice (adjusted  $P$  value  $< 0.05$ ; fold change  $> 2$ ; see **Figure 32A**). Highly differentially expressed genes are indicated in **Figure 31** (adjusted  $P$  value  $< 1 \times 10^{-5}$ ; fold change  $> 2$ ). Several genes contributing to fatty acid metabolism such as *Ffar3*, *Fabp1* were significantly downregulated. Genes that have been reported to positively correlate to coronary artery disease were identified in untreated mice, including *Mia*, *Serpina1d*, *Fn1*. Genes that are conventionally involved in cardiac contractile function and energy metabolism, such as *Myl7*, *Tnnt2*, *Acta2*, were profoundly upregulated upon NGM-D3 intervention.



resident-like macrophage marker genes such as *Lyve1* or *Ccl24*, were up-regulated in the NGM-D3 group (**Figure 32B**).

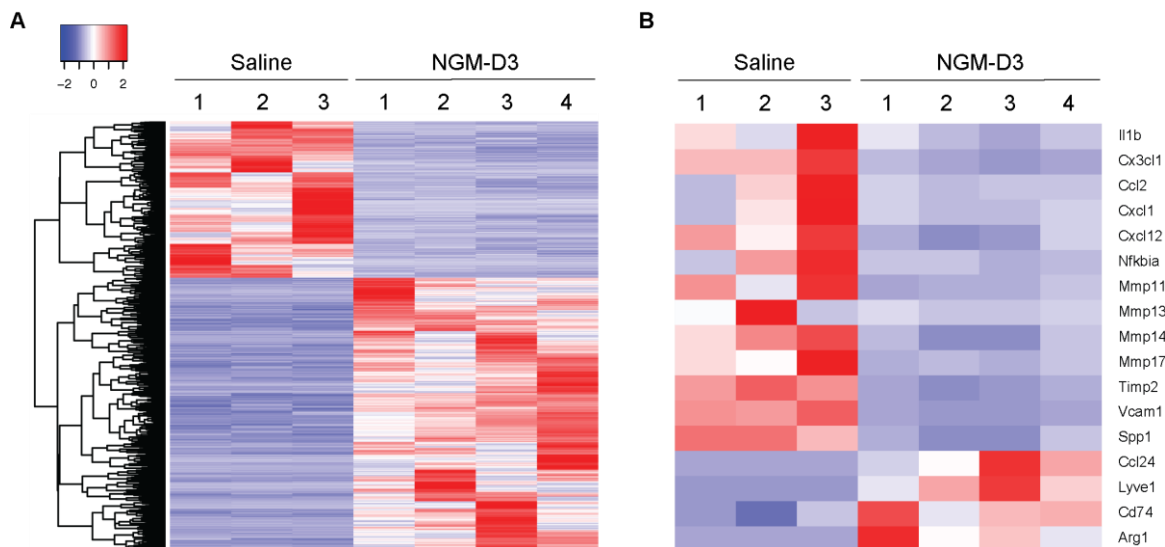


**Figure 32: Transcriptome analysis reveals distinct gene expression between saline and NGM-D3 treated mice.** **A** Heatmap shows all the differentially expressed genes in saline- and NGM-D3-treated mice. **B** Heatmap of selected pro-inflammatory and atherogenic genes enriched in mice receiving saline and selected genes enriched in mice receiving NGM-D3. Differentially regulated genes were filtered with an adjusted  $P < 0.05$  and fold change  $> 2$ .

NGM-D3 administration substantially altered the global transcriptomic atlas of plaques, which ultimately led to abundant downregulation of pro-atherogenic genes and augmentation of energy-promoting genes.

### 3.4.5 NGM-D3 attenuates multiple atherogenesis-related pathways

To gain more insights into understanding of the impact of NGM-D3 on the plaque transcriptome, I next performed pathway analyses. Gene ontology (GO) enrichment and KEGG pathway analysis displayed that the down-regulated genes are predominantly enriched in extracellular matrix (ECM) organization ( $P_{adj} = 2.61e-32$ ), focal adhesion ( $P_{adj} = 4.3e-11$ ), and positive regulation of migration ( $P_{adj} = 1.32e-31$ ) (**Figure 33A**). KEGG pathway analysis identified ECM-receptor interaction and multiple signaling pathways, including the TNF signaling pathway ( $P_{adj}$



= 0.0016), Ras signaling pathway ( $P_{\text{adj}} = 0.0098$ ), and PI3K-Akt signaling pathway ( $P_{\text{adj}} = 3.39\text{e-}11$ ) (**Figure 33B**).

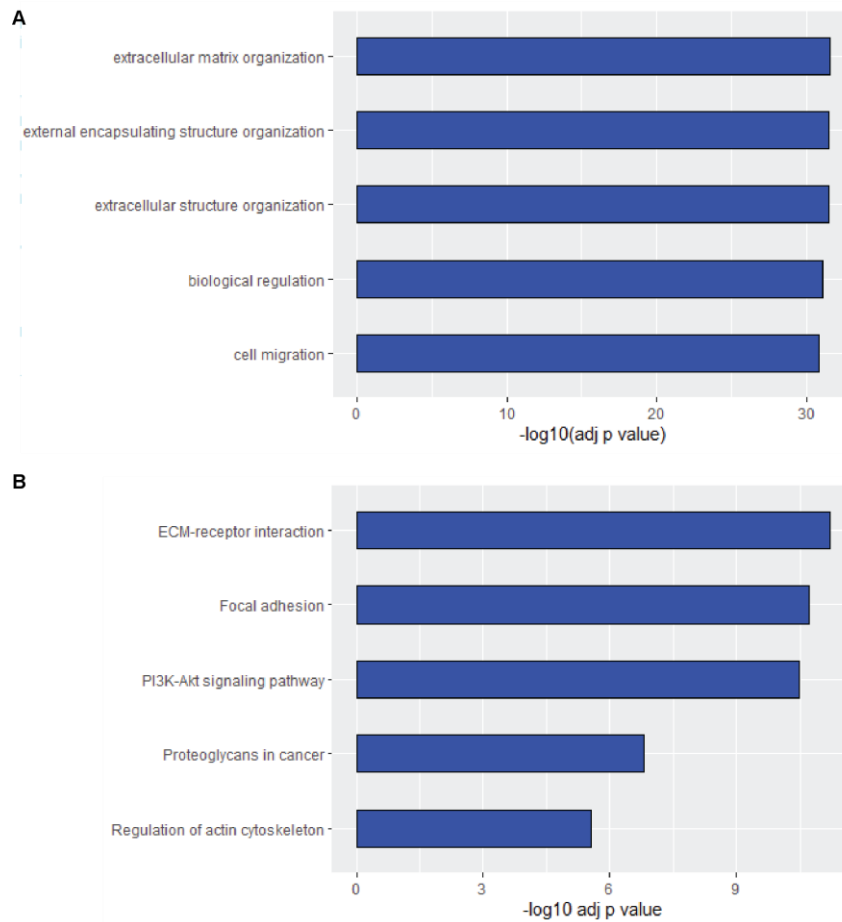


**Figure 33: Downstream enrichment analysis of genes down-regulated in the NGM-D3 group. A** Gene ontology (GO) terms and **B** Kyoto encyclopedia of genes and genomes (KEGG) pathways associated with down-regulated genes in NGM-D3-treated mice. All pathways listed are statistically highly significant with an adjust  $P \ll 0.05$ .

Expression levels of genes associated with pro-inflammatory TNF signaling, including *I11b*, *Tnfrsf1*, *Ccl2*, *Cx3cl1*, *Cxcl1*, *Nfkbia*, *Vcam1*, *Map3k8*, *Map2k1*, *Ptgs*, *Itch*, *Creb3l*, *Fas*, *Mmp14*, were markedly reduced in the treatment group (**Figure 34**).

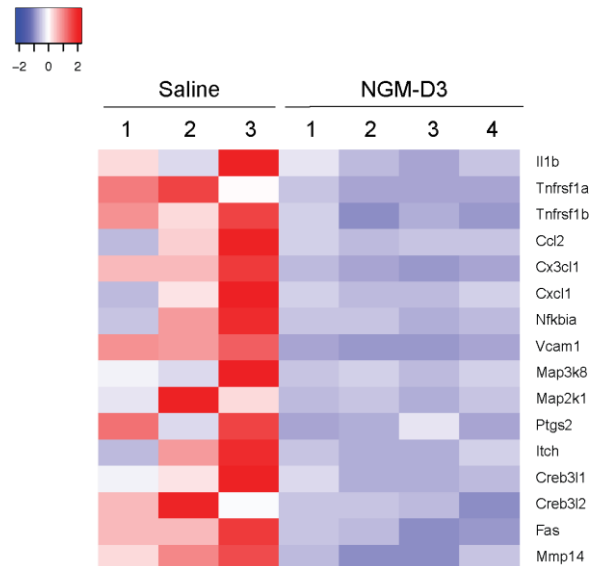


**Figure 34: Heatmap of genes mediating TNF signaling pathway in bulk RNA-seq.** Differentially downregulated genes in NGM-D3 treated mice involved in TNF signaling pathway are depicted.

Together, these data indicated that therapeutic intervention with NGM-D3 ameliorates pro-inflammatory pathways in early-stage atherosclerotic plaques.

### 3.4.6 NGM-D3 reprograms molecular landscape of plaques by downregulating non-immune cell-associated atherogenic genes and enhancing mitochondria metabolism

Furthermore, gene ontology (GO) enrichment and reactome pathway analysis indicated that the up-regulated genes in NGM-D3-treated mice are predominantly enriched in mitochondrial metabolism functions, such as oxidative phosphorylation ( $P$  adj =  $5.41e-24$ ), electron transport chain ( $P$  adj =  $3.68e-26$ ), citric acid (TCA) cycle ( $P$  adj =  $5.41e-24$ ), mitochondrial biogenesis ( $P$  adj =  $6.49e-10$ ) (**Figure 35**).

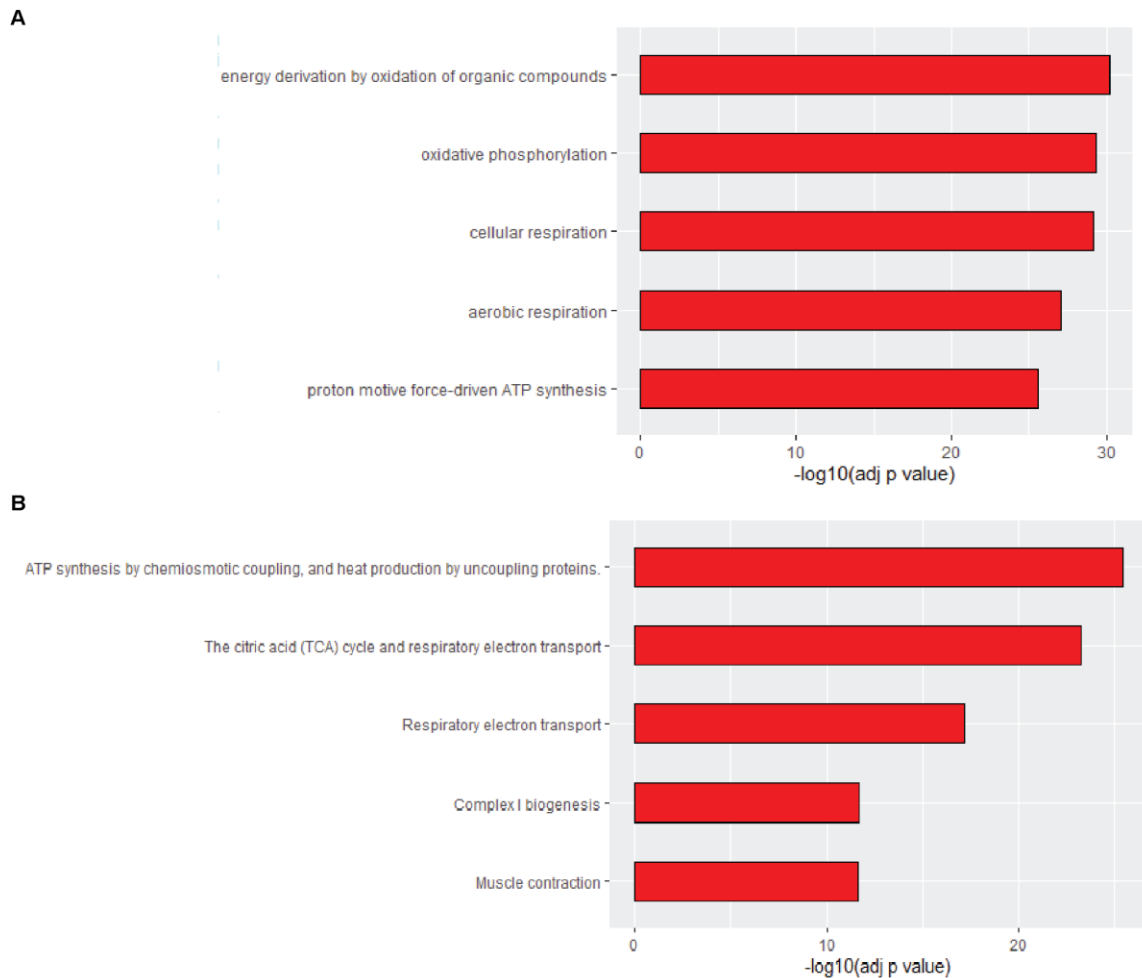


**Figure 35: Downstream enrichment analysis of upregulated genes in the NGM-D3 group. A** Gene ontology (GO) terms and **B** reactome pathways associated with the upregulated genes in NGM-D3-treated mice. All pathways listed are statistically highly significant with an adjust  $P \ll 0.05$ .

The data suggest that NGM-D3 reprograms the molecular landscape of plaques via multiple mitochondria metabolism pathways.

Furthermore, I extracted EC and SMC marker genes and compared their expression with publicly available single-cell transcriptomics data set of human atherosclerotic plaques (214). Decreased levels of endothelial cell markers (*Col4a1*, *Col4a2*, *Sulf1*, and *Vcam1*) and smooth muscle cell markers associated with the contractile phenotype (*Myh11*, *Mfap4*, *Acta2*, and *Tagln2*) as well as those associated with the synthetic phenotype (*Col1a1*, *Mgp*, and *Col3a1*) were identified (**Figure 36**). *Vcam1* is a marker of activated endothelium that is upregulated in the atherogenic response. SMCs undergo phenotype switching from a contractile to a synthetic state, which has

been suggested to exacerbate atherosclerosis (214, 215). My analysis indicated that intervention with NGM-D3 mitigated EC and SMC activation in athero-prone *ApoE*<sup>-/-</sup> mice in the early-stage model.

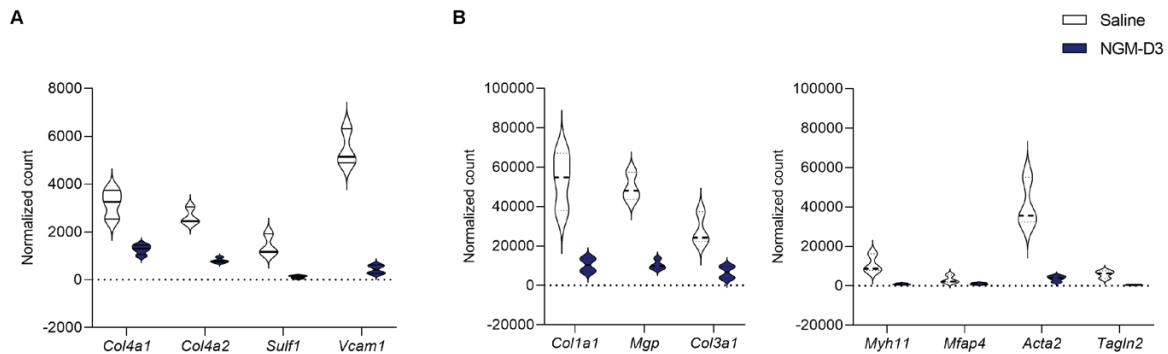


**Figure 36: Violin plots of non-immune cell signatures comparing control and NGM-D3 mice identified in bulk RNA-seq data.** Normalized counts were obtained from DESeq2. A EC signature genes (*Col4a1*, *Col4a2*, *Sulf1*, *Vcam1*). B Synthetic SMC signature genes (*Col1a1*, *Mgp*, *Col3a1*; left). Contractile SMC signature genes (*Myh11*, *Mfap4*, *Acta2*, *Tagln2*; right). EC, endothelial cell; SMC, smooth muscle cell.

Bulk RNA-seq of atherosclerotic plaques from control and NGM-D3-treated mice supported the notion that NGM-D3 treatment led to a downregulation of genes and pathways related to cell adhesion and migration, signaling and cell motility. Moreover, NGM-D3 appeared to substantially reprogram the early plaque transcriptomics through downregulation of extracellular matrix and TNF signaling pathways, while upregulating mitochondrial energy metabolism. In addition, an effect of ameliorating EC and SMC activation was noted. Together, these transcriptomics data suggest that the MIF/CXCR4 peptide inhibitor NGM-D3 may influence the transcriptional landscape of early plaque development towards a less inflammatory phenotype combined with an augmentation of mitochondrial energy metabolism. However, these changes do not yet lead to a reduction in plaque size in this early stage of atherogenesis.

## 4 Discussion

My Ph.D. thesis is composed of three parts. Work in the first part contributed to the characterization of the anti-inflammatory and anti-atherogenic activities of the MIF-selective CXCR4 ectodomain-derived 31-residue peptide inhibitor msR4M-L1, i.e. the parent peptide molecule of the NGMs that I then studied in chapters two and three of my thesis. To this end, the second part focused on characterizing a number of 20-residue peptide NGMs, which had been were designed, developed, and biophysically characterized by our collaborators at TUM, atherosclerosis-relevant cell-based *in vitro* assays, establishing their pharmacological dose-response ( $IC_{50}$ ) curves. I also evaluated the proteolysis stability of NGM-D3 in human plasma. Given its good stability in plasma, I continued to investigate its albumin binding potential using native gel electrophoresis. Lastly, I used an atherosclerosis animal model to evaluate the capacity of NGM-D3 to attenuate the development of atherosclerotic plaques. Since the first part has been published and discussed in the reference Kontos et al, Nat Commun 2020 (200), I only relatively briefly discuss this part regarding my own contributing data and will discuss the other parts in detail.

### 4.1 msR4M-L1

Our data suggest that the CXCR4 inhibitor, msR4M-L1, has a specific MIF-targeting effect regarding receptor interaction and inhibition of inflammatory responses, such as leukocyte adhesion and migration, and LDL/oxLDL uptake (200). More importantly, msR4M-L1 reduced atherosclerotic plaque progression in *ApoE*<sup>-/-</sup> mice. Those results highlight the promises of msR4M-L1 in the attenuation of chronic cardiovascular disease. It may open up new opportunities for therapeutics of inflammatory diseases.

Anti-cytokine therapies have been tested in the clinic for years and have revolutionized the treatment of several inflammatory diseases, including autoimmune disease, cancer, and psychiatric disorders (216, 217). As anti-cytokine therapies emerge to attract attention in the resolution of acute and chronic inflammation, they have been advanced into the cardiovascular field. There are monoclonal antibodies (e.g. canakinumab) and cytokine inhibitors (e.g. anakinra) modulating cytokine pathways (75, 218). On top of that, soluble cytokine receptors have been utilized to develop soluble cytokine inhibitors because most soluble receptors compete with membrane-bound receptors. Despite the general success of some anti-cytokine therapies in clinical applications, obtaining novel therapeutic approaches targeting chemokines, a sub-class of cytokines with chemoattractant capacity and key drivers of inflammatory leukocyte recruitment, has proven more challenging, because of the complexity of chemokine-receptor network. In my thesis, I contributed to the development of a novel anti-chemokine approach, namely soluble CXCR4 receptor mimics specifically targeting the atypical chemokine MIF and its pro-inflammatory signaling in atherosclerosis.

The candidate peptide msR4M-L1 is composed of 29 amino acids derived from segments of ECL1 and ECL2 of CXCR4, plus two unnatural amino acids of the linker moiety, i.e. 6-aminohexanoic acid (6-Ahx)/12-amino-dodecanoic acid (12-Ado), to yield ECL1[97-110]-6-Ahx-12-Ado-ECL2 [182-196]). The total molecular weight is less than 4 kDa which is more than 10 times smaller than that of CXCR4. Various biophysical assays have checked its binding affinity to MIF, ranging from 20 to 75 nM, while lacking appreciable affinity to CXCL12.

msR4M-L1 dose-dependently inhibits LDL and oxLDL uptake mediated by MIF in macrophages. In 2015, one study suggested that MIF/CXCR4 signaling drives Dil-LDL uptake into macrophages (211). Addition of MIF promoted, while knockdown of MIF markedly diminished LDL uptake in macrophages. This effect relied on CXCR4, verified by applying AMD3100 and CXCR4 gene knockdown. LDL is one of the essential lipid components. Imbalance of LDL

synthesis, uptake and degradation, and modification lead to excessive lipid retention in the arterial cells, resulting in cell phenotype switching, local immunity activation, and plaque initiation (219, 220). Inhibition of lipid accumulation holds promise for the therapeutics of atherosclerosis. Co-stimulation of MIF with its blocking antibody, 3-fold molar excess of IIID.9, fully abrogated the Dil-LDL signal enhancement, whereas the small molecule MIF inhibitor ISO-1 also decreased the phagocytized LDL as the concentration increased. Co-stimulation of a range of concentrations of msR4M-L1 with MIF gradually blocked MIF and CXCR4 interaction. The inhibitory potency of msR4M-L1 falls in the middle of IIID.9 and ISO-1. This is in line with the structural and pharmacological features of small peptide drugs. Moreover, the loss-of-function of msR4M-L1 variants seen in LDL uptake, such as msR4M-L1(2xAla) and msR4M-L1(7xAla), provides proof of the binding mechanism for MIF/msR4M-L1. That mechanism offers valuable insight into the design of next generation peptide inhibitors. Other than LDL, modified LDL forms, particularly oxLDL, are considered responsible for foam cell formation and have been linked to the progression of atherosclerosis (221). MIF can also increase oxLDL uptake by 1.6-fold in macrophages. msR4M-L1 inhibited MIF-induced oxLDL phagocytosis in a dose-dependent manner. The lipid clearance in macrophages is classically associated with scavenger receptors like LDLR, CD36, SR-A, and SR-BI (222). Therefore, CXCR4 might cooperatively interact and mobilize scavenger receptors to regulate LDL uptake.

DMR assay confirmed the msR4M-L1 inhibition on MIF-initiated integrated cellular responses. DMR is a very powerful tool for studying receptor biology and drug pharmacology (223). Overexpressed receptor on the cell surface allows the identification and detection of specific ligand agonism and inhibitor antagonism (224). Stably transfected HEK293-CXCR4 cells were utilized to track real-time dynamics of cells triggered by exogenous human recombinant MIF. MIF acted as a CXCR4 agonist to induce an increased DMR signal. Failure of pre-incubation of MIF with msR4M-L1 in the induction of cellular signal favors the notion that msR4M-L1 is specific in targeting MIF/CXCR4 axis.

CD74 receptor binding assay proved that msR4M-L1 could not disrupt the interaction of MIF with CD74. Due to the rescue the effect of MIF/CD74 axis on ischemic cardiomyocytes (116), msR4M-L1 selective targeting property on CXCR4 strengthens its potential use in CVD. HEK293-CD74 cells enabled a high expression of CD74 to study the impact of inhibitors on ligand/receptor dynamics on the surface. Furthermore, the further mobilization and influence on downstream AMPK signaling were checked by Western blot (200), which supported the data acquired for the binding assay.

Overall, msR4M-L1, as a proof-of-concept drug, manifests good inhibition on MIF/CXCR4 signaling in the setting of inflammation. By overcoming the issues in MIF and CXCR4 structure-activity relationship, msR4M-L1 was designed and synthesized with high specificity and selectivity to MIF and avoid interactions with CXCL12 and CD74. In comparison, MIF antibody kicks out adverse effects with high potency but interferes with the protective CD74/AMPK metabolic pathway. SMDs often lack specificity to a specific ligand and bind to other proteins due to their small sizes. For example, AMD3100 is also a clinically used CXCL12 inhibitor, but the only approved indication is autologous stem cell transplantation, due to adverse side effects such as neutrophilia. In addition, low production costs increase the chances for peptide drugs to go into manufacture and being accepted by patients. Targeting master players, IL-1 $\beta$  and IL-6, has been proven effective in clinical trials (75, 225). But cytokines and chemokines are part of defensive immunity, and utterly cut off would impair the normal defense of the body, consequently causing fatal complications like infections. Thus, distinguishing detrimental effects from beneficial effects for a molecule becomes essential in the initial phase of drug discovery. The same design strategy could be introduced to other cytokines and chemokines. A deep mechanistic understanding of SARs, disease status, and rational drug design could improve selectivity and reduce the occurrence of adverse clinical events.



## 4.2 Next generation mimics

### 4.2.1 *In vitro* screening

The previous study verified that engineered msR4M-L1 favors a MIF-binding conformation while sparing a CXCL12-interacting structure and demonstrated immunosuppression *in vitro* and *in vivo*. Although its size is smaller than 90% of CXCR4, it could still be improved to be smaller and more soluble while preserving the MIF-binding specificity and selectivity. Owing to the natural backbone, peptide drugs oftentimes present low bioavailability and are subjected to enzymatic degradation. Conversion of peptides to small molecules leads to the reduction of structural complexity and chemical lability, improvement of solubility and pharmacokinetics, and to establish administration routes (226). Solubility is one of the most crucial factors in achieving the desired concentration of a drug in circulation (227). Drugs with poor solubility require high dosing to reach the therapeutic plasma concentration. Low solubility also hinders formulation development, as drugs must be dissolved in an aqueous solution to be absorbed. Aside from all the above aspects, maintenance of the compound specificity and selectivity is of the utmost importance in the optimization process. The next step thus was identifying the amino acids critical for MIF binding activity, to then transform msR4M-L1 into a minimum active sequence.

Our collaborators at the Division of Peptide Biochemistry at TUM, chemically optimized the structure and tested binding selectivity of NGMs to MIF over CXCL12. I set out to characterize and establish dose-response relationships for the NGMs in three primary immune cell-based inflammatory models, including oxLDL uptake, human monocyte 3D chemotaxis, and murine B cell Transwell migration. Primary cells behave more closely to the cells in a living organism and provide more valuable relevancy to biomedical research than cell lines.

NGMs contain two minimal functional sequences of ECL1 and ECL2, consisting of 9 amino acids and 9 amino acids, respectively. Similar to msR4M-L1, the linker in NGM-O1Pen2 was kept unnatural. Instead, the linker moieties in NGM-D3, NGM-R3, and NGM-K3 were replaced by

natural hydrophilic amino acids. Their MIF binding affinities were determined by fluorescence titration spectroscopy (228). NGM-D3, NGM-R3, and NGM-K3 showed close affinities to msR4M-L1, whereas NGM-O1Pen2 revealed slightly higher affinity. The introduction of hydrophilic amino acids increased the water solubility of NGM-D3, NGM-R3, and NGM-K3, qualifying them for further testing. Regardless of the solubility, higher binding affinity to MIF licensed NGM-O1Pen2 into *in vitro* screening.

The data indicated that all NGMs, -D3, -R3, K3, -O1Pen2, can bind to MIF and suppress leukocyte activities induced by MIF. In terms of functional activity, NGMs sustained the inhibitory effects against MIF. The  $IC_{50}$  values from different experiments are in the nanomolar range and suggest NGM-D3, NGM-R3, and NGM-K3 are more robust MIF antagonists than NGM-O1Pen2.

Foam cell formation is a specific process throughout the entire phase of atherosclerosis. Foam cells have different origins, such as macrophages, smooth muscle cells, and endothelial cells. Macrophage-derived foam cells are the hallmark of early and progressing lesions. OxLDL is thought to be a dominant form of lipid component present in the lesions of animal models and humans (229, 230). CXCR4 has been linked to macrophage foam cell formation (211, 231). Thus, I used Dil-labeled oxLDL to monitor foam cell formation and examine inhibitor effects. The conventional method to evaluate lipid retention is Oil Red O staining. Compared with the conventional method, Dil fluorescence labeling has been optimized for superior sensitivity and reduces the unspecific background. Under unstimulated conditions (control), macrophages could spontaneously take up Dil-oxLDL due to the expression of scavenger receptors (211, 232). Stimulation with MIF enhanced Dil-oxLDL endocytosis by approximately 40%. A 30% reduction was seen when applying CXCR4 antagonist AMD3100, indicating CXCR4 contributes to the oxLDL increase regulated by MIF to a third. However, NGMs could ultimately bring the curve down (40%) to the same level as the control in the same concentration range. Multiple mechanisms might hold them accountable for the outcome. AMD3100 is a well-established

CXCR4 small molecular drug (233, 234). It requires a higher concentration to inhibit MIF-associated activity, implying distinct binding and inhibitory mechanisms. Besides, AMD3100 might be too small to block the interaction between MIF and CXCR4 entirely. On the other hand, lipid uptake and degradation are classically associated with scavenger receptors. In macrophages, the major scavenger receptors involved in oxLDL uptake are SRAI/II and CD36 (235, 236). CXCR4 may partner with those scavenger receptors, synergistically mediating oxLDL endocytosis. The precise mechanism needs to be further investigated.

MIF modulates monocyte and T-cell recruitment via CXCR4 and CXCR2 in an integrin-dependent way (102). msR4M-L1 showed the ability to block human monocyte chemotaxis in a dose-response fashion (200). 3D chemotaxis with cells floating in the gel is an excellent method to evaluate NGMs. As expected from the biophysical binding and oxLDL inhibition experiments, monocyte migration increased by MIF was blocked by all of the NGMs. NGM-D3 and NGM-K3 showed close, greater potency than NGM-R3 and NGM-O1Pen2 in inhibiting cell chemotaxis. NGM-O1Pen2 revealed lower efficacy than other candidates in the same concentration range. All the experiments so far have been done in human cells. Next, I used mouse B cells as they have been confirmed to be able to migrate towards MIF through CXCR4/CD74 (161). NGM-D3 showed unexpectedly high potency with an  $IC_{50}$  value of 0.6 nM. The  $IC_{50}$  values obtained from three assays indicate NGM-D3 appears to be the most potent drug candidate in response to MIF.

In the context of biochemical binding studies and cardiovascular-related bioassays, no CXCL12-binding of msR4M-L1 was noted. Since CXCL12 could drive leukocyte recruitment as a chemokine (63, 161), NGMs were tested to determine whether they also inhibit CXCL12-driven B cells and monocyte migration. Even though no inhibition was observed in B cell migration, the inhibition of NGM-R3 in the 5-fold molar excess of CXCL12 shown on monocytes suggests NGM-R3 binds to CXCL12 at certain level, which undermines the utility of NGM-R3 in MIF-driven atherosclerotic conditions. Nonetheless, the binding mechanism needs to be delineated.

Because context-specific regulations of CXCL12/CXCR4 axis likely occur, the CXCL12/MIF dual inhibitory feature of NGMs could be utilized in other conditions. For instance, the immune system participates in the process of tumorigenesis (237). MIF, an atypical chemokine, has been reported to regulate several tumor types, including glioblastoma, lung cancer, breast cancer, melanoma, and gastric cancer (238-242). MIF can trigger Akt pathway through CD74 to promote cell survival and angiogenesis in cancer (110, 243, 244). MIF also promotes the metastasis of tumor cells by reducing E-cadherin levels and increasing N-cadherin levels (245). CXCL12/CXCR4 axis has been found to be involved in tumor progression and metastasis. CXCL12 expression is up-regulated in gastric cancer, lung cancer, bladder cancer, and many other tumors (246-248). Peptides that inhibit CXCL12 and MIF could be tested in *in vitro* and *in vivo* models to define their therapeutic possibility in cancer. In addition, MIF and CXCL12 detrimental effects have also been implicated in the progression of the autoimmune disorder (249, 250). MIF-directed therapies have been suggested to ameliorate inflammatory responses in experimental studies of systemic lupus erythematosus (SLE) and rheumatoid arthritis (RA) (251). MIF and CXCL12 levels are associated with other diseases like multiple sclerosis (MS) and inflammatory bowel disease (252-255). MIF peptides with dual inhibitory effects could be efficacious in patients with high expression and pathologic roles of both CXCL12 and MIF.

#### **4.2.2 Degradation and albumin binding feature of NGM-D3**

The *in vitro* screening suggests NGM-D3 consistently showed good potency and efficacy without interfering with CXCL12-induced immune response, which permitted it for plasma stability evaluation. Studying the stability of peptides is fundamental. Fast degradation in biological fluids enormously compromise successful peptide drug development (256). Plasma is one of the easily accessible fluids and contains abundant amounts of proteases. TAMRA-msR4M-L1 can be detected after 48 hours incubation in plasma, showing fairly good proteolysis stability. TAMRA-NGM-D3 presented as dimer and monomer in the absence of DTT. DTT is a commonly used

reducing agent to disrupt protein disulfide bonds in gel electrophoresis. NGM-D3 possesses one cysteine in the sequence. And only monomer was observed in the presence of DTT, indicating NGM-D3 dimerization is dependent on disulfide bond formation. Indeed, interchain disulfide bonds can ensure protein stability and produce covalently linked protein dimers. TAMRA-NGM-D3 showed good stability in human plasma with a half-life of 23.2 h (with DTT) or a half-life of 15.6 h (without DTT) which are a relatively good number for an unmodified peptide. Dimerization could be one of the reasons why NGM-D3 is fairly resistant to plasma enzymatic degradation.

Albumin is the most prominent plasma protein in the blood with a normal concentration range of 35-50g/L (257). It has an extended half-life of 19 days in circulation due to neonatal Fc receptor (FcRn)-mediated recycling (258, 259). In the body, albumin serves as a carrier for various natural metabolites and exogenous compounds (258). The concentration and frequency of a drug at the target site is an important parameter in the evaluation of therapeutic efficiency. Drugs like small peptides often have a low-molecular weight below the renal filtration threshold, leading to rapid renal clearance and short plasma half-life (260, 261). Therefore, the long half-life of albumin has been strategized in the pharmaceutical industry to improve drug pharmacokinetics. Covalently binding and non-covalently binding to albumin could significantly alter drug distribution, clearance, and metabolism (262). In the paper, TAMRA-msR4M-L1 has demonstrated good plasma stability (detectable up to 48 h) and approximately 20 h half-life *in vivo* (200). This is considered exceptional as the half-life of a majority of unmodified peptides is between two and 30 minutes. However, the probability of single amino acid or partial cleavage needs to be excluded in future investigation. Also, these stability experiments were performed with TAMRA-labeled peptide and it is possible that the TAMRA moiety may confer some stability to the peptide sequence. Thus, measurements without fluorescence label need to be performed to further validate these findings.

A natural endogenous cleavage fraction of albumin, EPI-X4, was discovered as an antagonist of CXCR4 (263). It binds to a sequence close to the ECL2 of the receptor and blocks CXCL12 interaction with CXCR4. Interestingly, EPI-X4 behaves as an inverse agonist, reducing the CXCR4 signaling at the baseline level. The fragment originates from residues 408-423 of HSA which is positively charged on the surface. It interacts with the negatively charged extracellular face of CXCR4. All the evidence hints that msR4M-L1 and NGMs might be able to bind to serum albumin. Binding to albumin could likely stabilize MIF peptide inhibitors, giving rise to the observed good stability in plasma and reducing the renal clearance rate *in vivo*. Based on this hypothesis, I looked at the interaction of human albumin and NGM-D3 on the native gel. Native gel electrophoresis enables protein complexes to be separated according to the net charge, size, and shape while maintaining their subunit interactions. 2 h incubation allows Cy7.5-NGM-D3 to colocalize with FITC-HSA. This was not seen in 0 h incubation nor in the lanes loaded with Cy7.5-NGM-D3 or FITC-HSA alone, showing the interaction between the peptide and albumin. A similar pattern of bands was observed while replacing FITC-HSA with native HSA. The small size or the net charge could cause the missing signal in the last lane in **Figure 24**, where the peptide might be stuck in the upper chamber of the gel. The pattern of bands from samples processed without DTT on the SDS page gel indicates the cysteine in the sequence of NGM-D3 contributes to the binding of NGM-D3 to albumin. Albumin possesses 35 cysteine residues, the one at position 34 (Cys34) is free for covalent attachment. 34 of cysteines form a disulfide bond internally to maintain albumin structure stability. Cys34 is positioned at the outer surface of albumin and makes up 80% of thiols (-SH) in the plasma (264). One assumption could be that cysteine in NGM-D3 forms disulfide bond with free Cys34 of albumin. The strategy has been implicated in the application of covalent conjugation of drugs (257, 265). Additionally, albumin consists of three homologous domains I, II, and III. Each domain has two sub-domains (A and B). There are two primary drug-binding sites named site I and site II in albumin (266). Site I is located in subdomain IIA, and site II is located in subdomain IIIA (262). They could also potentially serve as the binding

sites for CXCR4-ectodomain peptide inhibitors. The surface of albumin is negatively charged, which enables it non-covalently interact with compounds (258).

#### 4.2.3 *In vivo* study

To recapitulate the pathophysiological features of human atherosclerosis, several animal models have been engineered and studied over decades (267). Different models are chosen based on the research interests, accessibility, and budgets. Owing to their cheap, easy-to-handle, and reproducible traits, mouse models are extensively used in atherosclerosis research. One of the models, LDL receptor deficiency mice, was generated in 1993 (268), developing intermediately elevated plasma cholesterol levels and small plaques when fed a regular diet (269). Cholesterol is predominantly accumulated in lipoprotein particles like chylomicron remnants, VLDL, and IDL (270, 271). Another standard model, *Apoe*<sup>-/-</sup> mice, was invented in 1992 (270, 272), showing severely impaired ability to clear plasma lipoproteins even when fed a regular diet. Lack of *Apoe* results in increased cholesterol levels, mainly in chylomicron and VLDL. Generally, *Apoe*<sup>-/-</sup> mice need a shorter timeframe to develop advanced lesions than *Ldlr*<sup>-/-</sup> mice (273). Unlike *Ldlr*, *Apoe* not only affects lipid levels but also has an impact on inflammation, oxidation, cell migration, and proliferation. The inflammatory profiling markers are more remarkable in *Apoe*-deficient mice (274). The earliest monocyte adhesion and foamy cells could be detected at the age of 6-8 weeks. Lesions enriched in SMCs, extracellular matrix, and necrotic core can be appreciated after 15 weeks. The course for lesion progression is markedly shortened when feeding a Western diet (274). The easy accessibility in my laboratory and all those advantages enable *Apoe*<sup>-/-</sup> to be the suitable atherosclerosis animal model to study the pharmacological effects of MIF peptide inhibitors.

Bulk RNA sequencing is a transcriptomic analysis of pooled cell populations, which measures the average expression level of genes across different cell types. It allowed us to identify regulatory molecules and pathways affected by NGM-D3. Mice receiving 5-week injection of

50 µg NGM-D3 three times per week exhibited downregulation of genes associated with extracellular matrix organization, cell adhesion and migration, cell proliferation as well as activation of several inflammatory signaling pathways including TNF signaling, PI3K-Akt signaling, Ras signaling. Upregulation of the central inflammation mediator *Il1β* and robust monocyte chemokines *Cx3cl1*, *Ccl2* in the untreated mice further validated anti-inflammatory effect of NGM-D3. RNA-seq data from our aging study in *Mif*-deficiency mice revealed downregulated gene enrichment in lipid synthesis and metabolism, lipid storage, and brown fat cell differentiation (162). Time duration of HFD and global gene knockout contribute to the variations between genetic modified and pharmacological models. Single-cell transcriptomics analysis of human carotid plaques found that ECs harbor a gene expression pattern in relation to activation and transdifferentiation with distinct expression in extracellular matrix and cell mobility. Activated endothelium marker *Vcam1*, a crucial leukocyte adhesion and transmigration mediator, was also recognized highly upregulated in human and our mice cohort. Moreover, synthetic SMCs in combination with upregulation of extracellular matrix genes dominates in human plaques (214). By comparing with human data, common genes indicative of activation of ECs and SMCs was observed in our saline-treated mice sequencing data. That provide evidence that NGM-D3 therapy modulates extracellular matrix construction and attenuates endothelium activation and inflammatory activities in the plaque (214).

In our early plaque model, the ORO and HE histology staining suggested NGM-D3 could not reduce early plaque burden in aortic root. The macrophage content was not altered by the peptide administration. During inflammatory atherogenesis, macrophages accumulate aggressively in the arterial wall, particularly in the initial phase (275, 276). Lesional macrophages have been believed to differentiate from infiltrating circulatory monocytes for centuries. However, sequencing and proteomic technologies have reinforced novel insights into the current understanding of macrophage origins. Not only do macrophages arise from the circulation, but they also derive locally in the vessel (277, 278). Macrophages are the first immune cells to



implant and reside in the cardiovascular system in mice (279, 280). Macrophage expansion does not only rely on monocyte recruitment from the blood but instead undergoes rapid proliferation in some circumstances (281). Šárka Lhoták et al characterized the proliferating residential cells across all stages of atherosclerosis in *ApoE*- and *Ldlr*-deficiency mice. Half of the activated macrophages were identified proliferating in situ in the early stage (282). This vision was revisited and validated by Clinton et al. in 2013 (283). Previously identified vascular dendritic cells, Mac<sup>AIR</sup> arising from monocyte progenitors, are seeded in the artery at birth. They differentiate into foam cells early on before monocytes come in and dominate the lesion growth (284). In advanced plaque, the plaque expansion capability of Mac<sup>AIR</sup> will be superseded by the recruited monocytes (284). Local macrophage proliferation declines as plaques progress. The rapid local macrophage turnover in the initial stage of atherosclerosis might explain the equivalent macrophage content in both groups and the subtle reduction in plaque size in NGM-D3 treated group. Although RNA-seq data revealed high expression of *Cx3c1*, the receptor *Cx3cr1* showed no difference. *Cx3cr1* is one of the markers of tissue resident macrophages (280, 285). Other resident macrophage markers including *Lyve1*, *Ccl24*, and *Pf4* were enhanced in treated mice. Interestingly, some macrophage markers that have been correlated with cholesterol metabolism *Cd9*, *Spp1* were increased in untreated mice. They are recognized as Trem2<sup>hi</sup> macrophage signatures (286). However, *Lgals3bp* was found upregulated in treated mice. Other than those genes, the majority of macrophage markers showed no differences, including MAC<sup>air</sup> expressing genes (*Mmp12*, *Mmp13*, *Rgs1*, *Gngt2*, *Itgax*). The RNA-seq data reflected the immunofluorescence staining of macrophage population. During the initial 4-5 weeks of HFD, macrophage content increases drastically and represents 50-60% plaque area in aortic root (287). Collagen begins to become notable in the initial 4 or 5 weeks, yet SMCs account for a small portion. Over time, monocytes and macrophages per plaque size decline (287). Further study needs to investigate the long-term effect of MIF peptide inhibitors.

The reduction of circulatory CD3<sup>+</sup> T cell percentage in the treated group is robust in the study cohort. The similar phenomenon was also seen in the genetic *MIF*-deficiency *ApoE*<sup>-/-</sup> mice model on 24-week HFD (288). T-cell immunity is part of adaptive immunity. T cells are not present in the healthy intima (289). They start to appear as the disease progresses. The most prevalent T cell subpopulation in the lesion is T helper cell 1 (Th1) (290). Single-cell sequencing uncovered the T-cell characteristics in human atherosclerotic plaque (33). However, there is a lack of correlation between circulatory immune cells and plaque growth. Besides, the subtype of the reduced T-cell population was not revealed in the study. Long-term pharmacological study needs to immuno-phenotype the T-cell population in blood, spleen, bone marrow, and plaque area.

The *in vivo* study investigated the therapeutic effect of NGMs in early plaque model, and characterized the inhibitory impact on plaque development and macrophage burden. Even though the inhibition was not prominent, peripheral immune cell profiling showed a promising trend that replicates the outcome from our aging study on *MIF* genetic modified model (162). Because local macrophage proliferation and activation dominates the early plaque growth, MIF antagonism might not be able to significantly reduce the plaque burden from early on. Genetic MIF knockout model should be incorporated as a comparison. Another limitation of the study is the therapeutic dosing regime and frequency. We employed one dose (50 µg) of NGM-D3 and three times a week of drug administration. The drug efficiency might be missed in the current therapeutic regimen. Additionally, finding the right therapeutic window of a drug is also critical to minimize the adverse effects. More dosing and reasonable therapeutic regimen could be tested in the follow-up study.

Future study could investigate the long-term effects of peptide inhibitors in an extended period of plaque development. Plaque and vessel obstruction are often identified when patients manifest symptoms and clinical complications. Clinical interventions usually start in the middle or very late phase of disease course. Establishing the pharmacological model in combination

with lipid-lowering therapy, which mimics the time course of human atherosclerosis, could also be interesting.

# References

1. Roth GA, Mensah GA, Fuster V. The Global Burden of Cardiovascular Diseases and Risks. *J Am Coll Cardiol*. 2020;76(25):2980-1.
2. Shattock SG. A Report upon the Pathological Condition of the Aorta of King Menephtah, Traditionally Regarded as the Pharaoh of the Exodus. *Proc R Soc Med*. 1909;2(Pathol\_Sect):122-7.
3. Zhou J, Li Y-S, Chien S. Shear Stress-Initiated Signaling and Its Regulation of Endothelial Function. *Arterioscler Thromb Vasc Biol*. 2014;34.
4. Nakajima H, Mochizuki N. Flow pattern-dependent endothelial cell responses through transcriptional regulation. *Cell Cycle*. 2017;16(20):1893-901.
5. Summerhill VI, Grechko AV, Yet S-F, Sobenin IA, Orekhov AN. The atherogenic role of circulating modified lipids in atherosclerosis. *Int J Mol Sci*. 2019;20(14):3561.
6. Poznyak AV, Nikiforov NG, Markin AM, Kashirskikh DA, Myasoedova VA, Gerasimova EV, et al. Overview of OxLDL and its impact on cardiovascular health: focus on atherosclerosis. *Front Pharmacol*. 2021:2248.
7. Tao Z, Smart FW, Figueroa JE, Glancy DL, Vijayagopal P. Elevated expression of proteoglycans in proliferating vascular smooth muscle cells. *Atherosclerosis*. 1997;135(2):171-9.
8. Little PJ, Tannock L, Olin KL, Chait A, Wight TN. Proteoglycans synthesized by arterial smooth muscle cells in the presence of transforming growth factor- $\beta$ 1 exhibit increased binding to LDLs. *Arterioscler Thromb Vasc Biol*. 2002;22(1):55-60.
9. Stary HC, Chandler AB, Glagov S, Guyton JR, Insull Jr W, Rosenfeld ME, et al. A definition of initial, fatty streak, and intermediate lesions of atherosclerosis. A report from the Committee on Vascular Lesions of the Council on Arteriosclerosis, American Heart Association. *Circulation*. 1994;89(5):2462-78.
10. Gisterå A, Hansson GK. The immunology of atherosclerosis. *Nat Rev Nephrol*. 2017;13(6):368-80.
11. Lutgens E, De Muinck ED, Kitslaar PJ, Tordoir JH, Wellens HJ, Daemen MJ. Biphasic pattern of cell turnover characterizes the progression from fatty streaks to ruptured human atherosclerotic plaques. *Cardiovasc Res*. 1999;41(2):473-9.
12. Seimon T, Tabas I. Mechanisms and consequences of macrophage apoptosis in atherosclerosis. *J Lipid Res*. 2009;50:S382-S7.
13. Ait-Oufella H, Kinugawa K, Zoll J, Simon T, Boddaert J, Heeneman S, et al. Lactadherin deficiency leads to apoptotic cell accumulation and accelerated atherosclerosis in mice. *Circulation*. 2007;115(16):2168-77.
14. Schrijvers DM, De Meyer GR, Kockx MM, Herman AG, Martinet W. Phagocytosis of apoptotic cells by macrophages is impaired in atherosclerosis. *Arterioscler Thromb Vasc Biol*. 2005;25(6):1256-61.
15. Stary HC, Chandler AB, Dinsmore RE, Fuster V, Glagov S, Insull Jr W, et al. A definition of advanced types of atherosclerotic lesions and a histological classification of atherosclerosis: a report from the Committee on Vascular Lesions of the Council on Arteriosclerosis, American Heart Association. *Circulation*. 1995;92(5):1355-74.
16. Virmani R, Kolodgie FD, Burke AP, Farb A, Schwartz SM. Lessons from sudden coronary death: a comprehensive morphological classification scheme for atherosclerotic lesions. *Arterioscler Thromb Vasc Biol*. 2000;20(5):1262-75.

17. Cheruvu PK, Finn AV, Gardner C, Caplan J, Goldstein J, Stone GW, et al. Frequency and distribution of thin-cap fibroatheroma and ruptured plaques in human coronary arteries: a pathologic study. *J Am Coll Cardiol*. 2007;50(10):940-9.
18. Burke AP, Farb A, Malcom GT, Liang Y-h, Smialek J, Virmani R. Coronary risk factors and plaque morphology in men with coronary disease who died suddenly. *N Engl J Med*. 1997;336(18):1276-82.
19. Deguchi J-o, Aikawa M, Tung C-H, Aikawa E, Kim D-E, Ntziachristos V, et al. Inflammation in atherosclerosis: visualizing matrix metalloproteinase action in macrophages in vivo. *Circulation*. 2006;114(1):55-62.
20. Partida RA, Libby P, Crea F, Jang I-K. Plaque erosion: a new in vivo diagnosis and a potential major shift in the management of patients with acute coronary syndromes. *Eur Heart J*. 2018;39(22):2070-6.
21. Bentzon JF, Otsuka F, Virmani R, Falk E. Mechanisms of plaque formation and rupture. *Circ Res*. 2014;114(12):1852-66.
22. Burke AP, Kolodgie FD, Farb A, Weber DK, Malcom GT, Smialek J, et al. Healed plaque ruptures and sudden coronary death: evidence that subclinical rupture has a role in plaque progression. *Circulation*. 2001;103(7):934-40.
23. De Beer F, Hind C, Fox K, Allan R, Maseri A, Pepys M. Measurement of serum C-reactive protein concentration in myocardial ischaemia and infarction. *Heart*. 1982;47(3):239-43.
24. Hofer IE, Steffens S, Ala-Korpela M, Bäck M, Badimon L, Bochaton-Piallat M-L, et al. Novel methodologies for biomarker discovery in atherosclerosis. *Eur Heart J*. 2015;36(39):2635-42.
25. Ohashi K, Burkart V, Flohé S, Kolb H. Cutting edge: heat shock protein 60 is a putative endogenous ligand of the toll-like receptor-4 complex. *J Immunol*. 2000;164(2):558-61.
26. Okamura Y, Watari M, Jerud ES, Young DW, Ishizaka ST, Rose J, et al. The extra domain A of fibronectin activates Toll-like receptor 4. *J Biol Chem*. 2001;276(13):10229-33.
27. Kawai T, Akira S, editors. TLR signaling. *Semin Immunol*; 2007: Elsevier.
28. Michelsen KS, Wong MH, Shah PK, Zhang W, Yano J, Doherty TM, et al. Lack of Toll-like receptor 4 or myeloid differentiation factor 88 reduces atherosclerosis and alters plaque phenotype in mice deficient in apolipoprotein E. *Proc Natl Acad Sci*. 2004;101(29):10679-84.
29. Zhu J, Paul WE. CD4 T cells: fates, functions, and faults. *Blood*. 2008;112(5):1557-69.
30. Wolf D, Ley K. Immunity and inflammation in atherosclerosis. *Circ Res*. 2019;124(2):315-27.
31. Emeson EE, Shen M-L, Bell C, Qureshi A. Inhibition of atherosclerosis in CD4 T-cell-ablated and nude (nu/nu) C57BL/6 hyperlipidemic mice. *Am J Clin Pathol*. 1996;149(2):675.
32. Zhou X, Robertson A-KL, Rudling M, Parini P, Hansson GrK. Lesion development and response to immunization reveal a complex role for CD4 in atherosclerosis. *Circ Res*. 2005;96(4):427-34.
33. Fernandez DM, Rahman AH, Fernandez NF, Chudnovskiy A, Amir E-aD, Amadori L, et al. Single-cell immune landscape of human atherosclerotic plaques. *Nat Med*. 2019;25(10):1576-88.
34. Li J, McArdle S, Gholami A, Kimura T, Wolf D, Gerhardt T, et al. CCR5+ T-bet+ FoxP3+ effector CD4 T cells drive atherosclerosis. *Circ Res*. 2016;118(10):1540-52.

35. Ait-Oufella H, Salomon BL, Potteaux S, Robertson A-KL, Gourdy P, Zoll J, et al. Natural regulatory T cells control the development of atherosclerosis in mice. *Nat Med*. 2006;12(2):178-80.
36. Cochain C, Koch M, Chaudhari SM, Busch M, Pelisek J, Boon L, et al. CD8+ T cells regulate monopoiesis and circulating Ly6Chigh monocyte levels in atherosclerosis in mice. *Circ Res*. 2015;117(3):244-53.
37. Kyaw T, Winship A, Tay C, Kanellakis P, Hosseini H, Cao A, et al. Cytotoxic and proinflammatory CD8+ T lymphocytes promote development of vulnerable atherosclerotic plaques in apoE-deficient mice. *Circulation*. 2013;127(9):1028-39.
38. van Duijn J, Kritikou E, Benne N, van der Heijden T, van Puijvelde GH, Kröner MJ, et al. CD8+ T-cells contribute to lesion stabilization in advanced atherosclerosis by limiting macrophage content and CD4+ T-cell responses. *Cardiovasc Res*. 2019;115(4):729-38.
39. Caligiuri G, Nicoletti A, Poirier B, Hansson GK. Protective immunity against atherosclerosis carried by B cells of hypercholesterolemic mice. *J Clin Invest*. 2002;109(6):745-53.
40. Major AS, Fazio S, Linton MF. B-lymphocyte deficiency increases atherosclerosis in LDL receptor-null mice. *Arterioscler Thromb Vasc Biol*. 2002;22(11):1892-8.
41. Raman D, Sobolik-Delmaire T, Richmond A. Chemokines in health and disease. *Exp Cell Res*. 2011;317(5):575-89.
42. Rajagopalan L, Rajarathnam K. Structural basis of chemokine receptor function—a model for binding affinity and ligand selectivity. *Biosci Rep*. 2006;26(5):325-39.
43. Gu L, Okada Y, Clinton SK, Gerard C, Sukhova GK, Libby P, et al. Absence of monocyte chemoattractant protein-1 reduces atherosclerosis in low density lipoprotein receptor-deficient mice. *Mol Cell*. 1998;2(2):275-81.
44. Lu B, Rutledge BJ, Gu L, Fiorillo J, Lukacs NW, Kunkel SL, et al. Abnormalities in monocyte recruitment and cytokine expression in monocyte chemoattractant protein 1-deficient mice. *J Exp Med*. 1998;187(4):601-8.
45. de Lemos JA, Morrow DA, Sabatine MS, Murphy SA, Gibson CM, Antman EM, et al. Association between plasma levels of monocyte chemoattractant protein-1 and long-term clinical outcomes in patients with acute coronary syndromes. *Circulation*. 2003;107(5):690-5.
46. Boring L, Gosling J, Cleary M, Charo IF. Decreased lesion formation in CCR2<sup>-/-</sup> mice reveals a role for chemokines in the initiation of atherosclerosis. *Nature*. 1998;394(6696):894-7.
47. Matsuo Y, Raimondo M, Woodward TA, Wallace MB, Gill KR, Tong Z, et al. CXC-chemokine/CXCR2 biological axis promotes angiogenesis in vitro and in vivo in pancreatic cancer. *Int J Cancer*. 2009;125(5):1027-37.
48. Koch AE, Polverini PJ, Kunkel SL, Harlow LA, DiPietro LA, Elner VM, et al. Interleukin-8 as a macrophage-derived mediator of angiogenesis. *Science*. 1992;258(5089):1798-801.
49. Keane MP, Arenberg DA, Moore BB, Addison CL, Strieter RM. CXC chemokines and angiogenesis/angiostasis. *Proc Assoc Am Physicians*. 1998;110(4):288-96.
50. Lv G, Zhu H, Li C, Wang J, Zhao D, Li S, et al. Inhibition of IL-8-mediated endothelial adhesion, VSMCs proliferation and migration by siRNA-TMEM98 suggests TMEM98's emerging role in atherosclerosis. *Oncotarget*. 2017;8(50):88043.

51. Tang X-E, Li H, Chen L-Y, Xia X-D, Zhao Z-W, Zheng X-L, et al. IL-8 negatively regulates ABCA1 expression and cholesterol efflux via upregulating miR-183 in THP-1 macrophage-derived foam cells. *Cytokine*. 2019;122:154385.
52. Noels H, Weber C, Koenen RR. Chemokines as therapeutic targets in cardiovascular disease: the road behind, the road ahead. *Arterioscler Thromb Vasc Biol*. 2019;39(4):583-92.
53. Nagasawa T, Hirota S, Tachibana K, Takakura N, Nishikawa S-i, Kitamura Y, et al. Defects of B-cell lymphopoiesis and bone-marrow myelopoiesis in mice lacking the CXC chemokine PBSF/SDF-1. *Nature*. 1996;382(6592):635-8.
54. Tachibana K, Hirota S, Iizasa H, Yoshida H, Kawabata K, Kataoka Y, et al. The chemokine receptor CXCR4 is essential for vascularization of the gastrointestinal tract. *Nature*. 1998;393(6685):591-4.
55. Yellowley C. CXCL12/CXCR4 signaling and other recruitment and homing pathways in fracture repair. *BoneKEy Rep*. 2013;2.
56. Nagasawa T. The chemokine CXCL12 and regulation of HSC and B lymphocyte development in the bone marrow niche. *Osteoimmunology: Springer*; 2007. p. 69-75.
57. Murad HA, Rafeeq MM, Alqurashi TM. Role and implications of the CXCL12/CXCR4/CXCR7 axis in atherosclerosis: still a debate. *Ann Med*. 2021;53(1):1598-612.
58. Janowski M. Functional diversity of SDF-1 splicing variants. *Cell Adh Migr*. 2009;3(3):243-9.
59. Janssens R, Struyf S, Proost P. The unique structural and functional features of CXCL12. *Cell Mol Immunol*. 2018;15(4):299-311.
60. Ziarek JJ, Kleist AB, London N, Raveh B, Montpas N, Bonnetterre J, et al. Structural basis for chemokine recognition by a G protein-coupled receptor and implications for receptor activation. *Sci Signal*. 2017;10(471):eaah5756.
61. Qin L, Kufareva I, Holden LG, Wang C, Zheng Y, Zhao C, et al. Crystal structure of the chemokine receptor CXCR4 in complex with a viral chemokine. *Science*. 2015;347(6226):1117-22.
62. Crump MP, Gong J-H, Loetscher P, Rajarathnam K, Amara A, Arenzana-Seisdedos F, et al. Solution structure and basis for functional activity of stromal cell-derived factor-1; dissociation of CXCR4 activation from binding and inhibition of HIV-1. *EMBO J*. 1997;16(23):6996-7007.
63. Décaillot FM, Kazmi MA, Lin Y, Ray-Saha S, Sakmar TP, Sachdev P. CXCR7/CXCR4 heterodimer constitutively recruits  $\beta$ -arrestin to enhance cell migration. *J Biol Chem*. 2011;286(37):32188-97.
64. Sjaarda J, Gerstein H, Chong M, Yusuf S, Meyre D, Anand SS, et al. Blood CSF1 and CXCL12 as causal mediators of coronary artery disease. *J Am Coll Cardiol*. 2018;72(3):300-10.
65. Ferdousie VT, Mohammadi M, Hassanshahi G, Khorramdelazad H, Falahati-Pour SK, Mirzaei M, et al. Serum CXCL10 and CXCL12 chemokine levels are associated with the severity of coronary artery disease and coronary artery occlusion. *Int J Cardiol*. 2017;233:23-8.
66. Samani NJ, Erdmann J, Hall AS, Hengstenberg C, Mangino M, Mayer B, et al. Genomewide association analysis of coronary artery disease. *N Engl J Med*. 2007;357(5):443-53.
67. Yamaguchi J-i, Kusano KF, Masuo O, Kawamoto A, Silver M, Murasawa S, et al. Stromal cell-derived factor-1 effects on ex vivo expanded endothelial progenitor cell recruitment for ischemic neovascularization. *Circulation*. 2003;107(9):1322-8.

68. Döring Y, van der Vorst EP, Duchene J, Jansen Y, Gencer S, Bidzhekov K, et al. CXCL12 derived from endothelial cells promotes atherosclerosis to drive coronary artery disease. *Circulation*. 2019;139(10):1338-40.
69. Zernecke A, Bot I, Djalali-Talab Y, Shagdarsuren E, Bidzhekov K, Meiler S, et al. Protective role of CXC receptor 4/CXC ligand 12 unveils the importance of neutrophils in atherosclerosis. *Circ Res*. 2008;102(2):209-17.
70. Döring Y, Noels H, Van Der Vorst EP, Neideck C, Egea V, Drechsler M, et al. Vascular CXCR4 limits atherosclerosis by maintaining arterial integrity: evidence from mouse and human studies. *Circulation*. 2017;136(4):388-403.
71. Libby P, Ridker PM, Hansson GK, Atherothrombosis LTNo. Inflammation in atherosclerosis: from pathophysiology to practice. *J Am Coll Cardiol*. 2009;54(23):2129-38.
72. Tabas I, Glass CK. Anti-inflammatory therapy in chronic disease: challenges and opportunities. *Science*. 2013;339(6116):166-72.
73. Tardif J-C, Tanguay J-F, Wright SR, Duchatelle V, Petroni T, Grégoire JC, et al. Effects of the P-selectin antagonist inclacumab on myocardial damage after percutaneous coronary intervention for non–ST-segment elevation myocardial infarction: results of the SELECT-ACS trial. *J Am Coll Cardiol*. 2013;61(20):2048-55.
74. Ridker PM. Testing the inflammatory hypothesis of atherothrombosis: scientific rationale for the cardiovascular inflammation reduction trial (CIRT). *J Thromb Haemost*. 2009;7:332-9.
75. Ridker PM, Everett BM, Thuren T, MacFadyen JG, Chang WH, Ballantyne C, et al. Antiinflammatory therapy with canakinumab for atherosclerotic disease. *N Engl J Med*. 2017;377(12):1119-31.
76. Nidorf SM, Fiolet AT, Mosterd A, Eikelboom JW, Schut A, Opstal TS, et al. Colchicine in patients with chronic coronary disease. *N Engl J Med*. 2020;383(19):1838-47.
77. Francisci D, Pirro M, Schiaroli E, Mannarino MR, Cipriani S, Bianconi V, et al., editors. Maraviroc intensification modulates atherosclerotic progression in HIV-suppressed patients at high cardiovascular risk. A randomized, crossover pilot study. *Open forum infectious diseases*; 2019: Oxford University Press US.
78. Joseph JP, Reyes E, Guzman J, O'Doherty J, McConkey H, Arri S, et al. CXCR2 Inhibition—a novel approach to treating CoronAry heart DiseAse (CICADA): study protocol for a randomised controlled trial. *Trials*. 2017;18:1-11.
79. Bloom BR, Bennett B. Mechanism of a reaction in vitro associated with delayed-type hypersensitivity. *Science*. 1966;153(3731):80-2.
80. David JR. Delayed hypersensitivity in vitro: its mediation by cell-free substances formed by lymphoid cell-antigen interaction. *Proc Natl Acad Sci*. 1966;56(1):72-7.
81. Weiser WY, Temple PA, Witek-Giannotti JS, Remold HG, Clark SC, David JR. Molecular cloning of a cDNA encoding a human macrophage migration inhibitory factor. *Proc Natl Acad Sci*. 1989;86(19):7522-6.
82. Bernhagen J, Calandra T, Mitchell R, Martin S, Tracey K, Voelter W, et al. MIF is a pituitary-derived cytokine that potentiates lethal endotoxaemia. *Nature*. 1993;365(6448):756-9.
83. Paralkar V, Wistow G. Cloning the human gene for macrophage migration inhibitory factor (MIF). *Genomics*. 1994;19(1):48-51.
84. Kozak CA, Adamson MC, Buckler CE, Segovia L, Paralkar V, Wistow G. Genomic cloning of mouse MIF (macrophage inhibitory factor) and genetic mapping of



- the human and mouse expressed gene and nine mouse pseudogenes. *Genomics*. 1995;27(3):405-11.
85. Sparkes A, De Baetselier P, Roelants K, De Trez C, Magez S, Van Ginderachter JA, et al. The non-mammalian MIF superfamily. *Immunobiology*. 2017;222(3):473-82.
86. Wasiel AA, Rozeboom HJ, Hauke D, Baas B-J, Zandvoort E, Quax WJ, et al. Structural and functional characterization of a macrophage migration inhibitory factor homologue from the marine cyanobacterium *Prochlorococcus marinus*. *Biochem*. 2010;49(35):7572-81.
87. Mitchell R, Bacher M, Bernhagen J, Pushkarskaya T, Seldin MF, Bucala R. Cloning and characterization of the gene for mouse macrophage migration inhibitory factor (MIF). *J Immunol*. 1995;154(8):3863-70.
88. Illescas O, Gomez-Verjan JC, García-Velázquez L, Govezensky T, Rodriguez-Sosa M. Macrophage migration inhibitory factor-173 G/C polymorphism: A global meta-analysis across the disease spectrum. *Front Genet*. 2018;9:55.
89. Donn R, Shelley E, Ollier W, Thomson W, Group BPRS. A novel 5'-flanking region polymorphism of macrophage migration inhibitory factor is associated with systemic-onset juvenile idiopathic arthritis. *Arthritis Rheum*. 2001;44(8):1782-5.
90. Weber C, Kraemer S, Drechsler M, Lue H, Koenen RR, Kapurniotu A, et al. Structural determinants of MIF functions in CXCR2-mediated inflammatory and atherogenic leukocyte recruitment. *Proc Natl Acad Sci*. 2008;105(42):16278-83.
91. Bucala R. MIF rediscovered: cytokine, pituitary hormone, and glucocorticoid-induced regulator of the immune response. *FASEB J*. 1996;10(14):1607-13.
92. Kamimura A, Kamachi M, Nishihira J, Ogura S, Isobe H, Dosaka-Akita H, et al. Intracellular distribution of macrophage migration inhibitory factor predicts the prognosis of patients with adenocarcinoma of the lung. *Cancer*. 2000;89(2):334-41.
93. Yao Y, Deng Q, Song W, Zhang H, Li Y, Yang Y, et al. MIF plays a key role in regulating tissue-specific chondro-osteogenic differentiation fate of human cartilage endplate stem cells under hypoxia. *Stem Cell Rep*. 2016;7(2):249-62.
94. Liu X, Li X, Zhu W, Zhang Y, Hong Y, Liang X, et al. Exosomes from mesenchymal stem cells overexpressing MIF enhance myocardial repair. *J Cell Physiol*. 2020;235(11):8010-22.
95. Fliieger O, Engling A, Bucala R, Lue H, Nickel W, Bernhagen J. Regulated secretion of macrophage migration inhibitory factor is mediated by a non-classical pathway involving an ABC transporter. *FEBS Lett*. 2003;551(1-3):78-86.
96. Merk M, Baugh J, Zierow S, Leng L, Pal U, Lee SJ, et al. The Golgi-associated protein p115 mediates the secretion of macrophage migration inhibitory factor. *J Immunol*. 2009;182(11):6896-906.
97. Kleemann R, Grell M, Mischke R, Zimmermann G, Bernhagen J. Receptor binding and cellular uptake studies of macrophage migration inhibitory factor (MIF): use of biologically active labeled MIF derivatives. *J Interferon Cytokine Res*. 2002;22(3):351-63.
98. Xie L, Qiao X, Wu Y, Tang J.  $\beta$ -Arrestin1 mediates the endocytosis and functions of macrophage migration inhibitory factor. *PLoS One*. 2011;6(1):e16428.
99. Dankers W, Hasnat MA, Swann V, Alharbi A, Lee JP, Cristofaro MA, et al. Necrotic cell death increases the release of macrophage migration inhibitory factor by monocytes/macrophages. *Immunol Cell Biol*. 2020;98(9):782-90.
100. Claret F-X, Hibi M, Dhut S, Toda T, Karin M. A new group of conserved coactivators that increase the specificity of AP-1 transcription factors. *Nature*. 1996;383(6599):453-7.

101. Kleemann R, Hausser A, Geiger G, Mischke R, Burger-Kentischer A, Flieger O, et al. Intracellular action of the cytokine MIF to modulate AP-1 activity and the cell cycle through Jab1. *Nature*. 2000;408(6809):211-6.
102. Bernhagen J, Krohn R, Lue H, Gregory JL, Zerneck A, Koenen RR, et al. MIF is a noncognate ligand of CXC chemokine receptors in inflammatory and atherogenic cell recruitment. *Nat Med*. 2007;13(5):587-96.
103. Stockinger B, Pessara U, Lin RH, Habicht J, Grez M, Koch N. A role of Ia-associated invariant chains in antigen processing and presentation. *Cell*. 1989;56(4):683-9.
104. Jones PP, Murphy DB, Hewgill D, McDevitt HO. Detection of a common polypeptide chain in IA and IE sub-region immunoprecipitates. *Mol Immunol*. 1979;16(1):51-60.
105. Leng L, Metz CN, Fang Y, Xu J, Donnelly S, Baugh J, et al. MIF signal transduction initiated by binding to CD74. *J Exp Med*. 2003;197(11):1467-76.
106. Merk M, Zierow S, Leng L, Das R, Du X, Schulte W, et al. The D-dopachrome tautomerase (DDT) gene product is a cytokine and functional homolog of macrophage migration inhibitory factor (MIF). *Proc Natl Acad Sci*. 2011;108(34):E577-E85.
107. Shi X, Leng L, Wang T, Wang W, Du X, Li J, et al. CD44 is the signaling component of the macrophage migration inhibitory factor-CD74 receptor complex. *Immunity*. 2006;25(4):595-606.
108. Mitchell RA, Liao H, Chesney J, Fingerle-Rowson G, Baugh J, David J, et al. Macrophage migration inhibitory factor (MIF) sustains macrophage proinflammatory function by inhibiting p53: regulatory role in the innate immune response. *Proc Natl Acad Sci*. 2002;99(1):345-50.
109. Djurdjaj S, Lue H, Rong S, Papatiriu M, Klinkhammer BM, Zok S, et al. Macrophage migration inhibitory factor mediates proliferative GN via CD74. *J Am Soc Nephrol*. 2016;27(6):1650-64.
110. Lue H, Thiele M, Franz J, Dahl E, Speckgens S, Leng L, et al. Macrophage migration inhibitory factor (MIF) promotes cell survival by activation of the Akt pathway and role for CSN5/JAB1 in the control of autocrine MIF activity. *Oncogene*. 2007;26(35):5046-59.
111. Starlets D, Gore Y, Binsky I, Haran M, Harpaz N, Shvidel L, et al. Cell-surface CD74 initiates a signaling cascade leading to cell proliferation and survival. *Blood*. 2006;107(12):4807-16.
112. Gore Y, Starlets D, Maharshak N, Becker-Herman S, Kaneyuki U, Leng L, et al. Macrophage migration inhibitory factor induces B cell survival by activation of a CD74-CD44 receptor complex. *J Biol Chem*. 2008;283(5):2784-92.
113. Assis DN, Leng L, Du X, Zhang CK, Grieb G, Merk M, et al. The role of macrophage migration inhibitory factor in autoimmune liver disease. *Hepatology*. 2014;59(2):580-91.
114. Fukuda Y, Bustos MA, Cho S-N, Roszik J, Ryu S, Lopez VM, et al. Interplay between soluble CD74 and macrophage-migration inhibitory factor drives tumor growth and influences patient survival in melanoma. *Cell Death Dis*. 2022;13(2):1-11.
115. Qi D, Young LH. AMPK: energy sensor and survival mechanism in the ischemic heart. *Trends Endocrinol Metab*. 2015;26(8):422-9.
116. Miller EJ, Li J, Leng L, McDonald C, Atsumi T, Bucala R, et al. Macrophage migration inhibitory factor stimulates AMP-activated protein kinase in the ischaemic heart. *Nature*. 2008;451(7178):578-82.

117. Qi D, Hu X, Wu X, Merk M, Leng L, Bucala R, et al. Cardiac macrophage migration inhibitory factor inhibits JNK pathway activation and injury during ischemia/reperfusion. *J Clin Invest.* 2009;119(12):3807-16.
118. Noe JT, Mitchell RA. MIF-dependent control of tumor immunity. *Front Immunol.* 2020;11:609948.
119. Murphy PM, Tiffany HL. Cloning of complementary DNA encoding a functional human interleukin-8 receptor. *Science.* 1991;253(5025):1280-3.
120. Damme JV, Decock B, Conings R, Lenaerts JP, Opdenakker G, Billiau A. The chemotactic activity for granulocytes produced by virally infected fibroblasts is identical to monocyte-derived interleukin 8. *Eur J Immunol.* 1989;19(7):1189-94.
121. Olson TS, Ley K. Chemokines and chemokine receptors in leukocyte trafficking. *Am J Physiol Regul Integr Comp Physiol.* 2002;283(1):R7-R28.
122. Hebert CA, Vitangcol R, Baker JB. Scanning mutagenesis of interleukin-8 identifies a cluster of residues required for receptor binding. *J Biol Chem.* 1991;266(28):18989-94.
123. Kraemer S, Lue H, Zerneck A, Kapurniotu A, Andreetto E, Frank R, et al. MIF-chemokine receptor interactions in atherogenesis are dependent on an N-loop-based 2-site binding mechanism. *FASEB J.* 2011;25(3):894-906.
124. Kleemann R, Kapurniotu A, Frank RW, Gessner A, Mischke R, Flieger O, et al. Disulfide analysis reveals a role for macrophage migration inhibitory factor (MIF) as thiol-protein oxidoreductase. *J Mol Biol.* 1998;280(1):85-102.
125. Kleemann R, Kapurniotu A, Mischke R, Held J, Bernhagen J. Characterization of catalytic centre mutants of macrophage migration inhibitory factor (MIF) and comparison to Cys81Ser MIF. *Eur J Biochem.* 1999;261(3):753-66.
126. Nguyen MT, Beck Jr, Lue H, Fünzig H, Kleemann R, Koolwijk P, et al. A 16-residue peptide fragment of macrophage migration inhibitory factor, MIF-(50–65), exhibits redox activity and has MIF-like biological functions. *J Biol Chem.* 2003;278(36):33654-71.
127. Triantafilou K, Triantafilou M, Dedrick RL. A CD14-independent LPS receptor cluster. *Nat Immunol.* 2001;2(4):338-45.
128. Wu B, Chien EY, Mol CD, Fenalti G, Liu W, Katritch V, et al. Structures of the CXCR4 chemokine GPCR with small-molecule and cyclic peptide antagonists. *Science.* 2010;330(6007):1066-71.
129. Martínez-Muñoz L, Rodríguez-Frade JM, Barroso R, Sorzano CÓS, Torreño-Pina JA, Santiago CA, et al. Separating actin-dependent chemokine receptor nanoclustering from dimerization indicates a role for clustering in CXCR4 signaling and function. *Mol Cell.* 2018;70(1):106-19. e10.
130. Uto-Konomi A, McKibben B, Wirtz J, Sato Y, Takano A, Nanki T, et al. CXCR7 agonists inhibit the function of CXCL12 by down-regulation of CXCR4. *Biochem Biophys Res Commun.* 2013;431(4):772-6.
131. Bleul CC, Farzan M, Choe H, Parolin C, Clark-Lewis I, Sodroski J, et al. The lymphocyte chemoattractant SDF-1 is a ligand for LESTR/fusin and blocks HIV-1 entry. *Nature.* 1996;382(6594):829-33.
132. Yu L, Yu L, Pham Q, Wang TT. Transcriptional and translational-uncoupling in regulation of the CXCL12 and its receptors CXCR4, 7 in THP-1 monocytes and macrophages. *Immun Inflamm Dis.* 2018;6(1):106-16.
133. Teixido J, Martinez-Moreno M, Diaz-Martinez M, Sevilla-Movilla S. The good and bad faces of the CXCR4 chemokine receptor. *Int J Biochem Cell Biol.* 2018;95:121-31.

134. Quoyer J, Janz JM, Luo J, Ren Y, Armando S, Lukashova V, et al. Pepducin targeting the CXC chemokine receptor type 4 acts as a biased agonist favoring activation of the inhibitory G protein. *Proc Natl Acad Sci.* 2013;110(52):E5088-E97.
135. Song Z-Y, Wang F, Cui S-X, Qu X-J. Knockdown of CXCR4 inhibits CXCL12-induced angiogenesis in HUVECs through downregulation of the MAPK/ERK and PI3K/AKT and the Wnt/ $\beta$ -catenin pathways. *Cancer Invest.* 2018;36(1):10-8.
136. Tian Y, Yin H, Deng X, Tang B, Ren X, Jiang T. CXCL12 induces migration of oligodendrocyte precursor cells through the CXCR4-activated MEK/ERK and PI3K/AKT pathways. *Mol Med Report.* 2018;18(5):4374-80.
137. Yang F, Takagaki Y, Yoshitomi Y, Ikeda T, Li J, Kitada M, et al. Inhibition of dipeptidyl peptidase-4 accelerates epithelial–mesenchymal transition and breast cancer metastasis via the CXCL12/CXCR4/mTOR axis. *Cancer Res.* 2019;79(4):735-46.
138. Kofuku Y, Yoshiura C, Ueda T, Terasawa H, Hirai T, Tominaga S, et al. Structural basis of the interaction between chemokine stromal cell-derived factor-1/CXCL12 and its G-protein-coupled receptor CXCR4. *J Biol Chem.* 2009;284(50):35240-50.
139. Rajasekaran D, Gröning S, Schmitz C, Zierow S, Drucker N, Bakou M, et al. Macrophage migration inhibitory factor-CXCR4 receptor interactions. *J Biol Chem.* 2016;291(30):15881-95.
140. Lacy M, Kontos C, Brandhofer M, Hille K, Gröning S, Sinitski D, et al. Identification of an Arg-Leu-Arg tripeptide that contributes to the binding interface between the cytokine MIF and the chemokine receptor CXCR4. *Sci Rep.* 2018;8(1):1-17.
141. Betterman KL, Harvey NL. Decoys and cardiovascular development: CXCR7 and regulation of adrenomedullin signaling. *Dev Cell.* 2014;30(5):490-1.
142. Naumann U, Cameroni E, Pruenster M, Mahabaleshwar H, Raz E, Zerwes H-G, et al. CXCR7 functions as a scavenger for CXCL12 and CXCL11. *PLoS One.* 2010;5(2):e9175.
143. Koenen J, Bachelierie F, Balabanian K, Schlecht-Louf G, Gallego C. Atypical chemokine receptor 3 (ACKR3): a comprehensive overview of its expression and potential roles in the immune system. *Mol Pharmacol.* 2019;96(6):809-18.
144. Torossian F, Anginot A, Chabanon A, Clay D, Guerton B, Desterke C, et al. CXCR7 participates in CXCL12-induced CD34+ cell cycling through  $\beta$ -arrestin-dependent Akt activation. *Blood.* 2014;123(2):191-202.
145. Rajagopal S, Kim J, Ahn S, Craig S, Lam CM, Gerard NP, et al.  $\beta$ -arrestin-but not G protein-mediated signaling by the “decoy” receptor CXCR7. *Proc Natl Acad Sci.* 2010;107(2):628-32.
146. Alampour-Rajabi S, El Bounkari O, Rot A, Müller-Newen G, Bachelierie F, Gawaz M, et al. MIF interacts with CXCR7 to promote receptor internalization, ERK1/2 and ZAP-70 signaling, and lymphocyte chemotaxis. *FASEB J.* 2015;29(11):4497-511.
147. Chatterjee M, von Ungern-Sternberg SN, Seizer P, Schlegel F, Büttcher M, Sindhu N, et al. Platelet-derived CXCL12 regulates monocyte function, survival, differentiation into macrophages and foam cells through differential involvement of CXCR4–CXCR7. *Cell Death Dis.* 2015;6(11):e1989-e.
148. Siervo F, Biben C, Martínez-Muñoz L, Mellado M, Ransohoff RM, Li M, et al. Disrupted cardiac development but normal hematopoiesis in mice deficient in the second CXCL12/SDF-1 receptor, CXCR7. *Proc Natl Acad Sci.* 2007;104(37):14759-64.

149. Ma W, Liu Y, Ellison N, Shen J. Induction of CXC chemokine receptor type 7 (CXCR7) switches stromal cell-derived factor-1 (SDF-1) signaling and phagocytic activity in macrophages linked to atherosclerosis. *J Biol Chem.* 2013;288(22):15481-94.
150. Li X, Zhu M, Penfold ME, Koenen RR, Thiemann A, Heyll K, et al. Activation of CXCR7 limits atherosclerosis and improves hyperlipidemia by increasing cholesterol uptake in adipose tissue. *Circulation.* 2014;129(11):1244-53.
151. Hao H, Hu S, Chen H, Bu D, Zhu L, Xu C, et al. Loss of endothelial CXCR7 impairs vascular homeostasis and cardiac remodeling after myocardial infarction: implications for cardiovascular drug discovery. *Circulation.* 2017;135(13):1253-64.
152. Burger-Kentischer A, Goebel H, Seiler Rd, Fraedrich G, Schaefer HE, Dimmeler S, et al. Expression of macrophage migration inhibitory factor in different stages of human atherosclerosis. *Circulation.* 2002;105(13):1561-6.
153. Lin S-G, Yu X-Y, Chen Y-X, Huang XR, Metz C, Bucala R, et al. De novo expression of macrophage migration inhibitory factor in atherogenesis in rabbits. *Circ Res.* 2000;87(12):1202-8.
154. Lourenco S, Teixeira VH, Kalber T, Jose RJ, Floto RA, Janes SM. Macrophage migration inhibitory factor–CXCR4 is the dominant chemotactic axis in human mesenchymal stem cell recruitment to tumors. *J Immunol.* 2015;194(7):3463-74.
155. Makino A, Nakamura T, Hirano M, Kitta Y, Sano K, Kobayashi T, et al. High plasma levels of macrophage migration inhibitory factor are associated with adverse long-term outcome in patients with stable coronary artery disease and impaired glucose tolerance or type 2 diabetes mellitus. *Atherosclerosis.* 2010;213(2):573-8.
156. Schmeisser A, Marquetant R, Illmer T, Graffy C, Garlachs CD, Böckler D, et al. The expression of macrophage migration inhibitory factor 1 $\alpha$  (MIF 1 $\alpha$ ) in human atherosclerotic plaques is induced by different proatherogenic stimuli and associated with plaque instability. *Atherosclerosis.* 2005;178(1):83-94.
157. Pan J-H, Sukhova GK, Yang J-T, Wang B, Xie T, Fu H, et al. Macrophage migration inhibitory factor deficiency impairs atherosclerosis in low-density lipoprotein receptor-deficient mice. *Circulation.* 2004;109(25):3149-53.
158. Burger-Kentischer A, Göbel H, Kleemann R, Zerneck A, Bucala R, Leng L, et al. Reduction of the aortic inflammatory response in spontaneous atherosclerosis by blockade of macrophage migration inhibitory factor (MIF). *Atherosclerosis.* 2006;184(1):28-38.
159. Schober A, Bernhagen Jr, Thiele M, Zeiffer U, Knarren S, Roller M, et al. Stabilization of atherosclerotic plaques by blockade of macrophage migration inhibitory factor after vascular injury in apolipoprotein E–deficient mice. *Circulation.* 2004;109(3):380-5.
160. Schmitz C, Noels H, El Bounkari O, Strausfeld E, Megens RT, Sternkopf M, et al. Mif-deficiency favors an atheroprotective autoantibody phenotype in atherosclerosis. *FASEB J.* 2018;32(8):4428.
161. Klasen C, Ohl K, Sternkopf M, Shachar I, Schmitz C, Heussen N, et al. MIF promotes B cell chemotaxis through the receptors CXCR4 and CD74 and ZAP-70 signaling. *J Immunol.* 2014;192(11):5273-84.
162. Krammer C, Yang B, Reichl S, Besson-Girard S, Ji H, Bolini V, et al. Pathways linking aging and atheroprotection in Mif-deficient atherosclerotic mice. *FASEB J.* 2023;37(3):e22752.

163. Sinitski D, Kontos C, Krammer C, Asare Y, Kapurniotu A, Bernhagen J. Macrophage migration inhibitory factor (MIF)-based therapeutic concepts in atherosclerosis and inflammation. *Thromb Haemost.* 2019;119(04):553-66.
164. Pantouris G, Syed MA, Fan C, Rajasekaran D, Cho TY, Rosenberg Jr EM, et al. An analysis of MIF structural features that control functional activation of CD74. *Chem Biol.* 2015;22(9):1197-205.
165. Cournia Z, Leng L, Gandavadi S, Du X, Bucala R, Jorgensen WL. Discovery of human macrophage migration inhibitory factor (MIF)-CD74 antagonists via virtual screening. *J Med Chem.* 2009;52(2):416-24.
166. Jorgensen WL, Gandavadi S, Du X, Hare AA, Trofimov A, Leng L, et al. Receptor agonists of macrophage migration inhibitory factor. *Bioorg Med Chem Lett.* 2010;20(23):7033-6.
167. Lubetsky JB, Dios A, Han J, Aljabari B, Ruzsicska B, Mitchell R, et al. The tautomerase active site of macrophage migration inhibitory factor is a potential target for discovery of novel anti-inflammatory agents. *J Biol Chem.* 2002;277(28):24976-82.
168. Rajasekaran D, Zierow S, Syed M, Bucala R, Bhandari V, Lolis EJ. Targeting distinct tautomerase sites of D-DT and MIF with a single molecule for inhibition of neutrophil lung recruitment. *FASEB J.* 2014;28(11):4961-71.
169. Mawhinney L, Armstrong ME, O'Reilly C, Bucala R, Leng L, Fingerle-Rowson G, et al. Macrophage migration inhibitory factor (MIF) enzymatic activity and lung cancer. *Mol Med.* 2014;20(1):729-35.
170. Fagone P, Mazzon E, Cavalli E, Bramanti A, Petralia MC, Mangano K, et al. Contribution of the macrophage migration inhibitory factor superfamily of cytokines in the pathogenesis of preclinical and human multiple sclerosis: In silico and in vivo evidences. *J Neuroimmunol.* 2018;322:46-56.
171. Soumoy L, Kindt N, Ghanem G, Saussez S, Journe F. Role of macrophage migration inhibitory factor (MIF) in melanoma. *Cancers (Basel).* 2019;11(4):529.
172. Ouertatani-Sakouhi H, El-Turk F, Fauvet B, Cho M-K, Karpinar DP, Le Roy D, et al. Identification and characterization of novel classes of macrophage migration inhibitory factor (MIF) inhibitors with distinct mechanisms of action. *J Biol Chem.* 2010;285(34):26581-98.
173. Bai F, Asojo OA, Cirillo P, Ciustea M, Ledizet M, Aristoff PA, et al. A novel allosteric inhibitor of macrophage migration inhibitory factor (MIF). *J Biol Chem.* 2012;287(36):30653-63.
174. Günther S, Fagone P, Jalce G, Atanasov AG, Guignabert C, Nicoletti F. Role of MIF and D-DT in immune-inflammatory, autoimmune, and chronic respiratory diseases: From pathogenic factors to therapeutic targets. *Drug Discov Today.* 2019;24(2):428-39.
175. Zernecke A, Bernhagen Jr, Weber C. Macrophage migration inhibitory factor in cardiovascular disease. *Circulation.* 2008;117(12):1594-602.
176. Calandra T, Echtenacher B, Roy DL, Pugin J, Metz CN, Hültner L, et al. Protection from septic shock by neutralization of macrophage migration inhibitory factor. *Nat Med.* 2000;6(2):164-70.
177. Mahalingam D, Patel M, Sachdev J, Hart L, Halama N, Ramanathan R, et al. PD-011 Safety and efficacy analysis of imalumab, an anti-oxidized macrophage migration inhibitory factor (oxMIF) antibody, alone or in combination with 5-fluorouracil/leucovorin (5-FU/LV) or panitumumab, in patients with metastatic colorectal cancer (mCRC). *Ann Oncol.* 2016;27:ii105.

178. Dolgin E. First GPCR-directed antibody passes approval milestone. *Nat Rev Drug Discov.* 2018;17(7):457-60.
179. Henninot A, Collins JC, Nuss JM. The Current State of Peptide Drug Discovery: Back to the Future? *J Med Chem.* 2018;61(4):1382-414.
180. Lau JL, Dunn MK. Therapeutic peptides: Historical perspectives, current development trends, and future directions. *Biorg Med Chem.* 2018;26(10):2700-7.
181. Lee AC-L, Harris JL, Khanna KK, Hong J-H. A comprehensive review on current advances in peptide drug development and design. *Int J Mol Sci.* 2019;20(10):2383.
182. Wells JA, McClendon CL. Reaching for high-hanging fruit in drug discovery at protein–protein interfaces. *Nature.* 2007;450(7172):1001-9.
183. Fosgerau K, Hoffmann T. Peptide therapeutics: current status and future directions. *Drug Discov Today.* 2015;20(1):122-8.
184. Davda J, Declerck P, Hu-Lieskovan S, Hickling TP, Jacobs IA, Chou J, et al. Immunogenicity of immunomodulatory, antibody-based, oncology therapeutics. *J Immunother Cancer.* 2019;7(1):105.
185. Imai K, Takaoka A. Comparing antibody and small-molecule therapies for cancer. *Nat Rev Cancer.* 2006;6:714-27.
186. Smith MC, Gestwicki JE. Features of protein–protein interactions that translate into potent inhibitors: topology, surface area and affinity. *Expert Rev Mol Med.* 2012;14:e16.
187. Petta I, Lievens S, Libert C, Tavernier J, De Bosscher K. Modulation of Protein–Protein Interactions for the Development of Novel Therapeutics. *Mol Ther.* 2016;24(4):707-18.
188. Diao L, Meibohm B. Pharmacokinetics and Pharmacokinetic–Pharmacodynamic Correlations of Therapeutic Peptides. *Clin Pharmacokinet.* 2013;52(10):855-68.
189. Koenen RR, von Hundelshausen P, Nesmelova IV, Zerneck A, Liehn EA, Sarabi A, et al. Disrupting functional interactions between platelet chemokines inhibits atherosclerosis in hyperlipidemic mice. *Nat Med.* 2009;15(1):97-103.
190. Koenen RR, Weber C. Therapeutic targeting of chemokine interactions in atherosclerosis. *Nat Rev Drug Discov.* 2010;9(2):141-53.
191. Leman LJ, Maryanoff BE, Ghadiri MR. Molecules That Mimic Apolipoprotein A-I: Potential Agents for Treating Atherosclerosis. *J Med Chem.* 2014;57(6):2169-96.
192. Figueiredo CR, Matsuo AL, Massaoka MH, Polonelli L, Travassos LR. Antitumor activities of peptides corresponding to conserved complementary determining regions from different immunoglobulins. *Peptides.* 2014;59:14-9.
193. Figueiredo CR, Azevedo RAd, Mousdell S, Resende-Lara PT, Ireland L, Santos A, et al. Blockade of MIF–CD74 Signalling on Macrophages and Dendritic Cells Restores the Antitumour Immune Response Against Metastatic Melanoma. *Front Immunol.* 2018;9.
194. Benedek G, Meza-Romero R, Jordan KR, Keenlyside L, Offner H, Vandebark AA. HLA-DR $\alpha$ 1-mMOG-35-55 treatment of experimental autoimmune encephalomyelitis reduces CNS inflammation, enhances M2 macrophage frequency, and promotes neuroprotection. *J Neuroinflammation.* 2015;12.
195. Benedek G, Meza-Romero R, Andrew S, Leng L, Burrows GG, Bourdette D, et al. Partial MHC class II constructs inhibit MIF/CD74 binding and downstream effects. *Eur J Immunol.* 2013;43(5):1309-21.

196. Tamamura H, Hori A, Kanzaki N, Hiramatsu K, Mizumoto M, Nakashima H, et al. T140 analogs as CXCR4 antagonists identified as anti-metastatic agents in the treatment of breast cancer. *FEBS Lett.* 2003;550(1-3):79-83.
197. DeMarco SJ, Henze H, Lederer A, Moehle K, Mukherjee R, Romagnoli B, et al. Discovery of novel, highly potent and selective  $\beta$ -hairpin mimetic CXCR4 inhibitors with excellent anti-HIV activity and pharmacokinetic profiles. *Biorg Med Chem.* 2006;14(24):8396-404.
198. Di Maro S, Di Leva FS, Trotta AM, Brancaccio D, Portella L, Aurilio M, et al. Structure–Activity Relationships and Biological Characterization of a Novel, Potent, and Serum Stable C-X-C Chemokine Receptor Type 4 (CXCR4) Antagonist. *J Med Chem.* 2017;60(23):9641-52.
199. Di Maro S, Trotta AM, Brancaccio D, Di Leva FS, La Pietra V, Ieranò C, et al. Exploring the N-Terminal Region of C-X-C Motif Chemokine 12 (CXCL12): Identification of Plasma-Stable Cyclic Peptides As Novel, Potent C-X-C Chemokine Receptor Type 4 (CXCR4) Antagonists. *J Med Chem.* 2016;59(18):8369-80.
200. Kontos C, El Bounkari O, Krammer C, Sinitski D, Hille K, Zan C, et al. Designed CXCR4 mimic acts as a soluble chemokine receptor that blocks atherogenic inflammation by agonist-specific targeting. *Nat Commun.* 2020;11(1):5981.
201. Tillmann S, Bernhagen J, Noels H. Arrest Functions of the MIF Ligand/Receptor Axes in Atherogenesis. *Front Immunol.* 2013;4.
202. Kraemer S, Lue H, Zerneck A, Kapurniotu A, Andreetto E, Frank R, et al. MIF-chemokine receptor interactions in atherogenesis are dependent on an N-loop-based 2-site binding mechanism. *FASEB J.* 2011;25(3):894-906.
203. Bernhagen J, Mitchell RA, Calandra T, Voelter W, Cerami A, Bucala R. Purification, bioactivity, and secondary structure analysis of mouse and human macrophage migration inhibitory factor (MIF). *Biochem.* 1994;33(47):14144-55.
204. Krammer C, Kontos C, Dewor M, Hille K, Dalla Volta B, El Bounkari O, et al. A MIF-derived cyclopeptide that inhibits MIF binding and atherogenic signaling via the chemokine receptor CXCR2. *ChemBioChem.* 2021;22(6):1012-9.
205. Yan L-M, Tatarek-Nossol M, Velkova A, Kazantzis A, Kapurniotu A. Design of a mimic of nonamyloidogenic and bioactive human islet amyloid polypeptide (IAPP) as nanomolar affinity inhibitor of IAPP cytotoxic fibrillogenesis. *Proc Natl Acad Sci.* 2006;103(7):2046-51.
206. Venegas-Pino DE, Banko N, Khan MI, Shi Y, Werstuck GH. Quantitative analysis and characterization of atherosclerotic lesions in the murine aortic sinus. *J Vis Exp.* 2013(82):e50933.
207. Ji H, Besson-Girard S, Androvic P, Bulut B, Liu L, Wang Y, et al. High-Resolution RNA Sequencing from PFA-Fixed Microscopy Sections. *Neural Repair: Methods and Protocols*: Springer; 2023. p. 205-12.
208. The Galaxy platform for accessible, reproducible and collaborative biomedical analyses: 2022 update. *Nucleic Acids Res.* 2022;50(W1):W345-W51.
209. Raudvere U, Kolberg L, Kuzmin I, Arak T, Adler P, Peterson H, et al. g: Profiler: a web server for functional enrichment analysis and conversions of gene lists (2019 update). *Nucleic Acids Res.* 2019;47(W1):W191-W8.
210. Kruth HS, Huang W, Ishii I, Zhang W-Y. Macrophage foam cell formation with native low density lipoprotein. *J Biol Chem.* 2002;277(37):34573-80.
211. Domschke G, Linden F, Pawig L, Hafner A, Akhavanpoor M, Reymann J, et al. Systematic RNA-interference in primary human monocyte-derived macrophages: A high-throughput platform to study foam cell formation. *Sci Rep.* 2018;8(1):1-11.



212. Al-Abed Y, Dabideen D, Aljabari B, Valster A, Messmer D, Ochani M, et al. ISO-1 binding to the tautomerase active site of MIF inhibits its pro-inflammatory activity and increases survival in severe sepsis. *J Biol Chem*. 2005;280(44):36541-4.
213. Zirafi O, Hermann PC, Münch J. Proteolytic processing of human serum albumin generates EPI-X4, an endogenous antagonist of CXCR4. *J Leukoc Biol*. 2016;99(6):863-8.
214. Depuydt MA, Prange KH, Slenders L, Örd T, Elbersen D, Boltjes A, et al. Microanatomy of the human atherosclerotic plaque by single-cell transcriptomics. *Circ Res*. 2020;127(11):1437-55.
215. Rensen S, Doevendans P, Van Eys G. Regulation and characteristics of vascular smooth muscle cell phenotypic diversity. *Neth Heart J*. 2007;15:100-8.
216. Fernandez-Botran R, Sun X, Crespo FA. Soluble cytokine receptors in biological therapy. *Expert Opin Biol Ther*. 2002;2(6):585-605.
217. Rose-John S. The soluble interleukin 6 receptor: advanced therapeutic options in inflammation. *Clin Pharmacol Ther*. 2017;102(4):591-8.
218. Morton AC, Rothman AM, Greenwood JP, Gunn J, Chase A, Clarke B, et al. The effect of interleukin-1 receptor antagonist therapy on markers of inflammation in non-ST elevation acute coronary syndromes: the MRC-ILA Heart Study. *Eur Heart J*. 2015;36(6):377-84.
219. Babaev VR, Fazio S, Gleaves LA, Carter KJ, Semenkovich CF, Linton MF. Macrophage lipoprotein lipase promotes foam cell formation and atherosclerosis in vivo. *J Clin Invest*. 1999;103(12):1697-705.
220. Linton MF, Yancey PG, Davies SS, Jerome WG, Linton EF, Song WL, et al. The role of lipids and lipoproteins in atherosclerosis. *Endotext* [Internet]. 2019.
221. Maiolino G, Rossitto G, Caielli P, Bisogni V, Rossi GP, Calò LA. The role of oxidized low-density lipoproteins in atherosclerosis: the myths and the facts. *Mediators Inflamm*. 2013;2013.
222. Moore KJ, Freeman MW. Scavenger receptors in atherosclerosis: beyond lipid uptake. *Arterioscler Thromb Vasc Biol*. 2006;26(8):1702-11.
223. Schröder R, Schmidt J, Blättermann S, Peters L, Janssen N, Grundmann M, et al. Applying label-free dynamic mass redistribution technology to frame signaling of G protein-coupled receptors noninvasively in living cells. *Nat Protoc*. 2011;6(11):1748-60.
224. Schröder R, Janssen N, Schmidt J, Kebig A, Merten N, Hennen S, et al. Deconvolution of complex G protein-coupled receptor signaling in live cells using dynamic mass redistribution measurements. *Nat Biotechnol*. 2010;28(9):943-9.
225. Ridker PM, Devalaraja M, Baeres FM, Engelman MD, Hovingh GK, Ivkovic M, et al. IL-6 inhibition with ziltivekimab in patients at high atherosclerotic risk (RESCUE): a double-blind, randomised, placebo-controlled, phase 2 trial. *Lancet*. 2021;397(10289):2060-9.
226. L Scognamiglio P, Di Natale C, Perretta G, Marasco D. From peptides to small molecules: an intriguing but intricate way to new drugs. *Curr Med Chem*. 2013;20(31):3803-17.
227. Vemula VR, Lagishetty V, Lingala S. Solubility enhancement techniques. *International journal of pharmaceutical sciences review and research*. 2010;5(1):41-51.
228. Eftink MR. [11] Fluorescence methods for studying equilibrium macromolecule-ligand interactions. *Methods Enzymol*. 1997;278:221-57.

229. Witztum JL, Steinberg D. The oxidative modification hypothesis of atherosclerosis: does it hold for humans? *Trends Cardiovasc Med.* 2001;11(3-4):93-102.
230. Ylä-Herttuala S. Is oxidized low-density lipoprotein present in vivo? *Curr Opin Lipidol.* 1998;9(4):337-44.
231. Martinez FO, Gordon S, Locati M, Mantovani A. Transcriptional profiling of the human monocyte-to-macrophage differentiation and polarization: new molecules and patterns of gene expression. *J Immunol.* 2006;177(10):7303-11.
232. Murphy JE, Tedbury PR, Homer-Vanniasinkam S, Walker JH, Ponnambalam S. Biochemistry and cell biology of mammalian scavenger receptors. *Atherosclerosis.* 2005;182(1):1-15.
233. Zabel BA, Wang Y, Lewén S, Berahovich RD, Penfold ME, Zhang P, et al. Elucidation of CXCR7-mediated signaling events and inhibition of CXCR4-mediated tumor cell transendothelial migration by CXCR7 ligands. *J Immunol.* 2009;183(5):3204-11.
234. Fricker SP, Anastassov V, Cox J, Darkes MC, Grujic O, Idzan SR, et al. Characterization of the molecular pharmacology of AMD3100: a specific antagonist of the G-protein coupled chemokine receptor, CXCR4. *Biochem Pharmacol.* 2006;72(5):588-96.
235. Endemann G, Stanton LW, Madden KS, Bryant CM, White RT, Protter AA. CD36 is a receptor for oxidized low density lipoprotein. *J Biol Chem.* 1993;268(16):11811-6.
236. Freeman M, Ashkenas J, Rees D, Kingsley DM, Copeland NG, Jenkins NA, et al. An ancient, highly conserved family of cysteine-rich protein domains revealed by cloning type I and type II murine macrophage scavenger receptors. *Proc Natl Acad Sci.* 1990;87(22):8810-4.
237. Coussens LM, Werb Z. Inflammatory Cells and Cancer Think Different! *J Exp Med.* 2001;193(6):F23-F6.
238. Bacher M, Schrader J, Thompson N, Kuschela K, Gemsa D, Waeber G, et al. Up-regulation of macrophage migration inhibitory factor gene and protein expression in glial tumor cells during hypoxic and hypoglycemic stress indicates a critical role for angiogenesis in glioblastoma multiforme. *Am J Clin Pathol.* 2003;162(1):11-7.
239. White ES, Flaherty KR, Carskadon S, Brant A, Iannettoni MD, Yee J, et al. Macrophage migration inhibitory factor and CXC chemokine expression in non-small cell lung cancer: role in angiogenesis and prognosis. *Clin Cancer Res.* 2003;9(2):853-60.
240. Verjans E, Noetzel E, Bektas N, Schütz AK, Lue H, Lennartz B, et al. Dual role of macrophage migration inhibitory factor (MIF) in human breast cancer. *BMC Cancer.* 2009;9(1):1-18.
241. He L-J, Xie D, Hu P-J, Liao Y-J, Deng H-X, Kung H-F, et al. Macrophage migration inhibitory factor as a potential prognostic factor in gastric cancer. *World J Gastroenterol.* 2015;21(34):9916.
242. Oliveira CS, de Bock CE, Molloy TJ, Sadeqzadeh E, Geng XY, Hersey P, et al. Macrophage migration inhibitory factor engages PI3K/Akt signalling and is a prognostic factor in metastatic melanoma. *BMC Cancer.* 2014;14(1):1-14.
243. Amin MA, Volpert OV, Woods JM, Kumar P, Harlow LA, Koch AE. Migration inhibitory factor mediates angiogenesis via mitogen-activated protein kinase and phosphatidylinositol kinase. *Circ Res.* 2003;93(4):321-9.

244. Chesney JA, Mitchell RA. 25 years on: a retrospective on migration inhibitory factor in tumor angiogenesis. *Mol Med*. 2015;21(1):S19-S24.
245. Funamizu N, Hu C, Lacy C, Schetter A, Zhang G, He P, et al. Macrophage migration inhibitory factor induces epithelial to mesenchymal transition, enhances tumor aggressiveness and predicts clinical outcome in resected pancreatic ductal adenocarcinoma. *Int J Cancer*. 2013;132(4):785-94.
246. Ishigami S, Natsugoe S, Okumura H, Matsumoto M, Nakajo A, Uenosono Y, et al. Clinical implication of CXCL12 expression in gastric cancer. *Ann Surg Oncol*. 2007;14(11):3154-8.
247. Imai H, Sunaga N, Shimizu Y, Kakegawa S, Shimizu K, Sano T, et al. Clinicopathological and therapeutic significance of CXCL12 expression in lung cancer. *Int J Immunopathol Pharmacol*. 2010;23(1):153-64.
248. Yang D, Xin M, Wang J, Xu H, Huo Q, Tang Z, et al. Chemokine receptor CXCR4 and its ligand CXCL12 expressions and clinical significance in bladder cancer. *Genet Mol Res*. 2015;14(4):17699-707.
249. Zraggen S, Huggenberger R, Kerl K, Detmar M. An important role of the SDF-1/CXCR4 axis in chronic skin inflammation. *PLoS One*. 2014;9(4):e93665.
250. Hansen I, Ellingsen T, Hornung N, Poulsen JH, Lottenburger T, Stengaard-Pedersen K. Plasma level of CXC-chemokine CXCL12 is increased in rheumatoid arthritis and is independent of disease activity and methotrexate treatment. *J Rheumatol*. 2006;33(9):1754-9.
251. Bilsborrow JB, Doherty E, Tilstam PV, Bucala R. Macrophage migration inhibitory factor (MIF) as a therapeutic target for rheumatoid arthritis and systemic lupus erythematosus. *Expert Opin Ther Targets*. 2019;23(9):733-44.
252. Benedek G, Meza-Romero R, Jordan K, Zhang Y, Nguyen H, Kent G, et al. MIF and D-DT are potential disease severity modifiers in male MS subjects. *Proc Natl Acad Sci*. 2017;114(40):E8421-E9.
253. Nishihira J, Mitsuyama K. Overview of the role of macrophage migration inhibitory factor (MIF) in inflammatory bowel disease. *Curr Pharm Des*. 2009;15(18):2104-9.
254. Calderon TM, Eugenin EA, Lopez L, Kumar SS, Hesselgesser J, Raine CS, et al. A role for CXCL12 (SDF-1 $\alpha$ ) in the pathogenesis of multiple sclerosis: regulation of CXCL12 expression in astrocytes by soluble myelin basic protein. *J Neuroimmunol*. 2006;177(1-2):27-39.
255. Dotan I, Werner L, Vigodman S, Weiss S, Brazowski E, Maharshak N, et al. CXCL12 is a constitutive and inflammatory chemokine in the intestinal immune system. *Inflamm Bowel Dis*. 2010;16(4):583-92.
256. Otvos Jr L, Wade J. Current challenges in peptide-based drug discovery. *Front Chem* 2014;2:62.
257. Kratz F. Albumin as a drug carrier: design of prodrugs, drug conjugates and nanoparticles. *J Control Release*. 2008;132(3):171-83.
258. Peters Jr T. All about albumin: biochemistry, genetics, and medical applications: Academic press; 1995.
259. Anderson CL, Chaudhury C, Kim J, Bronson C, Wani MA, Mohanty S. Perspective—FcRn transports albumin: relevance to immunology and medicine. *Trends Immunol*. 2006;27(7):343-8.
260. Markovsky E, Baabur-Cohen H, Eldar-Boock A, Omer L, Tiram G, Ferber S, et al. Administration, distribution, metabolism and elimination of polymer therapeutics. *J Control Release*. 2012;161(2):446-60.

261. Sleep D, Cameron J, Evans LR. Albumin as a versatile platform for drug half-life extension. *Biochim Biophys Acta - Gen Subj*. 2013;1830(12):5526-34.
262. Kragh-Hansen U, Chuang VTG, Otagiri M. Practical aspects of the ligand-binding and enzymatic properties of human serum albumin. *Biol Pharm Bull*. 2002;25(6):695-704.
263. Zirafi O, Kim K-A, Ständker L, Mohr KB, Sauter D, Heigele A, et al. Discovery and characterization of an endogenous CXCR4 antagonist. *Cell Rep*. 2015;11(5):737-47.
264. Quinlan GJ, Martin GS, Evans TW. Albumin: biochemical properties and therapeutic potential. *Hepatology*. 2005;41(6):1211-9.
265. Bertucci C, Domenici E. Reversible and covalent binding of drugs to human serum albumin: methodological approaches and physiological relevance. *Curr Med Chem*. 2002;9(15):1463-81.
266. Sudlow G, Birkett D, Wade D. The characterization of two specific drug binding sites on human serum albumin. *Mol Pharmacol*. 1975;11(6):824-32.
267. Perrotta P, De Meyer G, Roth L, Van der Donckt C, Martinet W, De Meyer G. Animal models of atherosclerosis. *Eur J Pharmacol*. 2017;816:3-13.
268. Ishibashi S, Brown MS, Goldstein JL, Gerard RD, Hammer RE, Herz J. Hypercholesterolemia in low density lipoprotein receptor knockout mice and its reversal by adenovirus-mediated gene delivery. *J Clin Invest*. 1993;92(2):883-93.
269. Ishibashi S, Goldstein JL, Brown MS, Herz J, Burns DK. Massive xanthomatosis and atherosclerosis in cholesterol-fed low density lipoprotein receptor-negative mice. *J Clin Invest*. 1994;93(5):1885-93.
270. Plump AS, Smith JD, Hayek T, Aalto-Setälä K, Walsh A, Verstuyft JG, et al. Severe hypercholesterolemia and atherosclerosis in apolipoprotein E-deficient mice created by homologous recombination in ES cells. *Cell*. 1992;71(2):343-53.
271. Zhang SH, Reddick RL, Piedrahita JA, Maeda N. Spontaneous hypercholesterolemia and arterial lesions in mice lacking apolipoprotein E. *Science*. 1992;258(5081):468-71.
272. Piedrahita JA, Zhang SH, Hagaman JR, Oliver PM, Maeda N. Generation of mice carrying a mutant apolipoprotein E gene inactivated by gene targeting in embryonic stem cells. *Proc Natl Acad Sci*. 1992;89(10):4471-5.
273. Silvestre-Roig C, De Winther MP, Weber C, Daemen MJ, Lutgens E, Soehnlein O. Atherosclerotic plaque destabilization: mechanisms, models, and therapeutic strategies. *Circ Res*. 2014;114(1):214-26.
274. Jawien J. Mouse models of experimental atherosclerosis as a tool for checking a putative anti-atherogenic action of drugs. *Atherogenesis: IntechOpen*; 2012. p. 1-24.
275. Hansson GK, Libby P. The immune response in atherosclerosis: a double-edged sword. *Nat Rev Immunol*. 2006;6(7):508-19.
276. Swirski FK, Nahrendorf M. Leukocyte behavior in atherosclerosis, myocardial infarction, and heart failure. *Science*. 2013;339(6116):161-6.
277. Epelman S, Lavine KJ, Randolph GJ. Origin and functions of tissue macrophages. *Immunity*. 2014;41(1):21-35.
278. Hoeffel G, Ginhoux F. Fetal monocytes and the origins of tissue-resident macrophages. *Cell Immunol*. 2018;330:5-15.
279. Weinberger T, Esfandyari D, Messerer D, Percin G, Schleifer C, Thaler R, et al. Ontogeny of arterial macrophages defines their functions in homeostasis and inflammation. *Nat Commun*. 2020;11(1):1-16.

280. Ensan S, Li A, Besla R, Degousee N, Cosme J, Roufaiel M, et al. Self-renewing resident arterial macrophages arise from embryonic CX3CR1+ precursors and circulating monocytes immediately after birth. *Nat Immunol.* 2016;17(2):159-68.
281. Jenkins SJ, Ruckerl D, Cook PC, Jones LH, Finkelman FD, Van Rooijen N, et al. Local macrophage proliferation, rather than recruitment from the blood, is a signature of TH2 inflammation. *Science.* 2011;332(6035):1284-8.
282. Lhoták Š, Gyulay G, Cutz JC, Al-Hashimi A, Trigatti BL, Richards CD, et al. Characterization of proliferating lesion-resident cells during all stages of atherosclerotic growth. *J Am Heart Assoc.* 2016;5(8):e003945.
283. Robbins CS, Hilgendorf I, Weber GF, Theurl I, Iwamoto Y, Figueiredo J-L, et al. Local proliferation dominates lesional macrophage accumulation in atherosclerosis. *Nat Med.* 2013;19(9):1166-72.
284. Williams JW, Zaitsev K, Kim K-W, Ivanov S, Saunders BT, Schrank PR, et al. Limited proliferation capacity of aortic intima resident macrophages requires monocyte recruitment for atherosclerotic plaque progression. *Nat Immunol.* 2020;21(10):1194-204.
285. Winkels H, Ehinger E, Vassallo M, Buscher K, Dinh HQ, Kobiyama K, et al. Atlas of the immune cell repertoire in mouse atherosclerosis defined by single-cell RNA-sequencing and mass cytometry. *Circ Res.* 2018;122(12):1675-88.
286. McArdle S, Buscher K, Ghosheh Y, Pramod AB, Miller J, Winkels H, et al. Migratory and dancing macrophage subsets in atherosclerotic lesions. *Circ Res.* 2019;125(12):1038-51.
287. Baumer Y, McCurdy S, Jin X, Weatherby TM, Dey AK, Mehta NN, et al. Ultramorphological analysis of plaque advancement and cholesterol crystal formation in Ldlr knockout mouse atherosclerosis. *Atherosclerosis.* 2019;287:100-11.
288. Krammer C, Yang B, Reichl S, Besson-Girard S, Ji H, Bolini V, et al. Pathways linking aging and atheroprotection in Mif-deficient atherosclerotic mice. *FASEB J.* 2023;37(3):e22752.
289. Galkina E, Kadl A, Sanders J, Varughese D, Sarembock IJ, Ley K. Lymphocyte recruitment into the aortic wall before and during development of atherosclerosis is partially L-selectin dependent. *J Exp Med.* 2006;203(5):1273-82.
290. Ketelhuth DF, Hansson GK. Adaptive response of T and B cells in atherosclerosis. *Circ Res.* 2016;118(4):668-78.

# Acknowledgements

I would like to express my gratitude to my thesis supervisor Prof. Dr. rer. nat. Jürgen Bernhagen for offering me the opportunity to do research and pursue my PhD in his laboratory and all the support I received from him in science as well as during the time of my PhD study. I would also like to thank my TAC committee members, Prof. Dr. Aphrodite Kapurniotu and Prof. Dr. med. Lutgens Esther, for their mentorship. Without their passionate participation and valuable input, I could not have successfully conducted the thesis.

I am grateful to being able to work in an international team with my co-workers and collaborators from diverse academic and cultural background. They have helped and supported me in academic research and daily life. Thanks to Sabrina Lukanovic and Barbara Hönig for supporting me with all the paperwork and living advice in Germany. To Dr. Dzmitry Sinitski and Dr. Omar El Bounkarri, for showing me how to work in the laboratory in the first place and for their scientific advice and discussions. To the collaborators Dr. Christos Kontos and Hendrik Wunderlich, for providing peptides as well as to Dr. Markus Brandhofer for answering my questions regarding the biochemistry aspects of the study. To our technicians Simona Gerra, Priscila Bourilhon, and Maida Avdic for their technical supports. To Dr. Chunfang Zan and Bishan Yang for sharing tips of the animal experiment. I would also like show my gratitude to some colleagues from the Gokce lab. Particularly, to Hao Ji and Prof. Özgün Gökce for their contribution to the sequencing study. Beyond the lab work, I enjoyed those wonderful gatherings and parties of the lab mates during the festivals. The experience with the whole team has shaped the way I think and address scientific questions. They have made this journey a wonderful time.

My appreciation also goes to my family and friends Laura, Lin, Yuan and many others for their tremendous understanding, encouragement, and support to help me get through the difficult times of the pandemic. I would like to thank my friend Jiayu for his generous sharing. Lastly, I feel honored in receiving scholarship from China Scholarship Council and would like to express my gratitude to the support from the Chinese government.

# Affidavit



## Affidavit

Gao, Ying

\_\_\_\_\_  
Surname, first name

\_\_\_\_\_  
Street

\_\_\_\_\_  
Zip code, town, country

I hereby declare, that the submitted thesis entitled:

First and Second Generation CXCR4 Peptide Mimics to Block MIF Pathways in Atherosclerosis  
.....

is my own work. I have only used the sources indicated and have not made unauthorised use of services of a third party. Where the work of others has been quoted or reproduced, the source is always given.

I further declare that the dissertation presented here has not been submitted in the same or similar form to any other institution for the purpose of obtaining an academic degree.

Munich, 27.10.2023




\_\_\_\_\_  
place, date

Ying Gao

\_\_\_\_\_  
Signature doctoral candidate



# Confirmation of congruency

	LUDWIG- MAXIMILIANS- UNIVERSITÄT MÜNCHEN	Promotionsbüro Medizinische Fakultät		
<b>Confirmation of congruency between printed and electronic version of the doctoral thesis</b>				

Gao, Ying  
\_\_\_\_\_  
Surname, first name

\_\_\_\_\_  
Street

\_\_\_\_\_  
Zip code, town, country

I hereby declare, that the submitted thesis entitled:  
First and Second Generation CXCR4 Peptide Mimics to Block MIF Pathways in Atherosclerosis  
.....  
is congruent with the printed version both in content and format.

Munich, 27.10.2023  
\_\_\_\_\_  
place, date

Ying Gao  
\_\_\_\_\_  
Signature doctoral candidate